NTIA Report 94-306

Building Penetration Loss Measurements at 900 MHz, 11.4 GHz, and 28.8 GHz

K.C. Allen
N. DeMinco
J.R. Hoffman
Y. Lo
P.B. Papazian

U.S. DEPARTMENT OF COMMERCE
Ronald H. Brown, Secretary

Larry Irving, Assistant Secretary
for Communications and Information

May 1994

CONTENTS

PAGE

FIGURES iv

TABLES ix

ABSTRACT 1

1. INTRODUCTION 1

2. DESCRIPTION OF THE EXPERIMENT 2

2.1 Instrumentation And Calibration 2

2.2 Measurement Sites 5

3. MEASUREMENT PROCEDURE 7

3.1 Radio Building 7

3.2 Private Residence 10

3.3 Storeroom With Metal Siding 10

4. DATA COLLECTION AND PROCESSING 13

4.1 Data Collection 13

4.2 Data Processing 13

5. DISCUSSION OF RESULTS 14

6. CONCLUSIONS 33

APPENDIX A: PENETRATION LOSS PLOTS FOR ALL MEASUREMENT PATHS

A.1 Radio Building Penetration Loss A-1

A.2 Private Residence Penetration Loss A-39

A.3 Storeroom Penetration Loss A-43

FIGURES

PAGE

Figure 1. ITS millimeter-wave measurement van (receiver) . . . 3

Figure 2. Remote source cart (transmitter) 3

Figure 3. Wing 4 of the Radio Building with ITS millimeter-wave measurement van 6

Figure 4. West side of Wing 4 of the Radio Building 6

Figure 5. Private residence 8

Figure 6. Storeroom with metal siding 8

Figure 7. Floor plan of Wing 4 of the Radio Building with measurement paths of the transmitters 9

Figure 8. Floor plan of single level wood-frame house 11

Figure 9. Floor plan of building with metal siding(storeroom) 12

Figure 10. Raw data, free-space correction factor, and penetration attenuation versus distance for a typical 900-MHz measurement in the Radio Building 15

Figure 11. Raw data, free-space correction factor, and penetration attenuation versus distance for a typical 11.4-GHz measurement in the Radio Building 16

Figure 12. Raw data, free-space correction factor, and penetration attenuation versus distance for a typical 28.4-GHz measurement in the Radio Building 17

Figure 13. Penetration loss versus distance at three frequencies for a typical run in the Radio Building 18

Figure 14. Penetration loss versus distance at three frequencies for a typical run in the storeroom building with metal siding 19

Figure 15. Penetration loss versus distance at three frequencies for a typical run in the private residence 20

Figure 16. Cumulative distribution for all data in the Radio Building 25

FIGURES (Cont'd)

PAGE

Figure 17. Cumulative distribution for all data in Radio Building with just one wall between the transmitter and receiver 26

Figure 18. Cumulative distribution for all data in Radio Building with two or three walls between the transmitter and receiver 27

Figure 19. Cumulative distribution for all data in Radio Building with three or more walls between the transmitter and receiver 28

Figure 20. Cumulative distribution for all data in the private residence 29

Figure 21. Cumulative distribution for all data in the private residence with one wall between the transmitter and receiver 30

Figure 22. Cumulative distribution for all data in the private residence with two walls between the transmitter and receiver 31

Figure 23. Cumulative distribution for all data in the storeroom building with metal siding 32

Figure A-1. Penetration loss for Radio Building path RB1D . . A-1

Figure A-2. Penetration loss for Radio Building path RB1E . . A-2

Figure A-3. Penetration loss for Radio Building path RB2B . . A-3

Figure A-4. Penetration loss for Radio Building path RB2C . . A-4

Figure A-5. Penetration loss for Radio Building path RB3B . . A-5

Figure A-6. Penetration loss for Radio Building path RB3C . . A-6

Figure A-7. Penetration loss for Radio Building path RB4C . . A-7

Figure A-8. Penetration loss for Radio Building path RB4D . . A-8

Figure A-9. Penetration loss for Radio Building path RB5A . . A-9

Figure A-10. Penetration loss for Radio Building path RB5B A-10

Figure A-11. Penetration loss for Radio Building path RB6A A-11

FIGURES (Cont'd)

Figure A-12. Penetration loss for Radio Building path RB6B A-12

Figure A-13. Penetration loss for Radio Building path RB7A A-13

Figure A-14. Penetration loss for Radio Building path RB7B A-14

Figure A-15. Penetration loss for Radio Building path RB8A A-15

Figure A-16. Penetration loss for Radio Building path RB8B A-16

Figure A-17. Penetration loss for Radio Building path RB9A A-17

Figure A-18. Penetration loss for Radio Building path RB9B A-18

Figure A-19. Penetration loss for Radio Building path RB10A A-19

Figure A-20. Penetration loss for Radio Building path RB10B A-20

Figure A-21. Penetration loss for Radio Building path RB11A A-21

Figure A-22. Penetration loss for Radio Building path RB11B A-22

Figure A-23. Penetration loss for Radio Building path RB12A A-23

Figure A-24. Penetration loss for Radio Building path RB12B A-24

Figure A-25. Penetration loss for Radio Building path RB13A A-25

Figure A-26. Penetration loss for Radio Building path RB13B A-26

Figure A-27. Penetration loss for Radio Building path RB14A A-27

Figure A-28. Penetration loss for Radio Building path RB14B A-28

FIGURES (Cont'd)

Figure A-29. Penetration loss for Radio Building path RB15A A-29

Figure A-30. Penetration loss for Radio Building path RB15B A-30

Figure A-31. Penetration loss for Radio Building path RB16A A-31

Figure A-32. Penetration loss for Radio Building path RB16B A-32

Figure A-33. Penetration loss for Radio Building path RB17A A-33

Figure A-34. Penetration loss for Radio Building path RB17B A-34

Figure A-35. Penetration loss for Radio Building path RB18A A-35

Figure A-36. Penetration loss for Radio Building path RB18B A-36

Figure A-37. Penetration loss for Radio Building path RB19A A-37

Figure A-38. Penetration loss for Radio Building path RB19B A-38

Figure A-39. Penetration loss for private residence path HL1B A-39

Figure A-40. Penetration loss for private residence path HL1C A-40

Figure A-41. Penetration loss for private residence path HL2A A-41

Figure A-42. Penetration loss for private residence path HL2B A-42

Figure A-43. Penetration loss for storeroom path SRR1A . . A-43

Figure A-44. Penetration loss for storeroom path SRR1B . . A-44

Figure A-45. Penetration loss for storeroom path SRR2A . . A-45

Figure A-46. Penetration loss for storeroom path SRR2B . . A-46

FIGURES (Cont'd)

Figure A-47. Penetration loss for storeroom path SRR3A . . A-47
Figure A-48. Penetration loss for storeroom path SRR3B . . A-48
Figure A-49. Penetration loss for storeroom path SRR4A . . A-49
Figure A-50. Penetration loss for storeroom path SRR4B . . A-50
Figure A-51. Penetration loss for storeroom path SRR5A . . A-51
Figure A-52. Penetration loss for storeroom path SRR5B . . A-52
Figure A-53. Penetration loss for storeroom path SRR6A . . A-53
Figure A-54. Penetration loss for storeroom path SRR6B . . A-54
Figure A-55. Penetration loss for storeroom path SRR7A . . A-55
Figure A-56. Penetration loss for storeroom path SRR7B . . A-56
Figure A-57. Penetration loss for storeroom path SRR8A . . A-57
Figure A-58. Penetration loss for storeroom path SRR8B . . A-58

TABLES

PAGE

Table 1. Mean and Standard Deviation For Radio Building Penetration Loss Path Data 21

Table 2. Mean and Standard Deviation For Private Residence Penetration Loss Path Data 22

Table 3. Mean and Standard Deviation For Storeroom Penetration Loss Path Data 22

Table 4. Mean and Standard Deviation for Building Penetration Loss for a Variety of Combinations of Data Paths 23

BUILDING PENETRATION LOSS MEASUREMENTS AT 900 MHZ, 11.4 GHZ, AND 28.8 GHZ

K. C. Allen, N. DeMinco, J. R. Hoffman, Y. Lo, and P. B. Papazian*

The feasibility of using radio frequencies in the super high frequency (SHF) band (3-30 GHz) for Personal Communications Services (PCS) in buildings depends on the multipath within the structure and the amount of attenuation experienced by the electromagnetic waves passing through the structures. This study measured these effects to obtain a quantitative estimate of the attenuation magnitude. This magnitude can then be used for link margin analysis to determine if personal communications at SHF is practical.

keywords: building attenuation, measurements, PCS, penetration attenuation, personal communications

1. INTRODUCTION

This report describes the results of a measurement program. The objective was to determine if frequencies in the super high frequency (SHF) band (3-30 GHz) can be used for Personal Communications Services (PCS) between the outside and inside of buildings in a manner like that currently used for cellular telephone at 900 MHz. The crowding of the radio frequency spectrum at 900 MHz makes it probable that PCS will be required to operate at the higher frequency bands. PCS is a class of telecommunications services that includes a wide range of capabilities, such as telephony, data transfer, paging, voice mail, and electronic messaging. PCS will provide portability and personalized telephone service to users. Many small cells similar to the cells used in cellular phone systems can be used to provide low-cost communication services through pocket-size, low-power, portable telephones to individuals wherever they may be in the service area.

The Institute for Telecommunication Sciences (ITS) has been active in the development of computer models and measurements to assess system losses in typical PCS operational environments for the proposed frequency bands. Models are being developed for urban outdoor microcells and within-building environments. The building penetration measurements described in this report will provide some insight into the degree of attenuation experienced by PCS signals when penetrating three typical structures.

*The authors are with the Institute for Telecommunication Sciences, National Telecommunications and Information Administration, U.S. Department of Commerce, Boulder, Colorado 80303-3328

The experimental results in this report have been obtained to help determine the excess path loss associated with reception inside buildings and its dependence on location within the building and the building type. The data contained herein will also help to quantify the spatial variation of signal due to severe multipath.

The constructive and destructive interference at SHF frequencies are expected to vary over a much smaller spatial separation than would occur at lower frequencies and hence provide a means of obtaining space diversity reception over a short distance comparable to the size of the personal communicator set. Over a narrow bandwidth, this should minimize signal fading variations due to multipath and provide good communication performance for such a system.

This report describes the results of signal strength measurements made inside three types of buildings at three separate frequencies. The three frequencies used in the measurement were: 900 MHz, 11.4 GHz, and 28.8 GHz. The three types of buildings used for the experiment were: the ITS Wing 4 of the Department of Commerce Radio Building in Boulder, CO, (concrete construction with steel reinforcement), a private residence (wood-frame house with brick veneer), and the storeroom between Wings 3 and 5 of the Radio Building (a building with metal siding).

2. DESCRIPTION OF THE EXPERIMENT

This section describes the instrumentation, calibration, and measurement sites used for the penetration measurements.

2.1 Instrumentation And Calibration

The measurement system included three transmitters mounted on a cart that could be moved inside buildings, and the ITS millimeter-wave van located outside the building for reception of the signals. The van is shown in Figure 1 and the transmitter cart is shown in Figure 2. The transmitter cart consisted of three separate calibrated signal generators connected to three separate antennas. The antennas on the cart were omnidirectional in the azimuthal plane to simulate the radiation coverage typical of the small antenna that would be used for a PCS handheld unit. The receiving antennas on the van consisted of two medium-gain horn antennas with 17 dBi at 11.4 GHz and 16 dBi at 28.8 GHz both with vertical polarization, and a vertically-polarized omnidirectional antenna at 900 MHz. The beamwidths in azimuth and elevation of the 11.4-GHz horn were both 22 degrees, and the beamwidths for the 28.8-GHz horn were both 25 degrees. The horn antennas provided adequate angular coverage for receiving most of the multipath signals radiated from the transmitters inside the buildings under test, but favored the direct path and multipath signals arriving within their beamwidths.

Figure 1. ITS millimeter-wave measurement van (receiver).

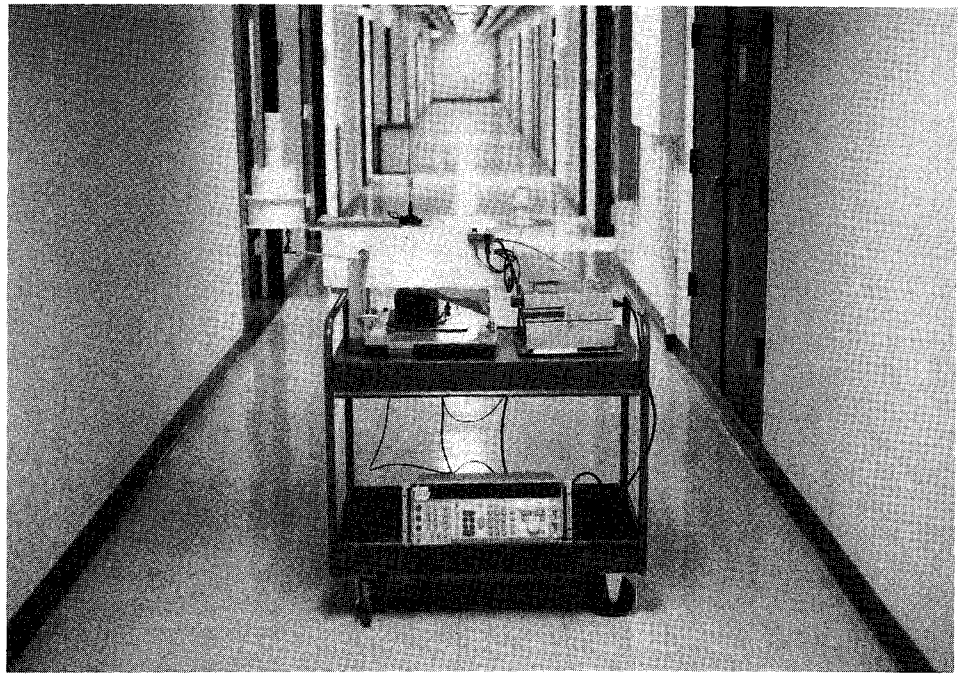

Figure 2. Remote source cart (transmitter).

This was not the case for the omnidirectional antennas. The omnidirectional antenna used at 900 MHz provided near equal response to the direct signal and all multipath signals arriving at the receiver, and therefore the destructive interference phenomenon was more likely to produce signal cancellation with deeper nulls than that attained at the higher frequencies with the horn antennas. The omnidirectional antenna vectorially adds all of the multipath return signals from all directions.

The outputs from the receiver antennas at 11.4 and 28.8 GHz were first converted down in frequency and then passed through separate logarithmic amplifiers. The output of each of the logarithmic amplifiers was a DC voltage proportional to the logarithm of the RF input power. This DC voltage was then sampled using an analog-to-digital (A/D) converter and the samples were stored in data files by a data acquisition program on the computer. The noise figure of the receiver system for the 11.4- and 28.8-GHz measurement was approximately 7 dB.

The output signal from the 900-MHz receiver antenna was applied directly to the spectrum analyzer input. The amplitude of the signal at 900-MHz was measured by the spectrum analyzer and sent to the data logging computer via the IEEE 488 BUS. The spectrum analyzer had a noise figure of approximately 20 dB at 900 MHz.

The system was calibrated to power levels relative to free space for each of the three frequency bands at a distance of 25.6 m over a grass-covered field at the end of Wing 4 of the Radio Building.

The measured free-space signal level at 25.6 m was used to normalize the signal level at each data point during the data processing to determine the actual free-space signal level at each distance. The free-space signal level was determined by averaging the signal received over a 2-min data collection interval at the 25.6-m receiver-to-transmitter distance. This free-space signal level was corrected for the actual distance and then subtracted from the measured signal level at each data point to determine the penetration loss for a signal propagating between the interior and the exterior of the building.

The received signal for all configurations consists of a direct wave and at least one wave reflected from the ground or some other obstruction. The vector addition of the direct and single or multiple reflected waves results in both constructive and destructive interference as a function of receiver-to-transmitter distance, antenna heights, and the radio frequency. The geometry for all sets of data provided a measurement of the excess attenuation experienced by the electromagnetic waves passing through the building structures for any situation that would be encountered for personal communications.

The signals at all three frequencies were sampled at sufficent intervals (1 sample/s) to characterize the data even though they were not sampled every half wavelength at the two upper frequencies (11.4 and 28.8 GHz). The linear distance between nulls and peaks for the sampled waveform created by constructive and destructive interference does not repeat every half wavelength. It is a function of the signal frequency, distance between the transmitter and receiver, transmitter antenna height, and receiver antenna height. If the receiver or transmitter moves horizontally, as was the case in the measurements performed here, the distance between two consecutive minima or maxima is given by

$$D = LR^2/2H_1H_2,$$

where D is the distance between two successive minima or maxima in meters, L is the wavelength in meters, R is the distance between the receiver and the transmitter in meters, H_1 is the transmitter antenna height in meters, and H_2 is the receiver antenna height in meters.

This distance was calculated for each of the three frequencies using the parameters that would result in the smallest distance between minima or maxima. The shortest distance R used during the measurements was 15 m. The transmitter height H_1 was 1 m. The receiver height H_2 was 3 m. The resulting distances D between minima or maxima for 900 MHz, 11.4 GHz, and 28.8 GHz were 12.50, 0.99, and 0.40 m, respectively. Referring to any of the Figures in the Appendix (A-1 through A-58), the data were sampled at least every 0.2 m, so there are at least two samples for each periodic variation of the signal as the transmitter cart was moved along all of the measurement paths. The formula above is for the periodicity of the minima and maxima variation for only the direct and reflected waves. Waves from higher order multipath signals would tend to fill in these nulls, so the case considered here is the worst-case multipath condition. The sampling of the data is therefore adequate to describe the signal fluctuation and hence compute the building attenuation.

2.2 Measurement Sites

Radio Building:

The Department of Commerce Radio Building in Boulder, CO is a concrete structure with steel reinforcement throughout. Wing 4 of the Radio Building is shown in Figure 3, with the ITS measurement van located at the end for the first sequence of measurements. There is a large amount of metal within the building for electrical conduit and structural support. The external walls of the building are concrete with re-bar reinforcement. The interior walls are mostly of cinder block with additional partitions with wood studs and gypsum dry wall. The metal-frame windows in each of the

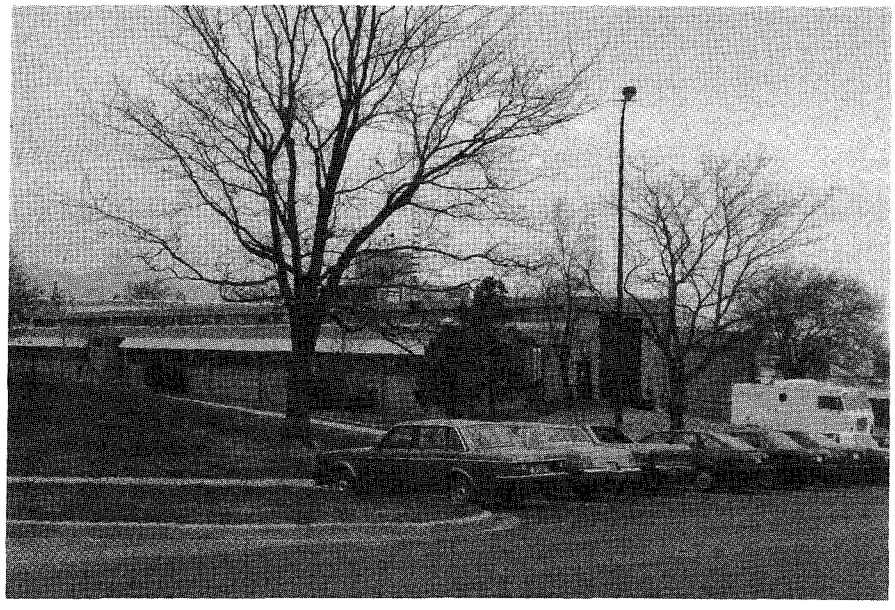

Figure 3. Wing 4 of the Radio Building with ITS millimeter-wave measurement van.

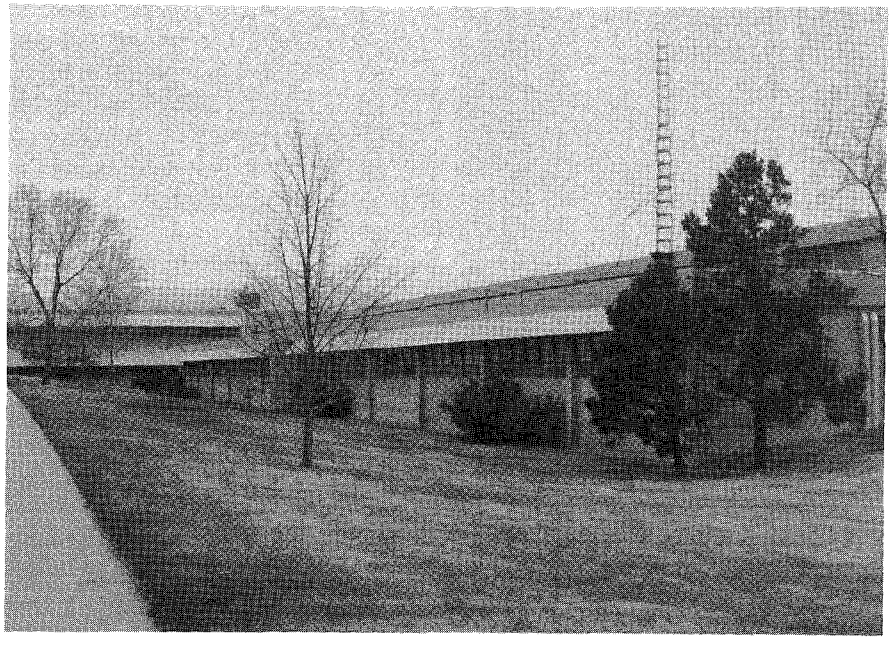

Figure 4. West side of Wing 4 of the Radio Building.

offices cover approximately 6 m^2. Figure 4 is a view of the west side of Wing 4 showing these windows. All offices in Wing 4 have these windows, and as a result the building may be relatively transparent to the electromagnetic energy from the signal sources when the van was positioned on the side of the building. The office doors are of wood construction with approximately 2.3 m^2 of area. The rooms are filled with conventional metal office furniture including desks, file cabinets, tables, and chairs.

Private Residence:

The building shown in Figure 5 is a standard wood-frame house with brick veneer on the outside. The gypsum wallboard did not have a metallic foil on one side. The insulation has a paper vapor barrier. The furniture inside this structure is predominantly of wood and non-metallic construction typical of a private residence. The shrubbery and trees outside did not obstruct the line-of-sight between the transmitter and receiver. Window area on the street side of the house was approximately 4 m^2 per room. There were two major paths traversed during the measurement. One interior wall separated the two paths. The rear path had the exterior wall plus an interior wall between the receiver and transmitter. The front path had just one exterior wall between the receiver and the transmitter.

Storeroom Building With Metal Siding:

The building shown in Figure 6 is a metal frame structure with metal siding. There are a few windows, with approximately 1 m^2 of area each. The storeroom loading dock door and all entrance doors are made of steel. The storeroom has metal shelves along the width of the building with wide aisles between them. This structure is expected to present a large attenuation to the electromagnetic waves passing through it.

3. MEASUREMENT PROCEDURE

This section describes the measurement procedure used for each of the three sites.

3.1 Radio Building

For the first set of Radio Building measurements, the signal was radiated from the cart antennas inside the building and received by the van antennas located 17.1 m from the loading dock end of Wing 4, in the driveway. Figure 7 contains a floor plan of Wing 4 of the Radio Building with the paths traversed during the measurements indicated by arrows.

Figure 5. Private residence.

Figure 6. Storeroom with metal siding.

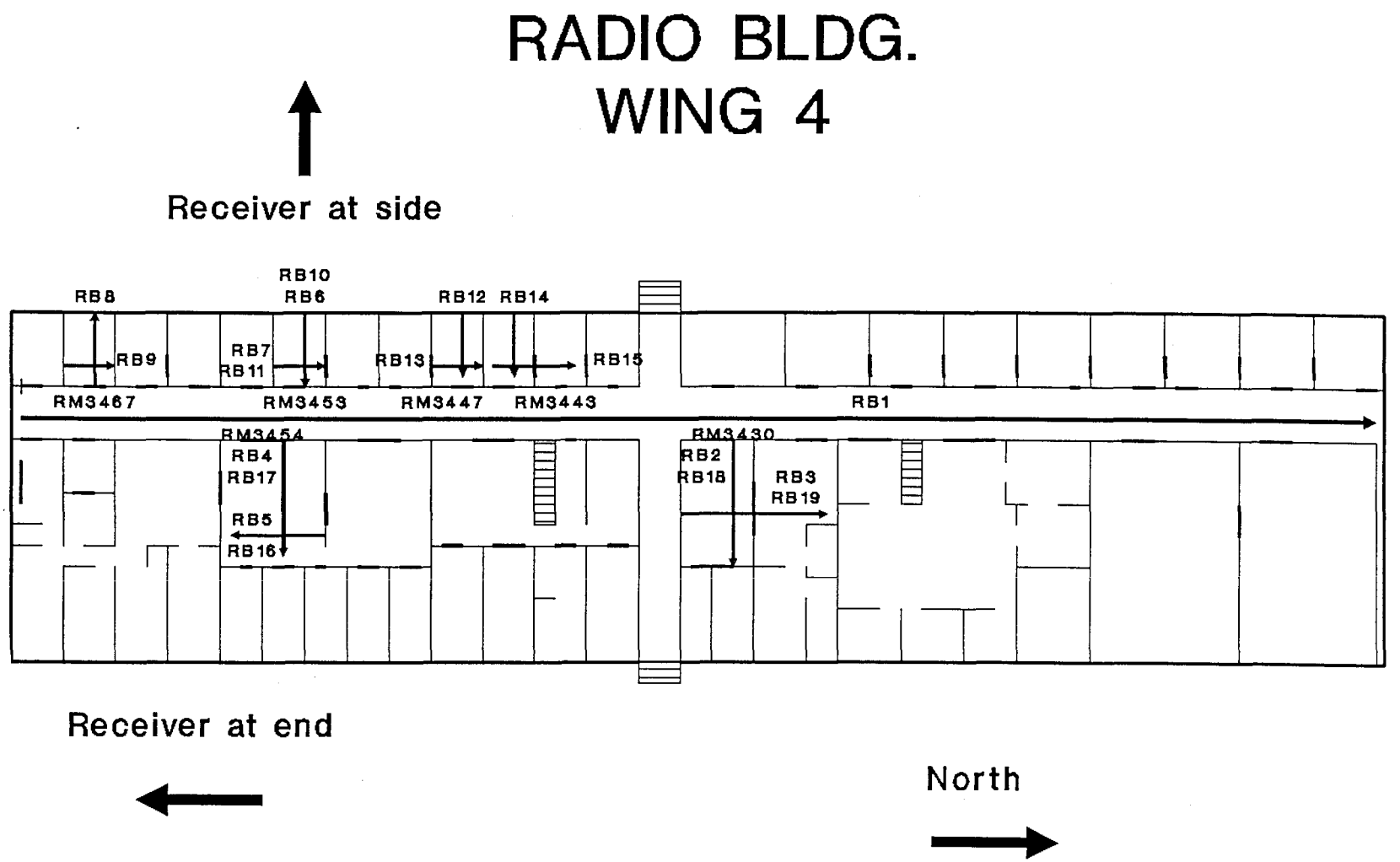

Figure 7. Floor plan of Wing 4 of the Radio Building with measurement paths of the transmitters.

The points of the arrows indicate the endpoints of each of the paths traversed during the measurements and the arrows indicate the direction of the path. The cart was moved down the main hallway and into offices and labs on both sides of the hallway along paths with measured distances. The receiving van was stationary during all of these measurements.

For the second set of Radio Building measurements, the signal was radiated from the cart antennas inside the building and received at the van antennas located outside the West side of the building on the sidewalk between Wing 4 and Wing 6 of the Radio Building. Figure 7 also contains the measurement paths for the new position of the van at the West side of the Radio Building. The van and the cart were located opposite each other along the length of the building wing. For a portion of the measurements, the cart was moved into some of the offices and labs on both sides of the hallway. The position of the van along the length of either wing was such that it was directly opposite of the cart. This alignment was easily performed by viewing the van through the windows of the closest office.

3.2 Private Residence

For this building, the van was located in the street appproximately 19.5 m from the closest outside wall. The cart was moved through several rooms along a straight line parallel to the street and data were recorded with the van stationary. The distance to the cart from the van was also determined for each data measurement group. The floor plan of the house was convenient for making two such runs and covering most of the length of the house. Figure 8 contains the floor plan with paths traversed during the measurements indicated by arrows. The arrows indicate the direction of the paths traversed during the measurements. The first path passed through the kitchen area and family room in the rear half of the house. The second path passed through the front half of the house through the dining room and living room.

3.3 Storeroom With Metal Siding

For this building structure, the van was located in the parking lot of the Department of Commerce Radio Building between Wings 3 and 5, adjacent to the storeroom and approximately 17.1 m from the door. Figure 9 contains the floor plan of the storeroom with the measurement paths indicated by arrows. The points of the arrows indicate the endpoints of the paths traversed. The source cart was moved up and down all of the aisles inside the storeroom to provide a matrix of data with the variation of electromagnetic energy at three frequencies in two coordinates.

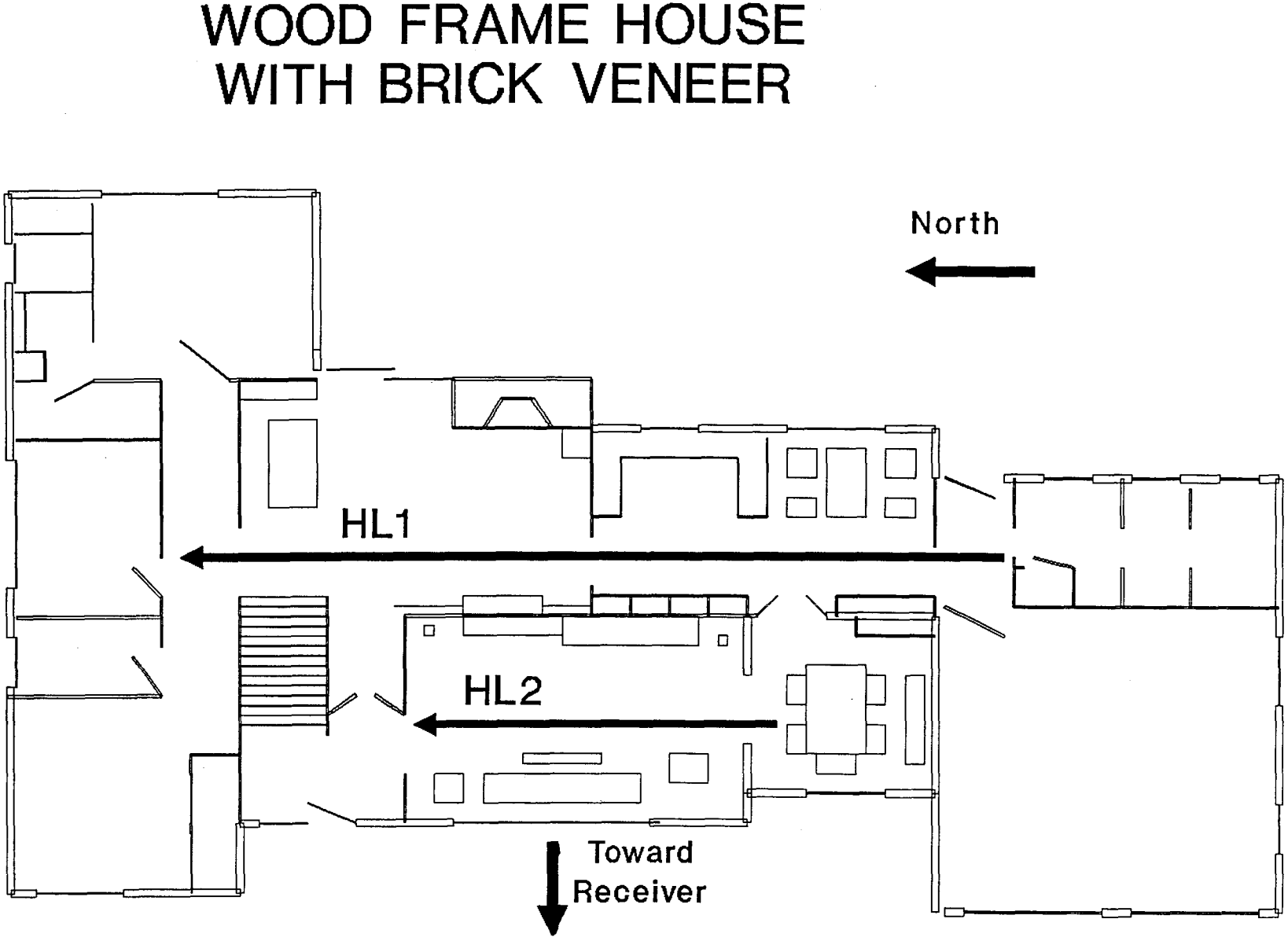

Figure 8. Floor plan of single level wood-frame house.

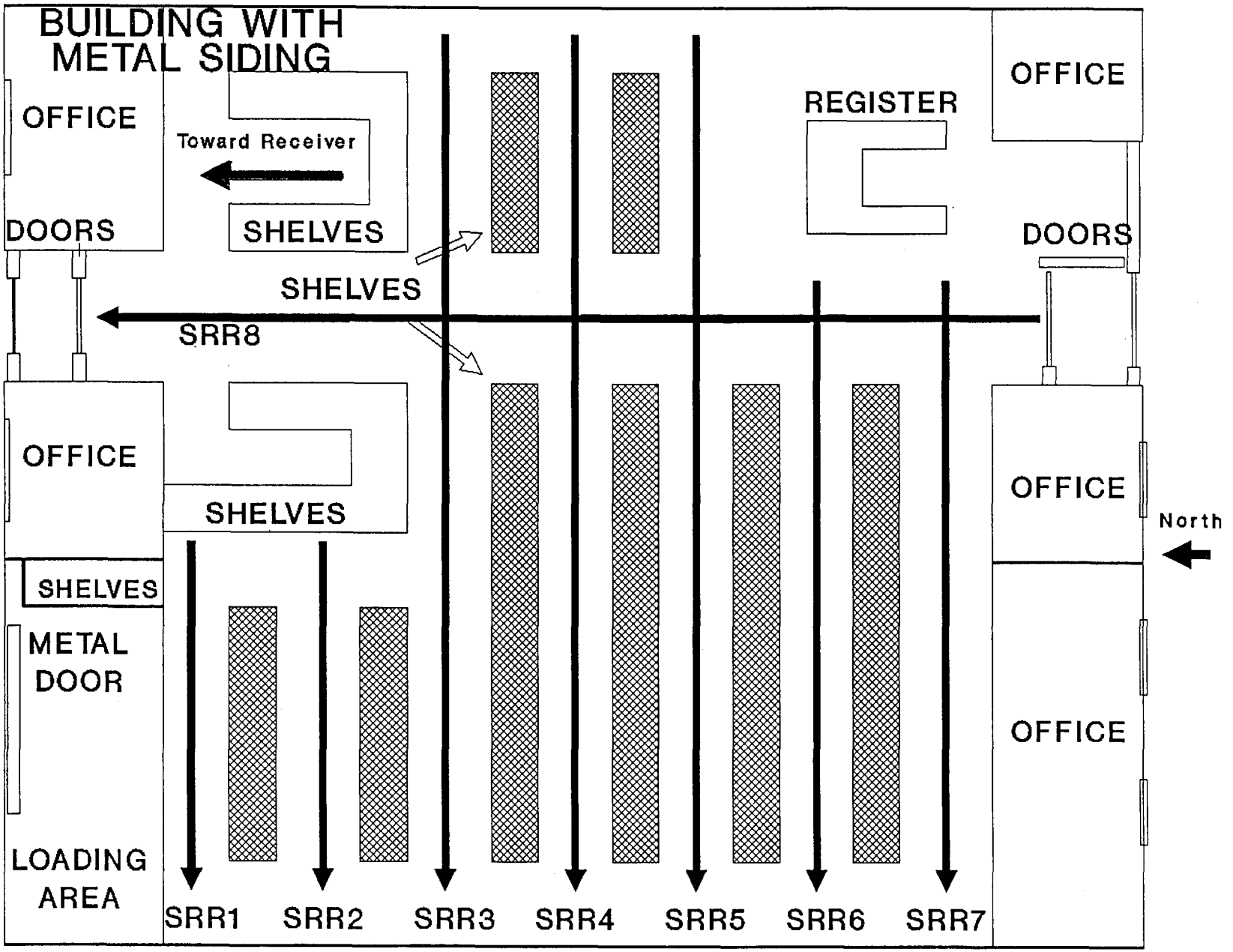

Figure 9. Floor plan of storeroom with metal siding.

4. DATA COLLECTION AND PROCESSING

This section describes the data collection and processing of the data taken for the penetration measurements.

4.1 Data Collection

The data collection for all sites consisted of recording received signal level at each frequency at a rate of one sample per second for the period of time it took the cart to traverse the desired path length for each particular room or hallway. The cart was moving at a speed of approximately 0.5 m/s. All receivers and transmitters at the three frequencies were operating simultaneously. The antennas were oriented in a line and the cart was positioned so that all antennas had a clear field of view of the van in a manner such that none of the antennas were blocking each other. For the Radio Building Stockroom, the signal level was recorded as the cart was moved along two paths within the room. One was parallel to the line-of-sight path between the van and the cart and the other was perpendicular to this line-of-sight path. For the private residence (the wood-frame house), the cart moved along only one path perpendicular to the line-of-site between the van and the cart for the measurement. Measurements of all cart/van distances at each sample site were obtained so that the distance to the van could be determined and the free-space signal level could be calculated at that particular distance. This free-space signal level was then subtracted from the measured data to determine the building penetration loss.

The data were stored in separate files for each of the paths in each room. For example, there were a number of files recorded for each of two orthogonal paths within an office. The data were recorded in separate files for each of three frequencies. A start and stop time was also part of the data. A description of what the data are and how the data were taken is also correlated with the file name. The files can be treated separately or combined in any number of meaningful combinations. This could include: hallway data only, office data only, data taken moving through all the stations along the length of the hallway, or the total of all data taken in a particular building type. The files are listed separately and can be combined to look at effects covering certain situations. During analysis, the data can be separated by functional experiment or combined together.

4.2 Data Processing

The data taken during the collection path runs for any of the building structures were processed to remove the free-space loss from the measurements. This was done by putting coordinates on the layout of each structure to locate all positions on the path in an

x-y coordinate system with reference to the van location. The radial distance from the van could then be determined for each particular data point from the geometry. The free-space signal level for each particular data point is then corrected for free-space loss by using the measured free-space calibration signal level at a reference distance and adding the value necessary to correct to the radial distance between the van and the particular data point. This value in decibels is 20*log(R/Ro), where Ro is the reference distance at which the free-space calibration was taken, and R is the actual radial distance of the particular data point under consideration. The measured signal level at the particular data point is then subtracted from the free-space signal level to obtain the attenuation through the structure.

Figures 10, 11, and 12 are examples of this process for each of the three frequencies: 900 MHz, 11.4 GHz, and 28.8 GHz. Each figure demonstrates what has been done to the data files. The raw data, free-space correction factor, and final penetration attenuation are shown in each figure. The position on the horizontal axis is the distance in meters traversed along the path.

The penetration attenuation for all paths in the three building structures at the three frequencies was then plotted for analytical purposes. The data were also examined statistically. This is discussed in the next section.

5. DISCUSSION OF RESULTS

The attenuation versus distance traversed for all three frequencies was also plotted for each of the path runs made in all three building structures. Figures 13, 14, and 15 show selected runs for this penetration loss comparison. Figure 13 is a typical run for one of the paths taken in the Radio Building. Figure 14 is a typical run for one of the paths taken in the storeroom building with metal siding. Figure 15 is a typical run for the private residence (single-level wood-frame house with brick veneer). The complete set of attenuation plots for all paths is contained in the Appendix A. The paths in Figures 10 through 15, as well as those figures in Appendix A, are keyed by an alphanumeric code corresponding to those given in the floor-plan Figures 7, 8, and 9 to identify the runs. These plots provide a direct comparison of the penetration attenuation for the three frequencies in each of the three building structures.

Statistical analyses of the separate paths, as well as combinations of these paths, were performed to better characterize the data. The mean and standard deviation of the mean are summarized in Table 1 for the Radio Building, Table 2 for the private residence, and Table 3 for the storeroom. Table 4 contains the results for selected combinations of paths for each of the three building structures. The codes for the paths listed in the first column of

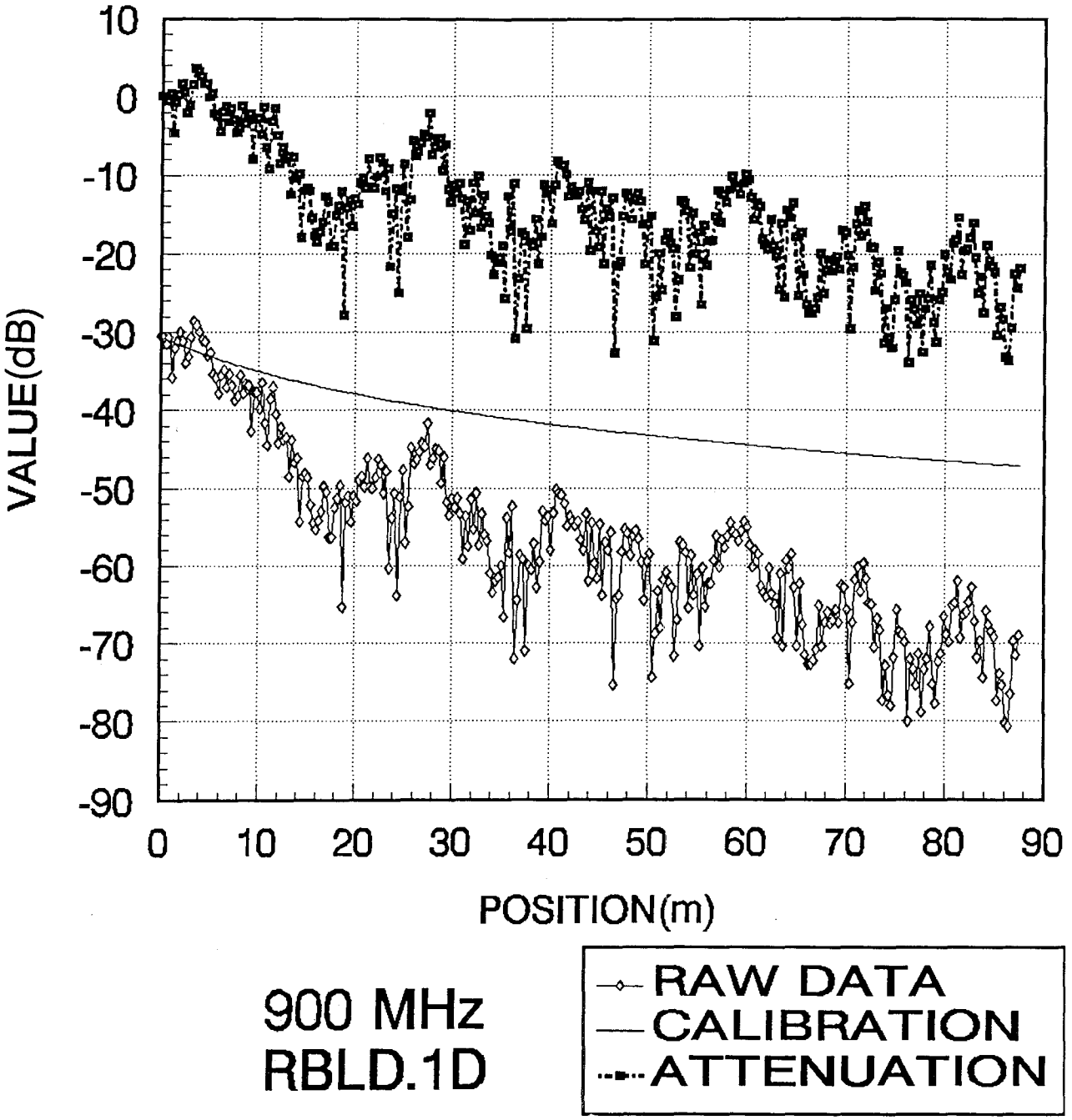

Figure 10. Raw data, free-space correction factor, and penetration attenuation versus distance for a typical 900-MHz measurement in the Radio Building.

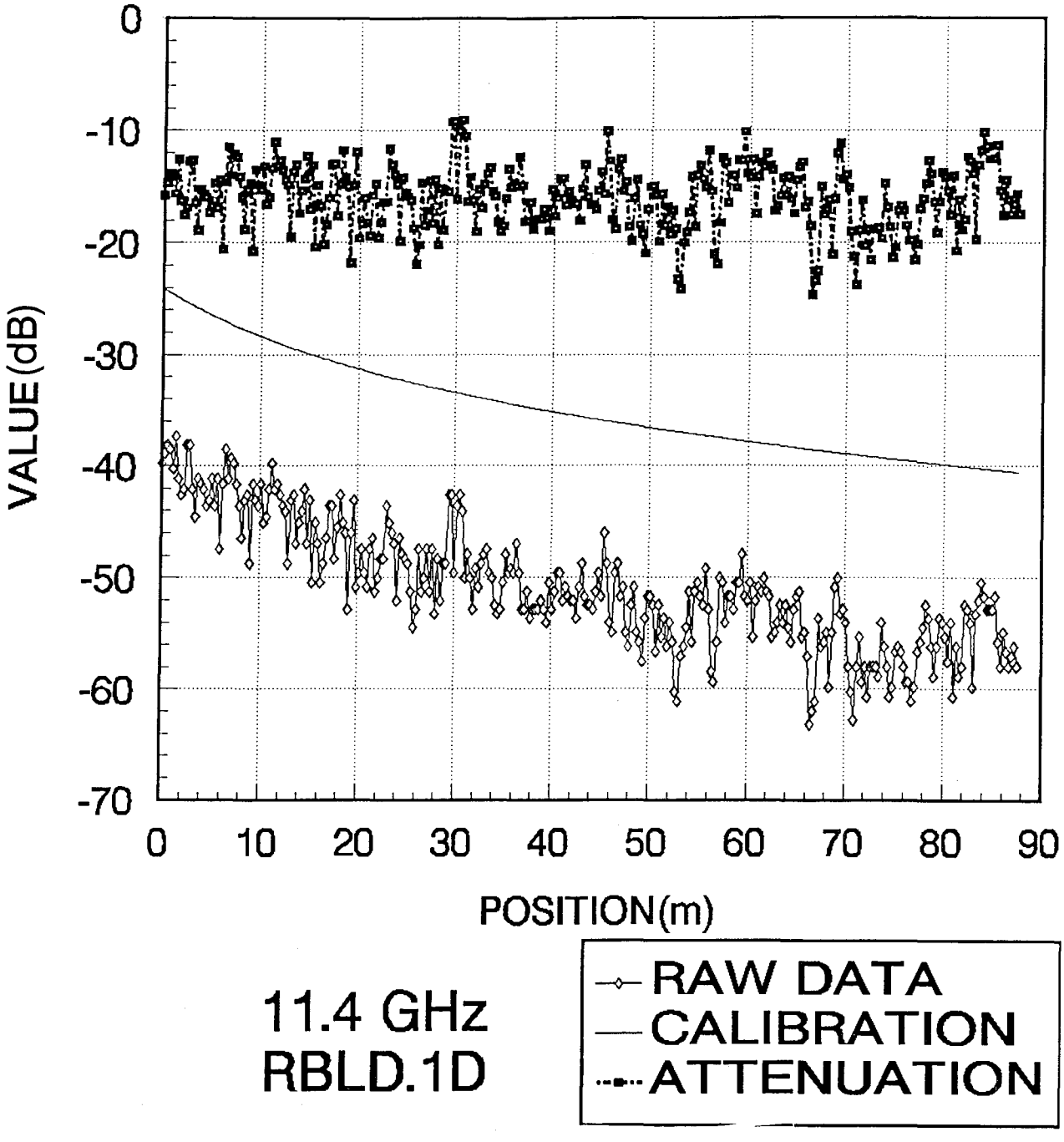

Figure 11. Raw data, free-space correction factor, and penetration attenuation versus distance for a typical 11.4-GHz measurement in the Radio Building.

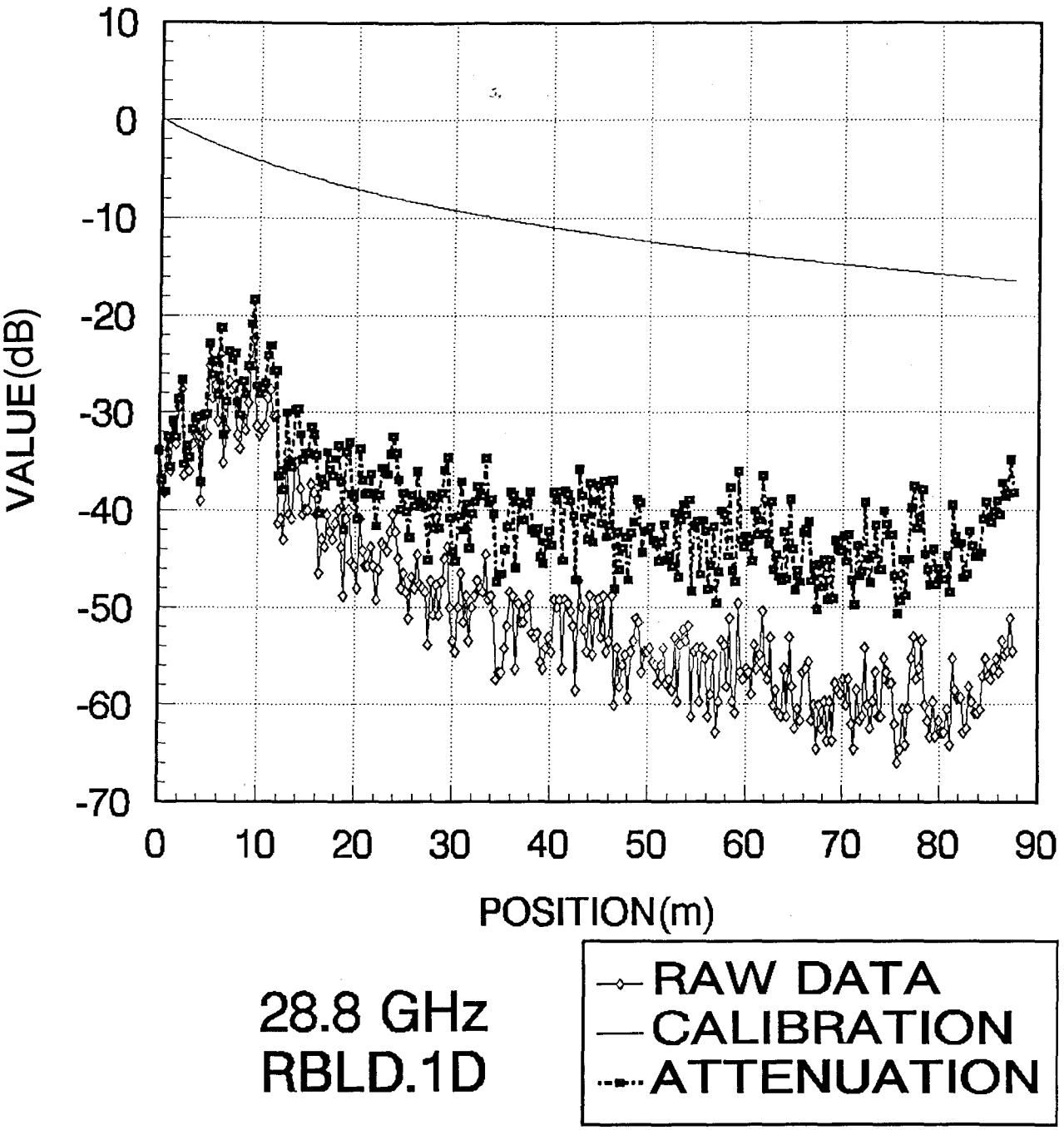

Figure 12. Raw data, free-space corection factor, and penetration attenuation versus distance for a typical 28.4 GHz measurement in the Radio Building.

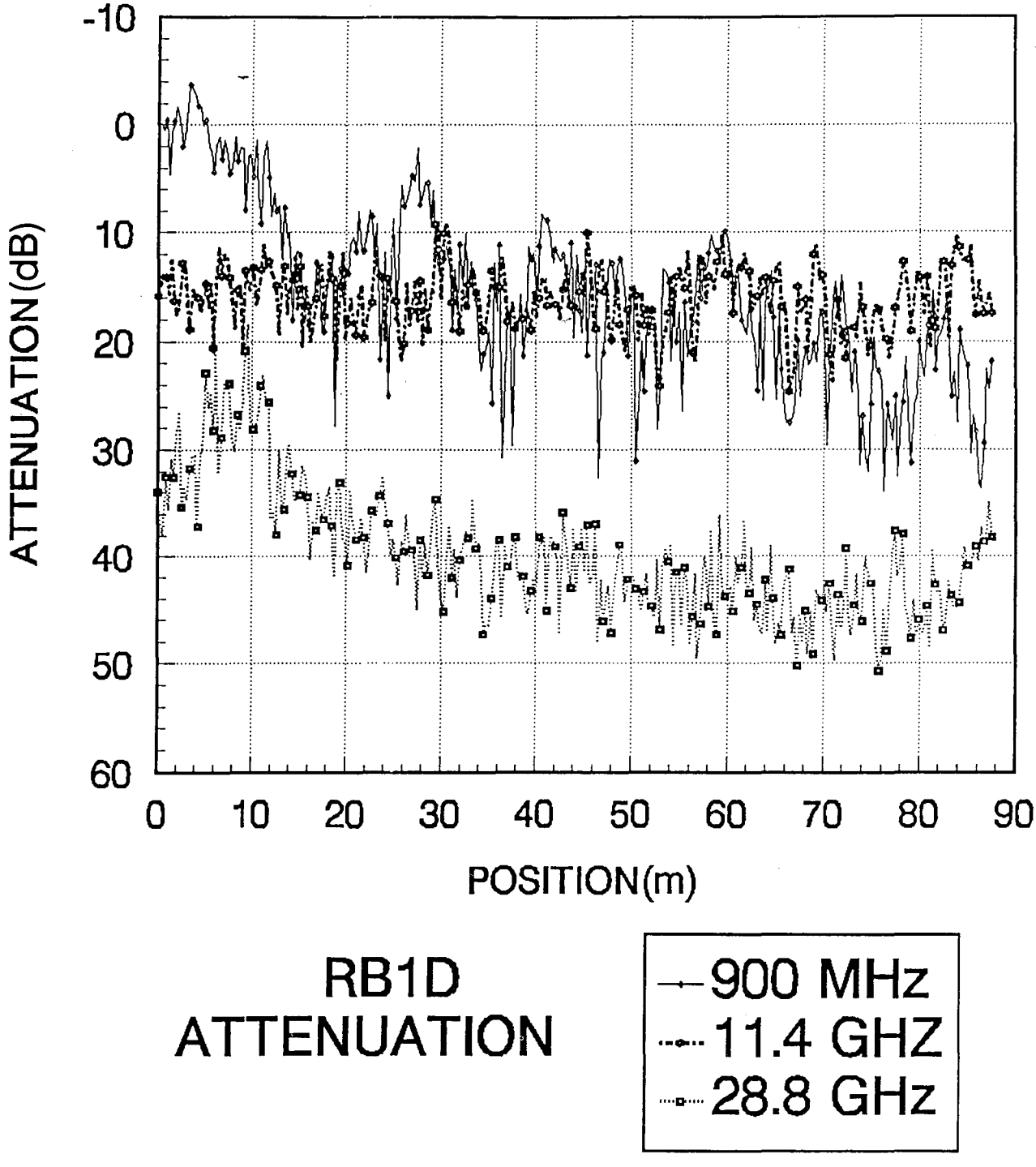

Figure 13. Penetration loss versus distance at three frequencies for a typical run in the Radio Building.

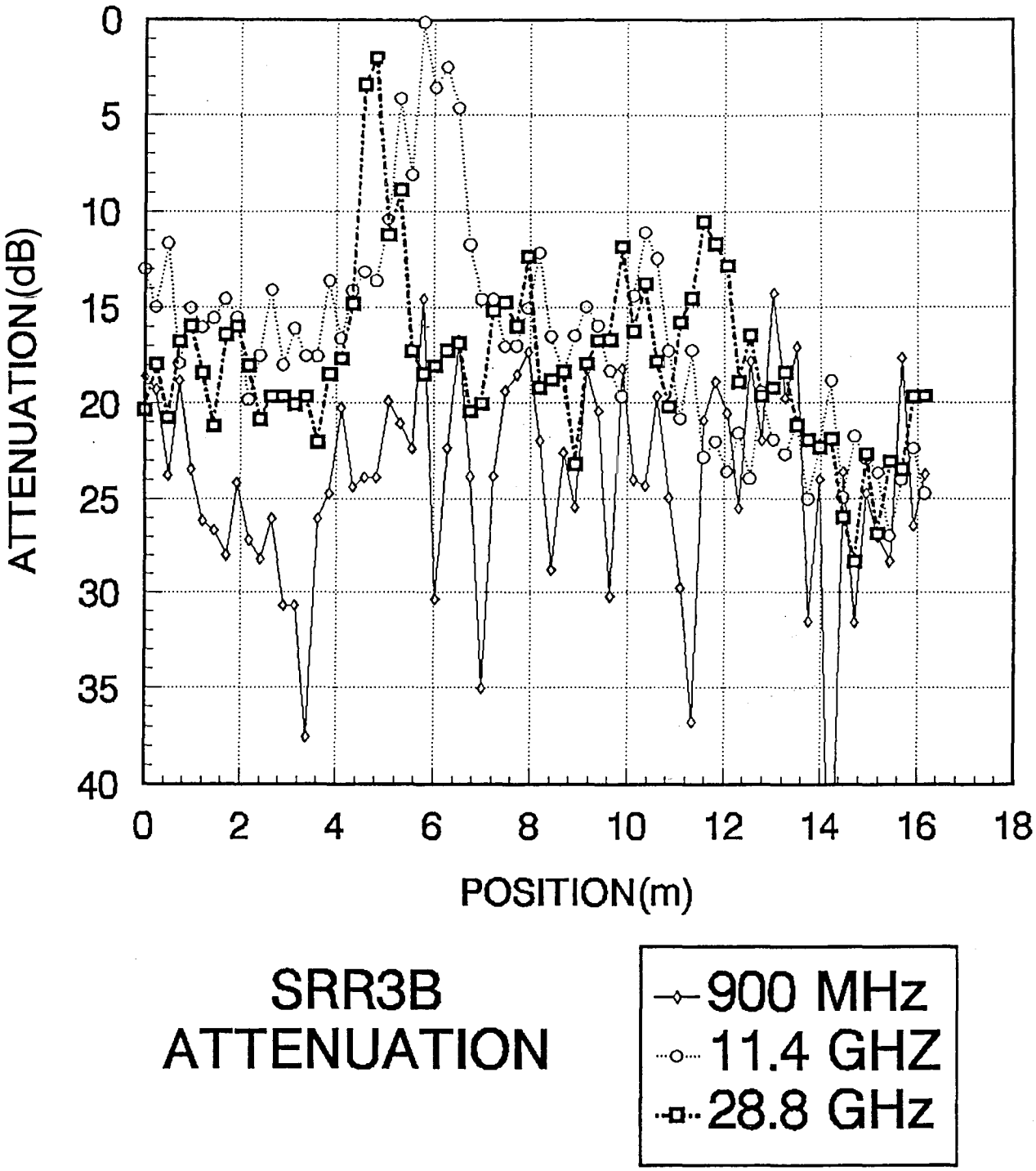

Figure 14. Penetration loss versus distance at three frequencies for a typical run in the storeroom building with metal siding.

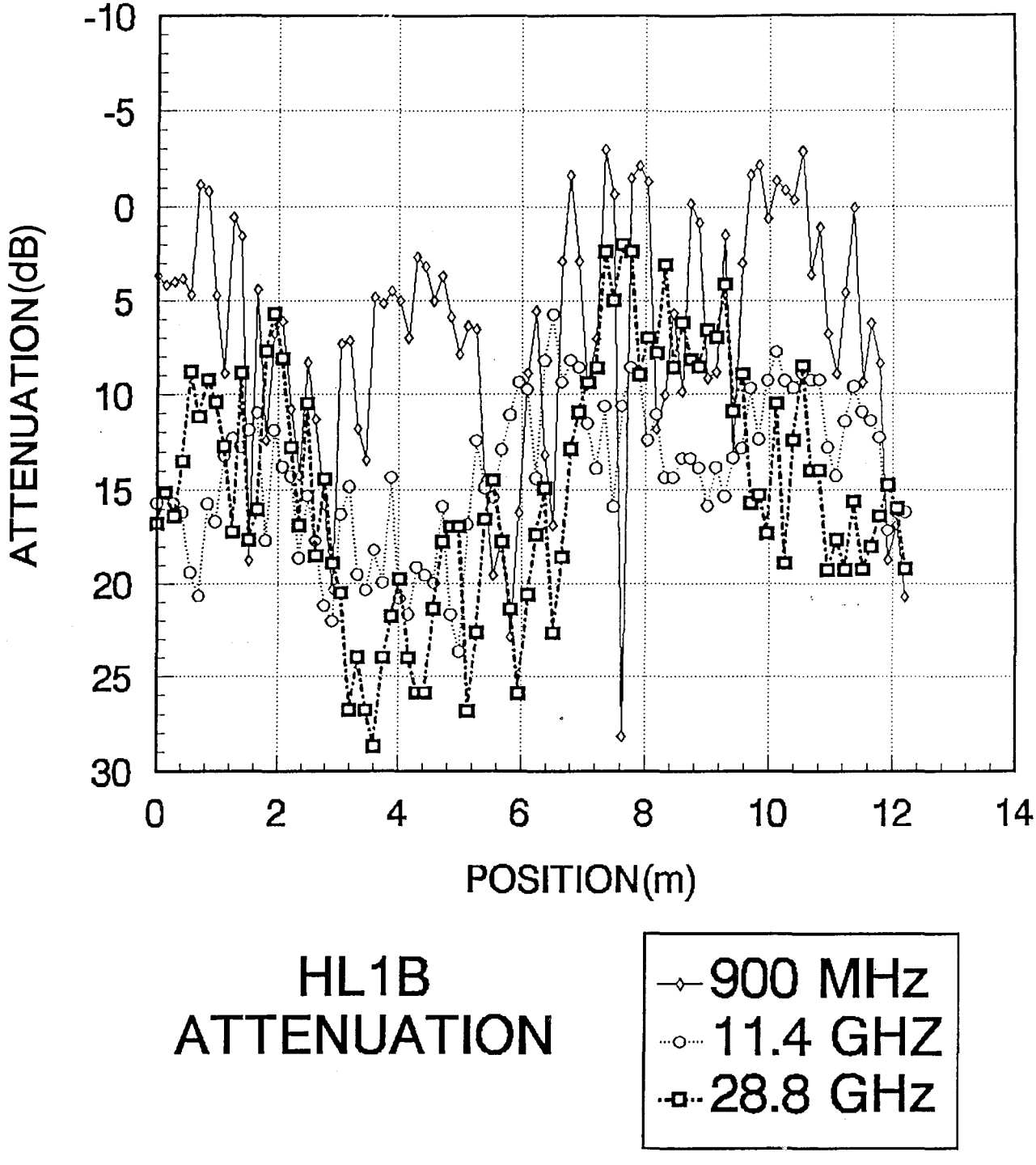

Figure 15. Penetration loss versus distance at three frequencies for a typical run in the private residence.

Table 1. Mean and Standard Deviation of attenuation (dB) for Radio Building Penetration Loss Path Data

	900 MHz		11.4 GHz		28.8 GHz		
path	mean	stdev	mean	stdev	mean	stdev	comments
RB1D	15.3	8.2	16.0	2.8	39.6	6.2	main hall,van at end
RB1E	15.9	7.7	17.2	3.0	39.5	5.6	main hall,van at end
RB2B	29.2	5.3	33.9	4.0	52.5	1.5	Rm3430lab,van at end
RB2C	29.0	5.3	34.1	3.8	53.0	1.5	Rm3430lab,van at end
RB3B	28.0	4.6	35.6	2.7	53.5	1.3	Rm3430lab,van at end
RB3C	28.4	4.4	35.1	2.9	53.4	1.4	Rm3430lab,van at end
RB4C	29.4	5.5	31.1	3.4	53.8	3.5	Rm3454lab,van at end
RB4D	29.7	5.9	32.2	3.6	52.6	3.9	Rm3454lab,van at end
RB5A	27.9	5.4	37.6	1.9	54.6	2.2	Rm3454lab,van at end
RB5B	28.3	3.5	37.6	2.3	53.3	2.7	Rm3454lab,van at end
RB6A	20.0	3.9	32.1	1.6	42.7	2.5	Rm3453ofc,van at end
RB6B	19.6	5.0	30.7	2.3	41.9	4.1	Rm3453ofc,van at end
RB7A	20.9	5.7	31.3	1.2	42.1	3.5	Rm3453ofc,van at end
RB7B	21.2	5.0	31.6	1.8	41.5	2.4	Rm3453ofc,van at end
RB8A	9.4	6.1	5.9	2.3	4.1	0.8	Rm3467ofc,van on sdw
RB8B	8.7	6.6	5.7	2.5	3.9	0.8	Rm3467ofc,van on sdw
RB9A	11.1	6.2	3.8	2.3	3.3	1.2	Rm3467ofc,van on sdw
RB9B	10.0	5.9	3.1	1.3	3.2	1.1	Rm3467ofc,van on sdw
RB10A	5.5	4.5	3.8	2.0	6.0	2.3	Rm3453ofc,van on sdw
RB10B	8.1	7.3	2.9	1.5	4.9	1.5	Rm3453ofc,van on sdw
RB11A	11.2	5.6	2.9	1.9	4.3	1.1	Rm3453ofc,van on sdw
RB11B	9.3	6.2	2.3	1.8	4.2	1.0	Rm3453ofc,van on sdw
RB12A	9.9	5.8	4.6	2.4	6.6	2.6	Rm3447ofc,van on sdw
RB12B	9.6	6.5	4.7	3.6	6.5	2.8	Rm3447ofc,van on sdw
RB13A	11.3	5.3	4.3	2.1	5.0	1.4	Rm3447ofc,van on sdw
RB13B	7.8	6.1	3.5	2.0	4.7	1.3	Rm3447ofc,van on sdw
RB14A	7.3	5.0	3.0	1.9	6.4	2.0	Rm3443ofc,van on sdw
RB14B	8.4	4.5	3.1	2.0	6.2	1.3	Rm3443ofc,van on sdw
RB15A	11.3	5.6	5.2	2.9	8.8	3.8	Rm3443ofc,van on sdw
RB15B	11.0	6.4	5.2	3.3	7.4	3.5	Rm3443ofc,van on sdw
RB16A	17.7	4.9	18.9	3.6	26.8	4.0	Rm3454lab,van on sdw
RB16B	17.4	5.2	17.4	2.8	26.1	3.2	Rm3454lab,van on sdw
RB17A	20.4	6.5	16.2	2.5	21.9	3.1	Rm3454lab,van on sdw
RB17B	19.2	4.8	16.3	2.5	21.3	3.4	Rm3454lab,van on sdw
RB18A	21.3	7.5	31.3	3.0	43.3	4.1	Rm3430lab,van on sdw
RB18B	21.1	6.6	30.7	2.2	43.1	3.2	Rm3430lab,van on sdw
RB19A	16.3	5.0	29.8	1.9	41.7	2.9	Rm3430lab,van on sdw
RB19B	15.4	4.9	30.5	2.4	41.8	2.1	Rm3430lab,van on sdw

Table 2. Mean and Standard Deviation of attenuation for Private Residence Penetration Loss Path Data

	900 MHz		11.4 GHz		28.8 GHz		
path	mean	stdev	mean	stdev	mean	stdev	comments
HL1B	6.9	6.6	14.1	3.9	14.8	6.4	rear path,two walls
HL1C	6.3	6.5	13.3	4.0	14.1	6.6	rear path,two walls
HL2A	2.7	4.6	9.7	2.9	8.6	4.8	front path,one wall
HL2B	3.6	6.1	9.8	3.9	8.6	4.4	front path,one wall

Table 3. Mean and Standard Deviation of attenuation for Storeroom Penetration Loss Path Data

	900 MHz		11.4 GHz		28.8 GHz		
path	mean	stdev	mean	stdev	mean	stdev	comments
SRR1A	17.6	5.6	17.1	3.6	16.1	6.4	side aisle path
SRR1B	17.3	5.1	17.1	3.1	17.6	6.4	side aisle path
SRR2A	21.3	5.4	20.5	3.6	17.5	4.2	side aisle path
SRR2B	21.6	6.0	20.8	3.5	17.6	4.8	side aisle path
SRR3A	23.7	5.6	16.5	5.7	16.9	4.6	side aisle path
SRR3B	24.3	5.9	16.6	5.6	17.8	4.5	side aisle path
SRR4A	25.1	5.3	17.0	5.4	18.4	4.2	side aisle path
SRR4B	24.8	5.0	16.4	5.5	17.7	4.8	side aisle path
SRR5A	27.7	5.7	17.7	5.2	19.5	4.4	side aisle path
SRR5B	26.6	4.4	17.1	5.3	19.5	4.4	side aisle path
SRR6A	26.1	6.6	17.4	6.7	20.1	2.9	side aisle path
SRR6B	27.4	5.8	17.5	5.9	20.1	3.1	side aisle path
SRR7A	24.9	5.6	17.2	5.5	18.7	3.6	side aisle path
SRR7B	25.8	6.5	16.5	6.2	18.6	3.3	side aisle path
SRR8A	21.7	6.1	4.3	2.7	13.2	2.7	main aisle path
SRR8B	22.5	6.7	4.3	2.7	13.0	4.4	main aisle path

Table 4. Mean and Standard Deviation of attenuation for Building Penetration Loss for a Variety of Combinations of Data Paths

	900 MHz		11.4 GHz		28.8 GHz		File
	mean	stdev	mean	stdev	mean	stdev	
All Data In Radio Building Combined	17.7	9.3	19.8	11.5	34.1	17.4	ALLRB
All Data In Radio Building With Only One Wall Between XMTR And RCVR	9.4	6.1	4.1	2.6	5.6	2.7	RBOFF2
All Data In Radio Building With 2 Or 3 Walls Between XMTR And RCVR	18.9	6.4	26.0	7.0	36.2	9.5	RBLAB2
All Data In Radio Building With More Than 3 Walls Between XMTR And RCVR	28.8	5.1	34.4	3.8	53.3	2.4	RBLAB1
All Data In Private Residence Combined	5.4	6.4	12.3	4.3	12.4	6.6	ALLHL
All Data In Private Residence With One Wall Between XMTR And RCVR	3.2	5.4	9.7	3.5	8.6	4.6	HLFRNT
All Data In Private Residence With Two Walls Between XMTR And RCVR	6.6	6.6	13.7	4.0	14.5	6.6	HLREAR
All Data In Stockroom Combined	24.3	6.3	15.0	7.1	17.5	4.8	ALLSRR

each of these tables are also used to identify the paths in Figures 7, 8, and 9. Two runs are shown for each path. The letter suffix on the end of the path name separately identifies each of these path runs.

Cumulative distribution functions of certain files or combinations of files representing certain communications scenarios were performed to look at the statistics of the particular situation.

An example of one practical situation would be an evaluation of communications capability from anywhere in an office building (Radio Building) for a fixed external base station (represented by the van). This would require combining all of the separate files taken in that building. Figure 16 is a cumulative distribution function for all the data in the Radio Building. Analyzing all data files would allow determination of the link margin necessary for designing Personal Communication Systems using these higher frequencies. Figure 16 shows the cumulative distribution function for all of the Radio Building data at the three frequencies. This figure indicates that less than 0.1 % of the data points will have penetration attenuation of more than 47 dB at 900 MHz, 41 dB at 11.4 GHz, and 58 dB at 28.8 GHz.

Figure 16 is a composite of a large amount of data repesenting many diverse conditions. Some measurement points on certain data paths had one wall present between the transmitter and the receiver, but other data contains paths with more than three walls between the transmitter and the receiver. Figure 17 contains data paths where only one wall separates the transmitter and receiver in the Radio Building. This wall had a lot of window area. The mean attenuation is much smaller (less than 10 dB). The attenuation was more than 28 dB at 900 MHz, 13 dB at 11.4 GHz, and 16 dB at 28.8 GHz less than 0.1 % of the time. Figure 18 contains data paths with two or three walls between the transmitter and the receiver. The mean attenuation can be as great as 39 dB. Figure 19 contains path data where more than three walls are involved and the mean attenuation can be as high as 53 dB.

Table 4 contains the mean attenuation and its standard deviation for all of these cases. All of these separate cases for the Radio Building indicate an increasing penetration attenuation at all frequencies as the number of wall penetrations increases in the building structure. This behavior was noted in the data taken for the private residence (wood-frame structure with brick veneer). Figure 20 is the cumulative distribution function of the combined data for all of the paths in the private residence. Figure 21 is the cumulative distribution function for the condition of one wall separation between the transmitter and receiver (front hallway traverse). Figure 22 is for the case of two wall separations (rear hallway traverse). Figure 23 is for the case of one wall separation in the storeroom. Data was not collected for the case of more than one wall separation for the storeroom.

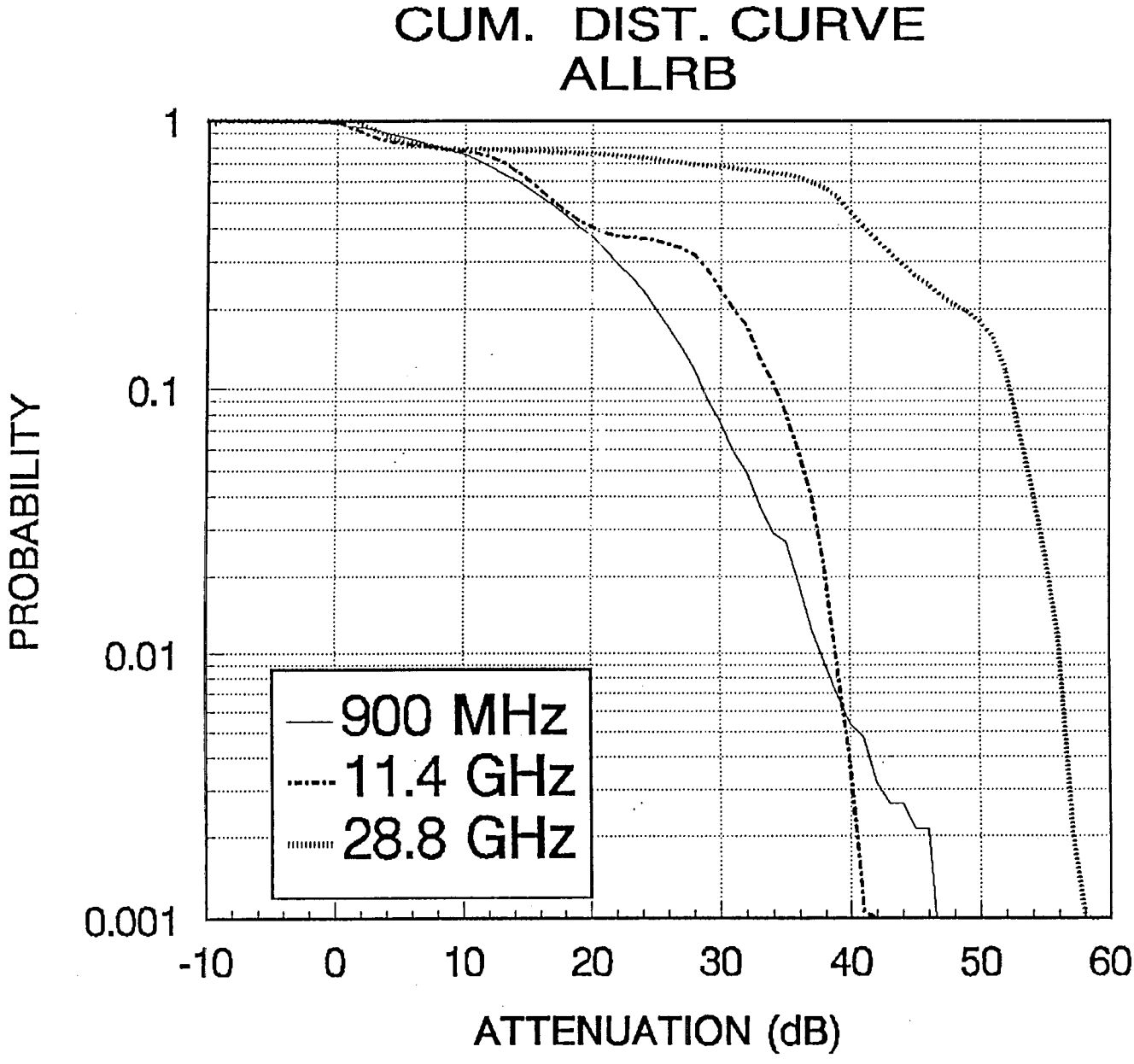

Figure 16. Cumulative distribution for all data in the Radio Building.

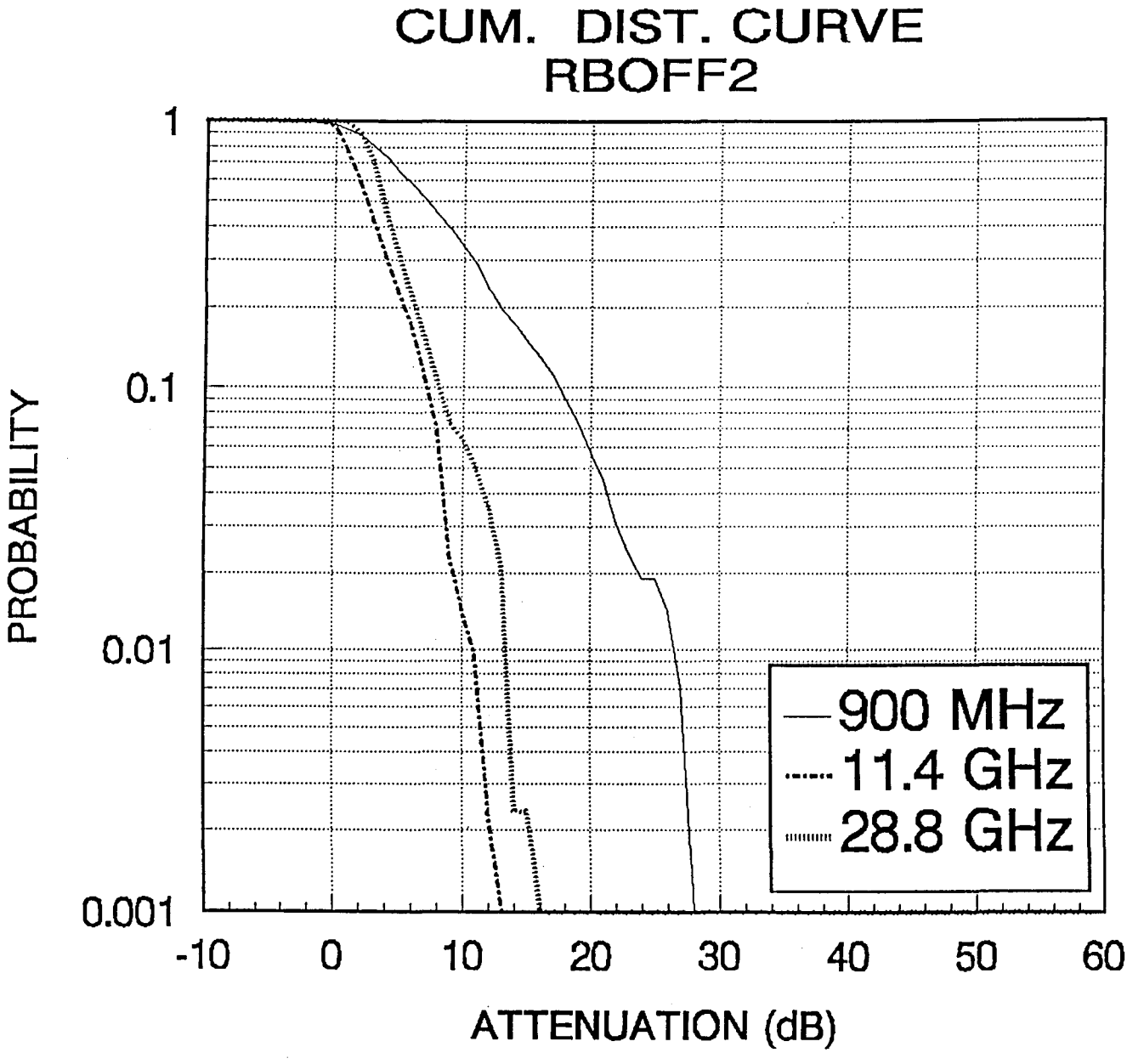

Figure 17. Cumulative distribution for all data in the Radio Building with just one wall between the transmitter and receiver.

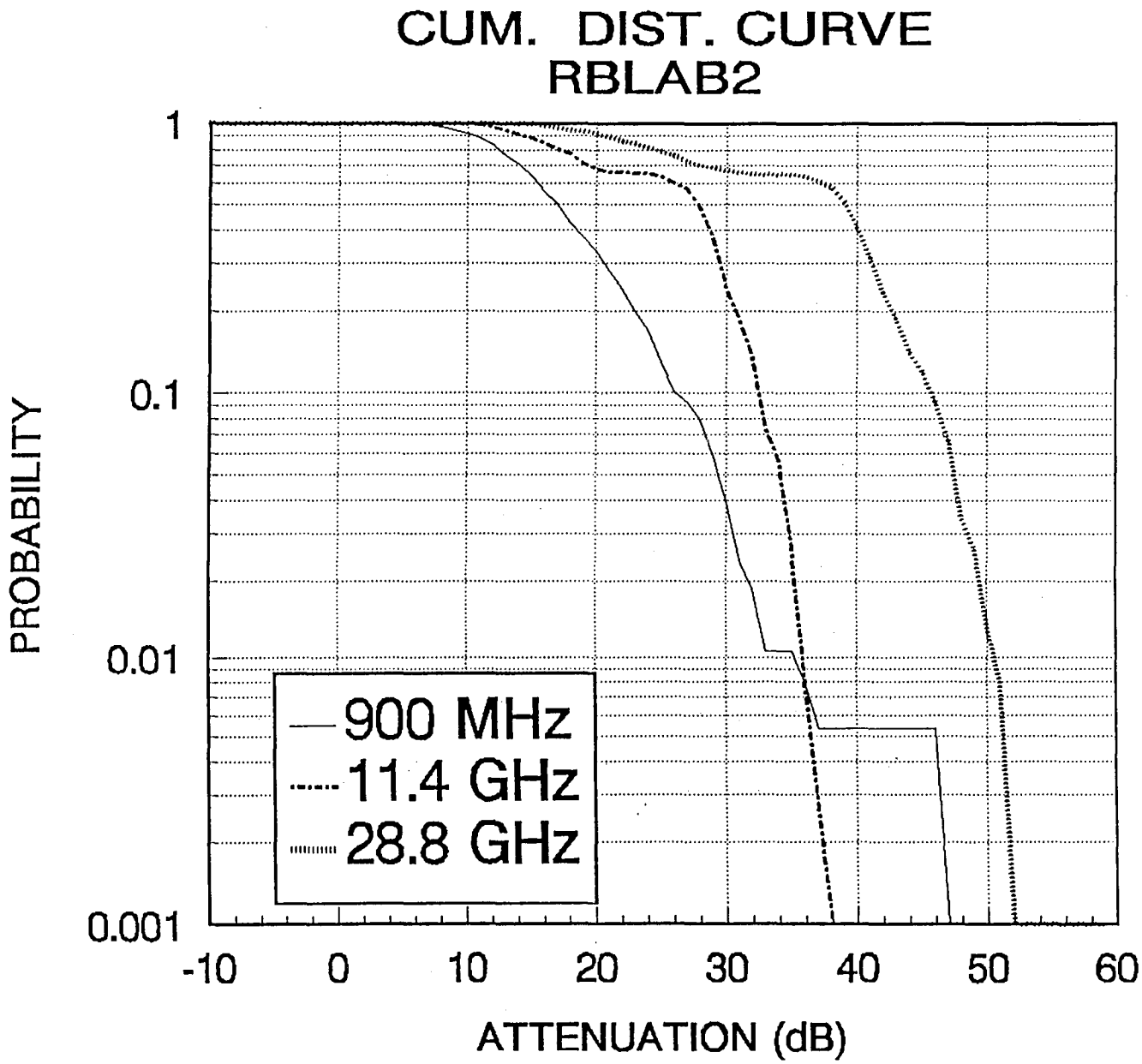

Figure 18. Cumulative distribution for all data in Radio Building with two or three walls between the transmitter and receiver.

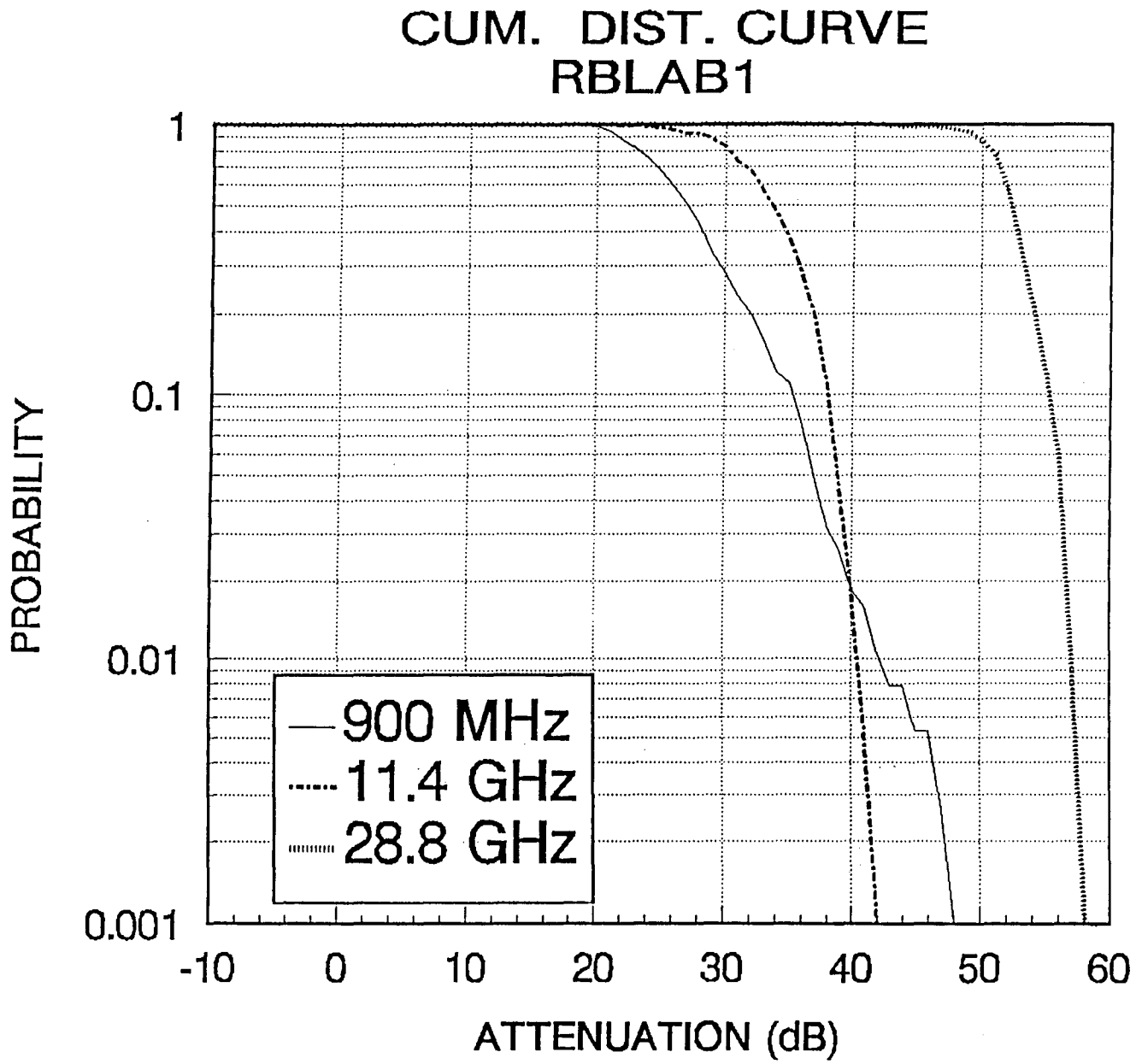

Figure 19. Cumulative distribution for all data in Radio Building with three or more walls between the transmitter and receiver.

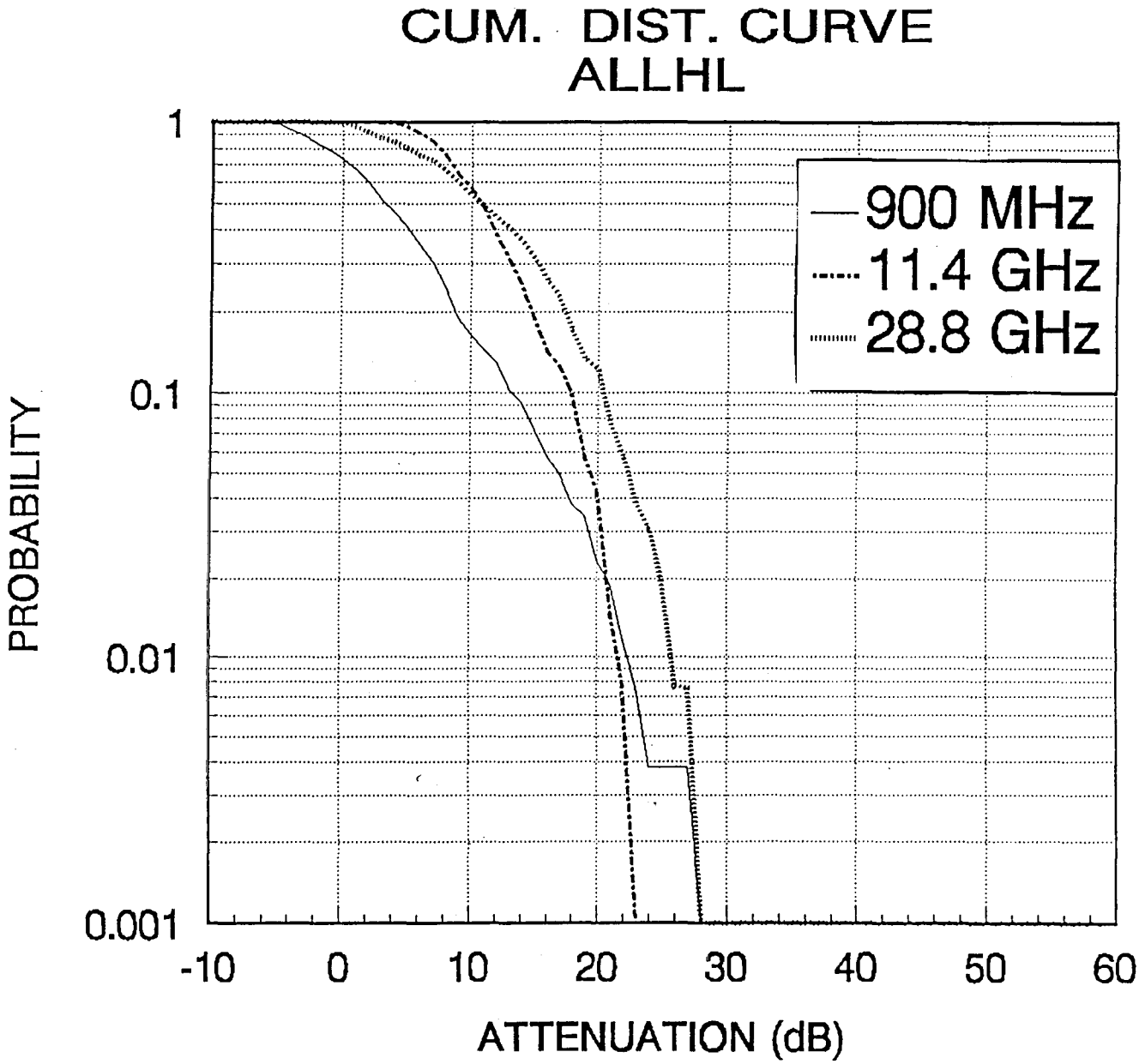

Figure 20. Cumulative distribution for all data in the private residence.

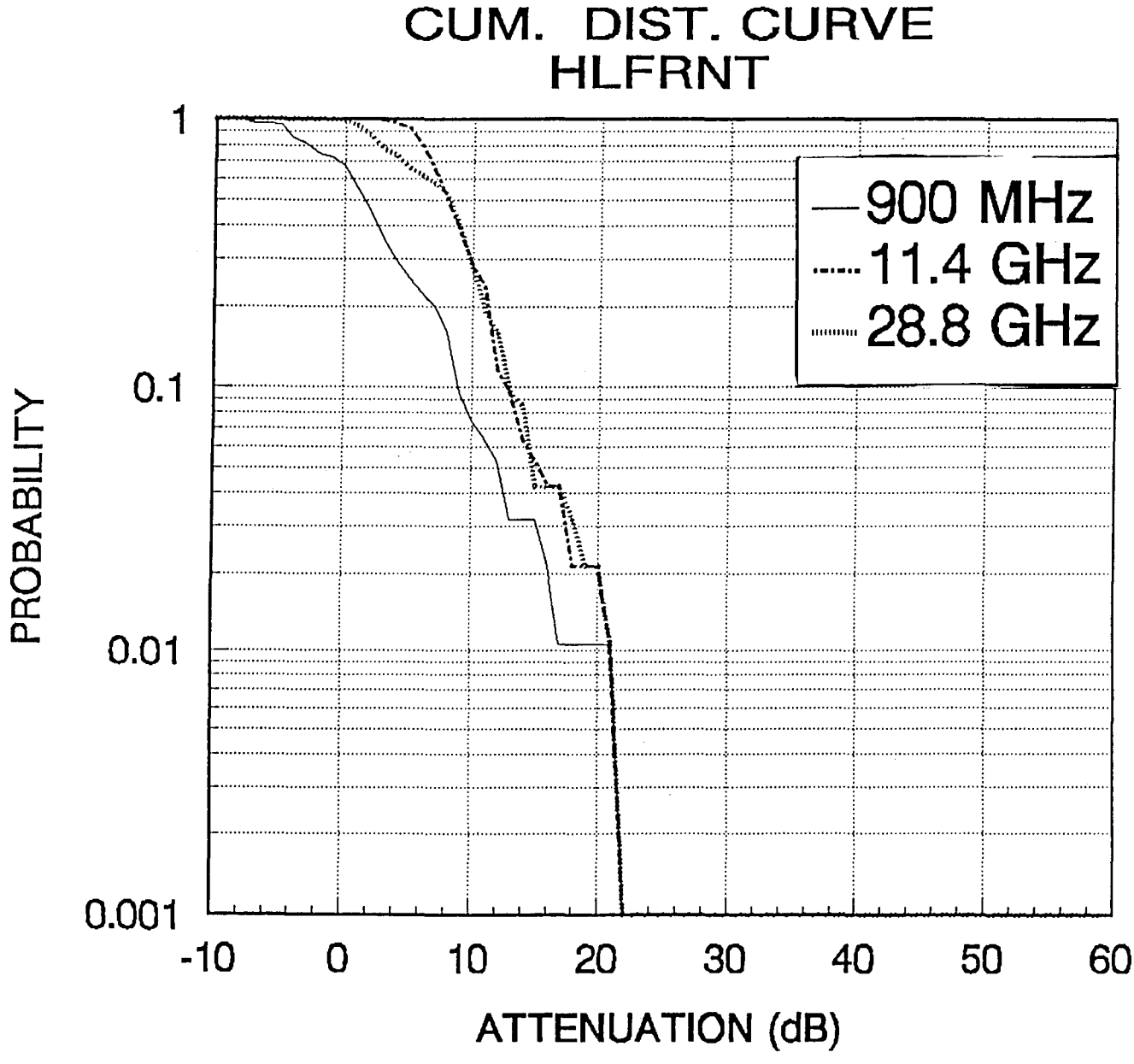

Figure 21. Cumulative distribution for all data in the private residence with one wall between the transmitter and receiver.

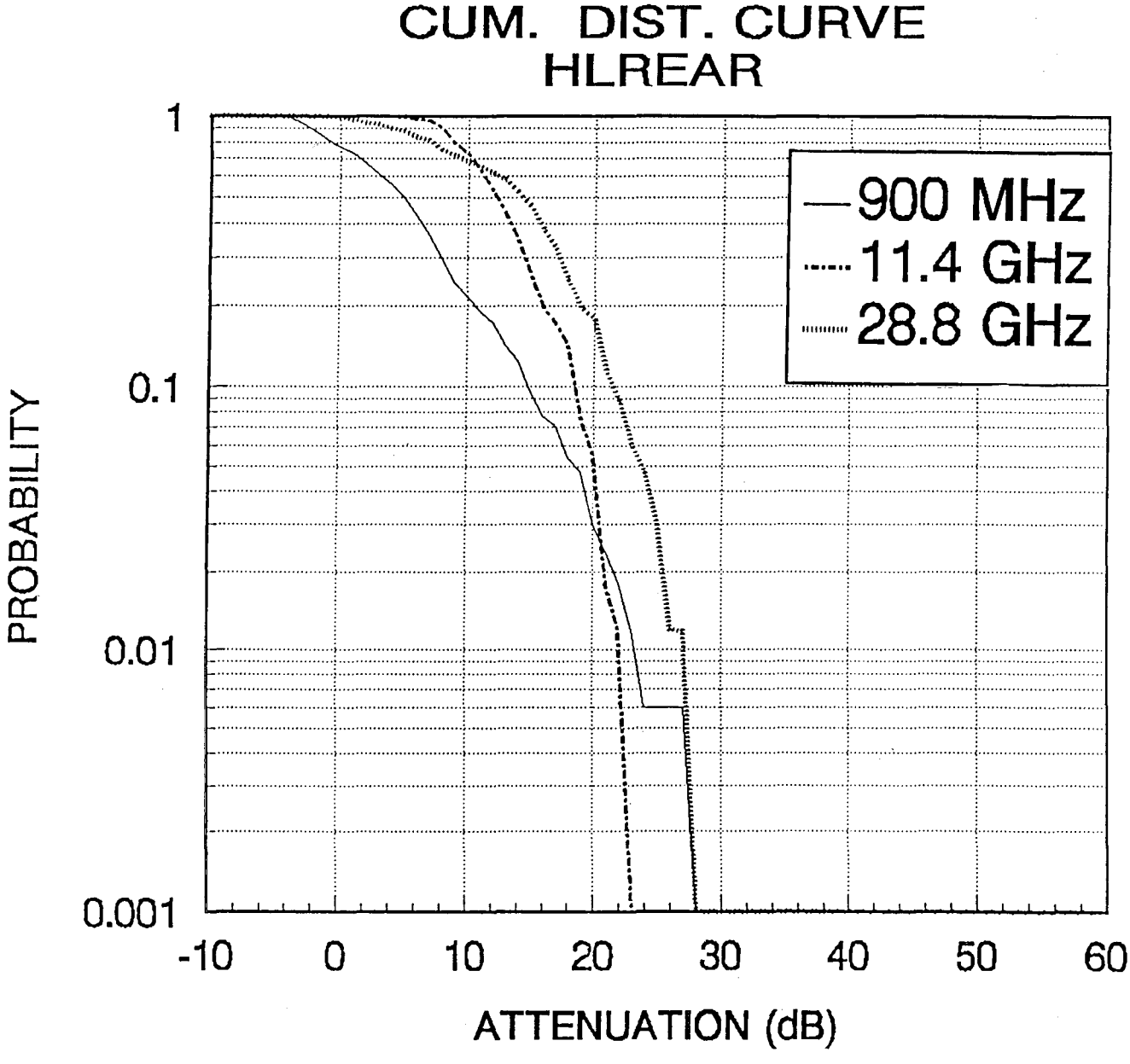

Figure 22. Cumulative distribution for all data in the private residence with two walls between the transmitter and receiver.

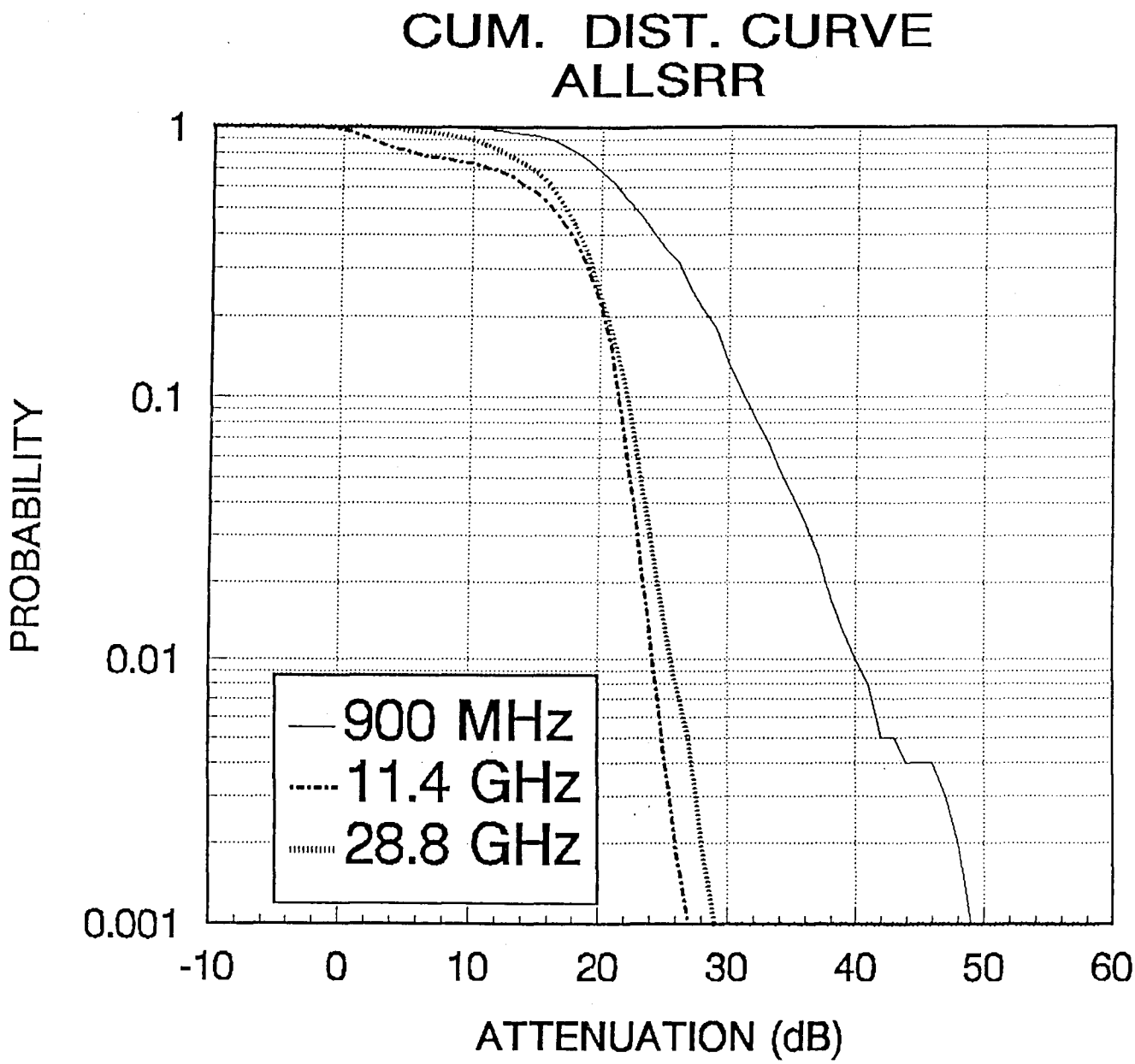

Figure 23. Cumulative distribution for all data in the storeroom building with metal siding.

The maximum attenuation that will be present less than a certain percentage of time can be read off these figures. This number can be used for the link margin at different link reliabilities. Table 4 has the mean attenuation and its standard deviation for all three data combinations. The means at all frequencies are greater for the two-wall case.

Figure 23 shows the cumulative distribution function for all of the data collected in the storeroom (metal structure with metal siding). The mean attenuation and its standard deviation are listed in Table 4. The attenuation is highest (greater than 49 dB less than 0.1 % of the time) at 900 MHz, because of the shielding effect of the metal siding on the building and the small windows (with respect to a wavelength at 900 MHz). The attenuation at 11.4 and 28.8 GHz was greater than 27 and 29 dB respectively less than 0.1 % of the time.

6.0 CONCLUSIONS

The penetration attenuation for the Radio Building and the private residence tend to increase with frequency. The penetration attenuation for the storeroom decreases with increasing frequency.

The separate cases for the Radio Building and private residence also indicate a progressively increasing amount of penetration attenuation at all frequencies as the number of wall penetrations increase in the building structure.

The electromagnetic energy at 11.4 and 28.8 GHz can couple into the storeroom building more effectively than that energy at 900 MHz. The shielding effectiveness (ratio in dB of the power outside the structure to the power inside the structure) of the structure is less at the two higher frequencies and allows more energy to couple through the walls. The shielding effectiveness of a metal structure is dependent on the size of the openings in the outer shell of the structure. These may be windows, doors, heating and/or air conditioning penetrations, holes, etc. When the size of the opening in the structure is greater than or comparable to a wavelength, then the opening in the structure provides a strong coupling path for electromagnetic energy to flow into or out of the structure. This reduces the penetration attenuation of the structure.

The penetration attenuation values derived from the measurements conducted in this study can be used determine the feasibility of personal communications. The cumulative distribution functions of the penetration attenuation can provide information on what link margins are necessary for different communication probabilities or reliabilities. The penetration attenuation provides a quantitative margin for link calculations to use in analyzing and designing personal communication systems.

APPENDIX: ATTENUATION PLOTS FOR ALL MEASUREMENT PATHS

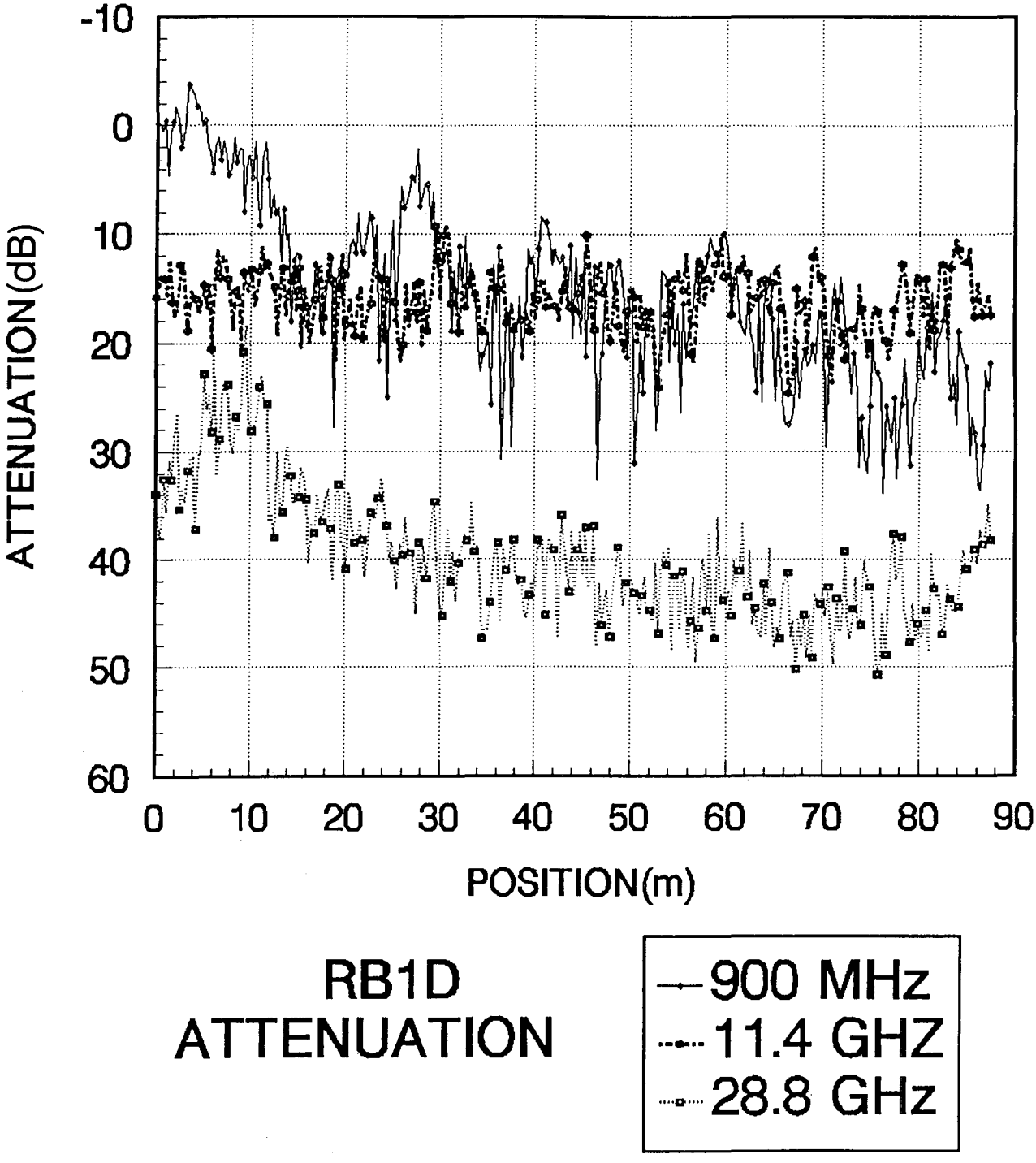

Figure A-1. Penetration loss for Radio Building path RB1D.

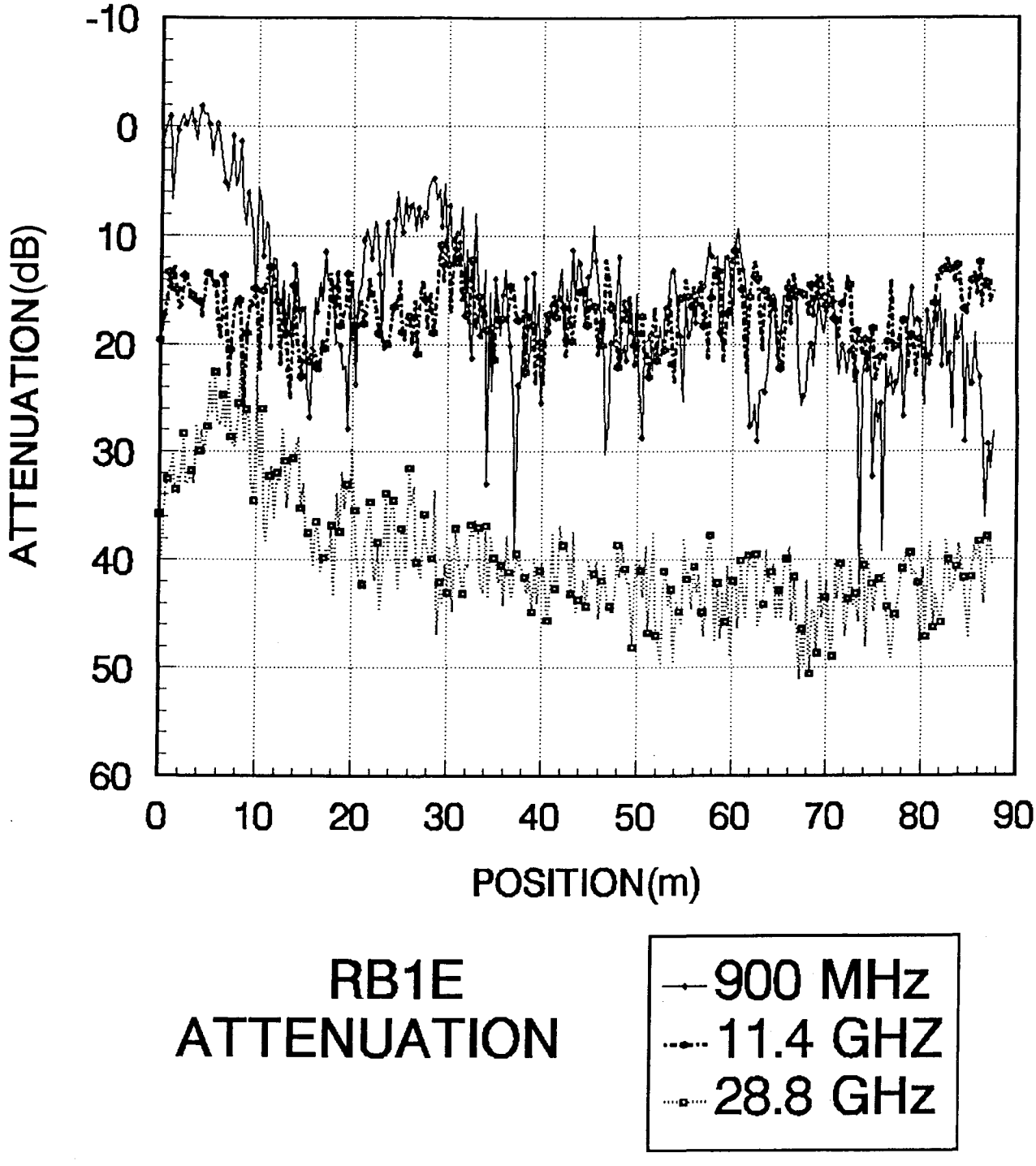

Figure A-2. Penetration loss for Radio Building path RB1E.

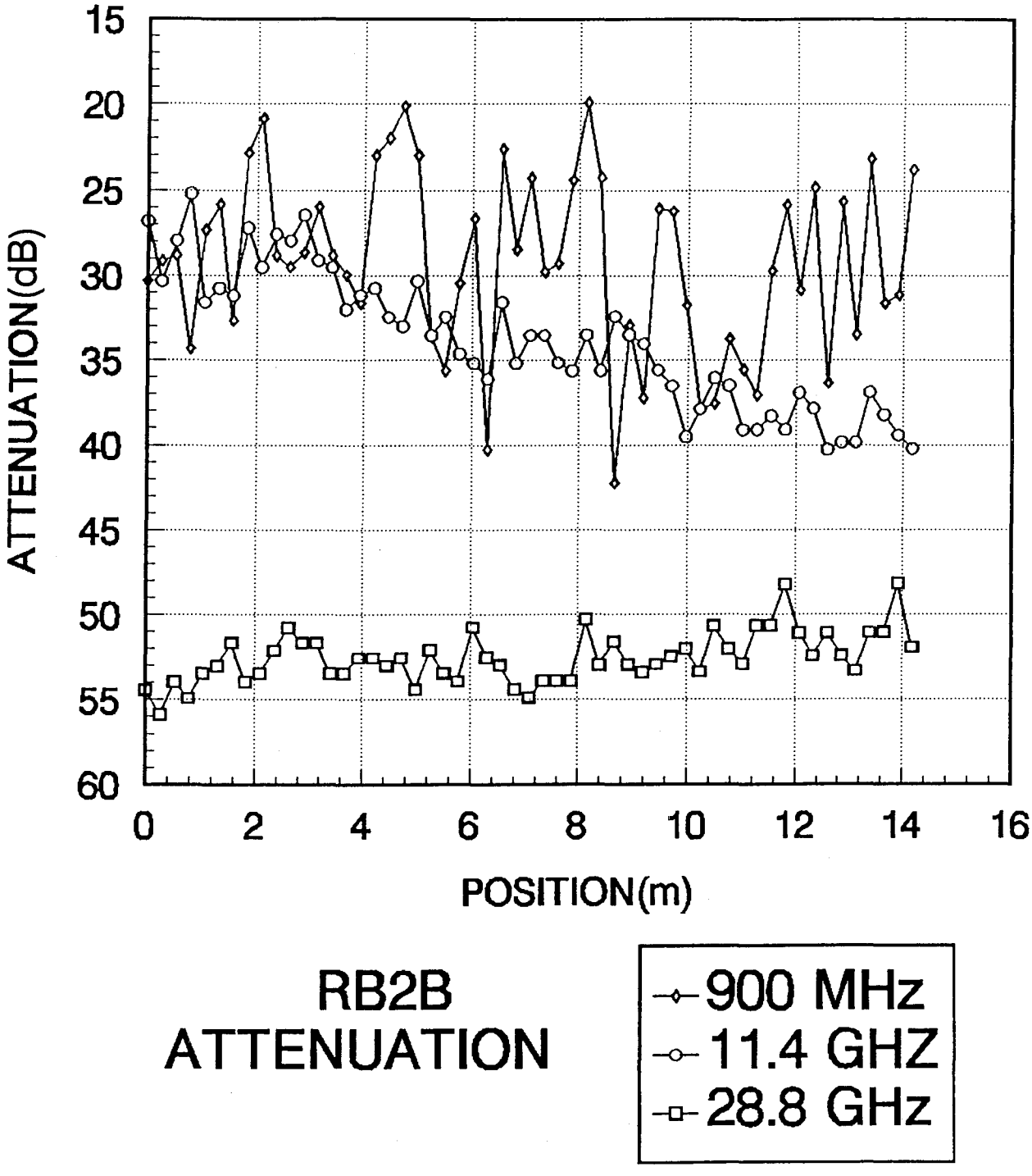

Figure A-3. Penetration loss for Radio Building path RB2B.

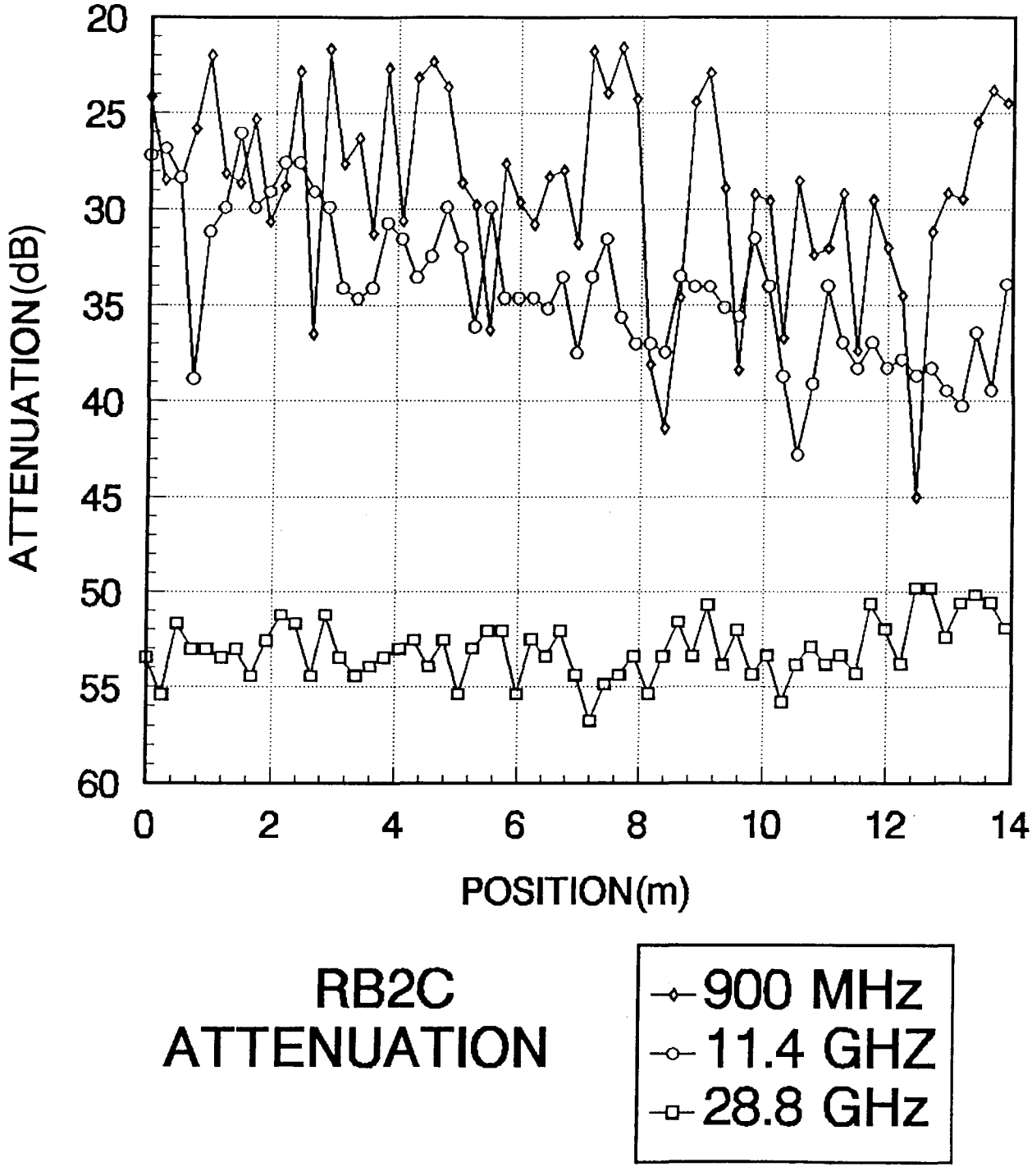

Figure A-4. Penetration loss for Radio Building path RB2C.

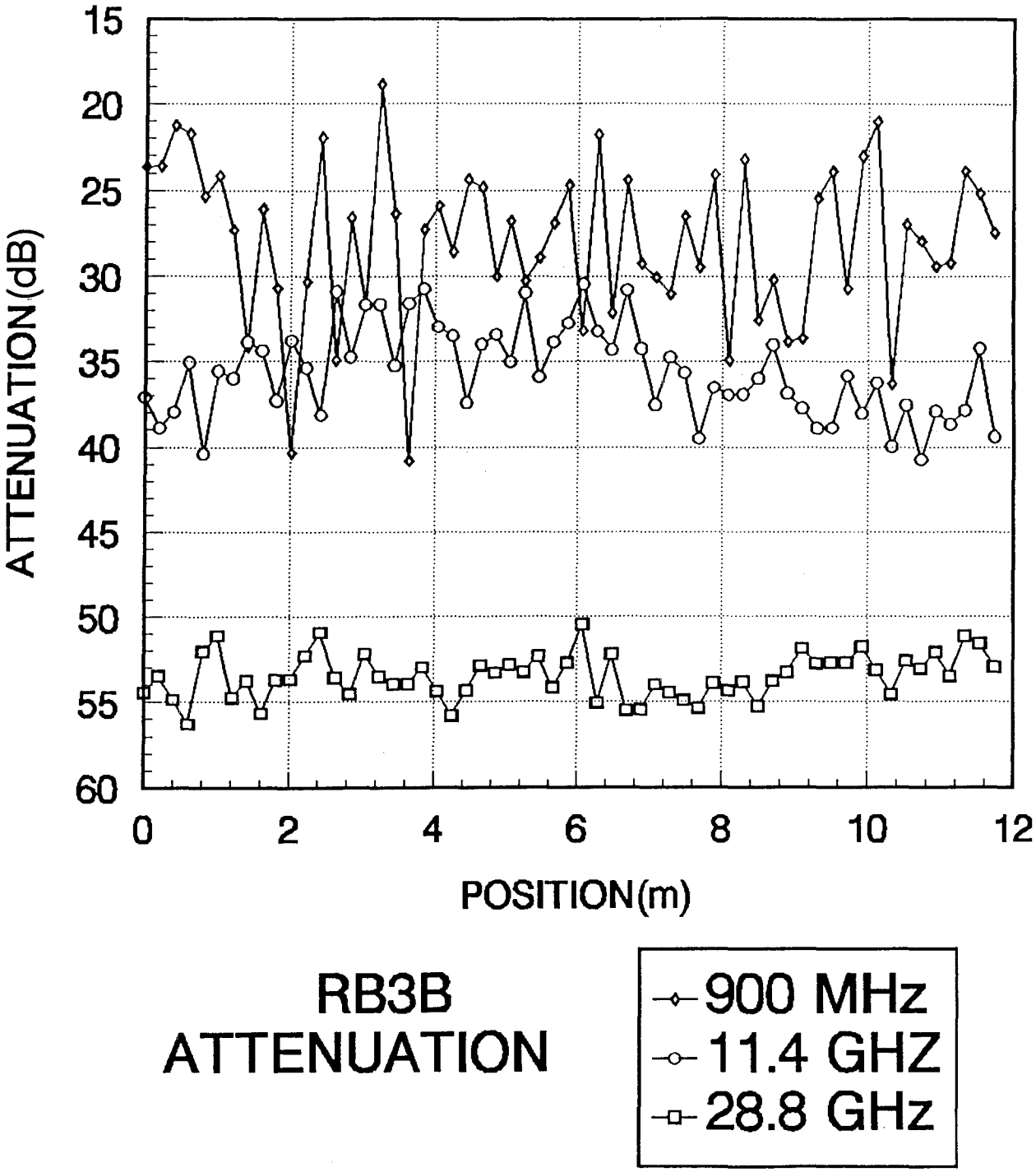

Figure A-5. Penetration loss for Radio Building path RB3B.

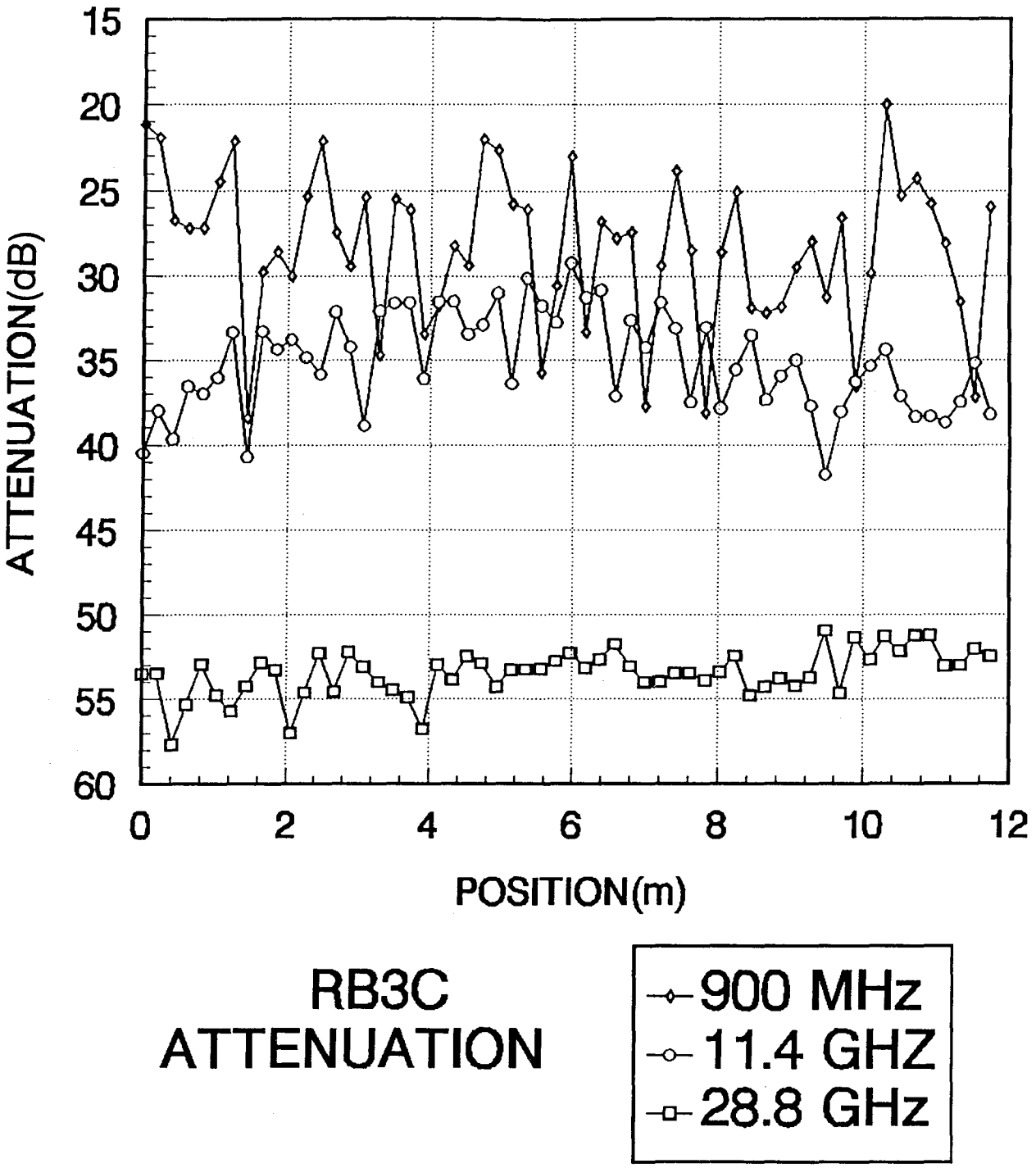

Figure A-6. Penetration loss for Radio Building path RB3C.

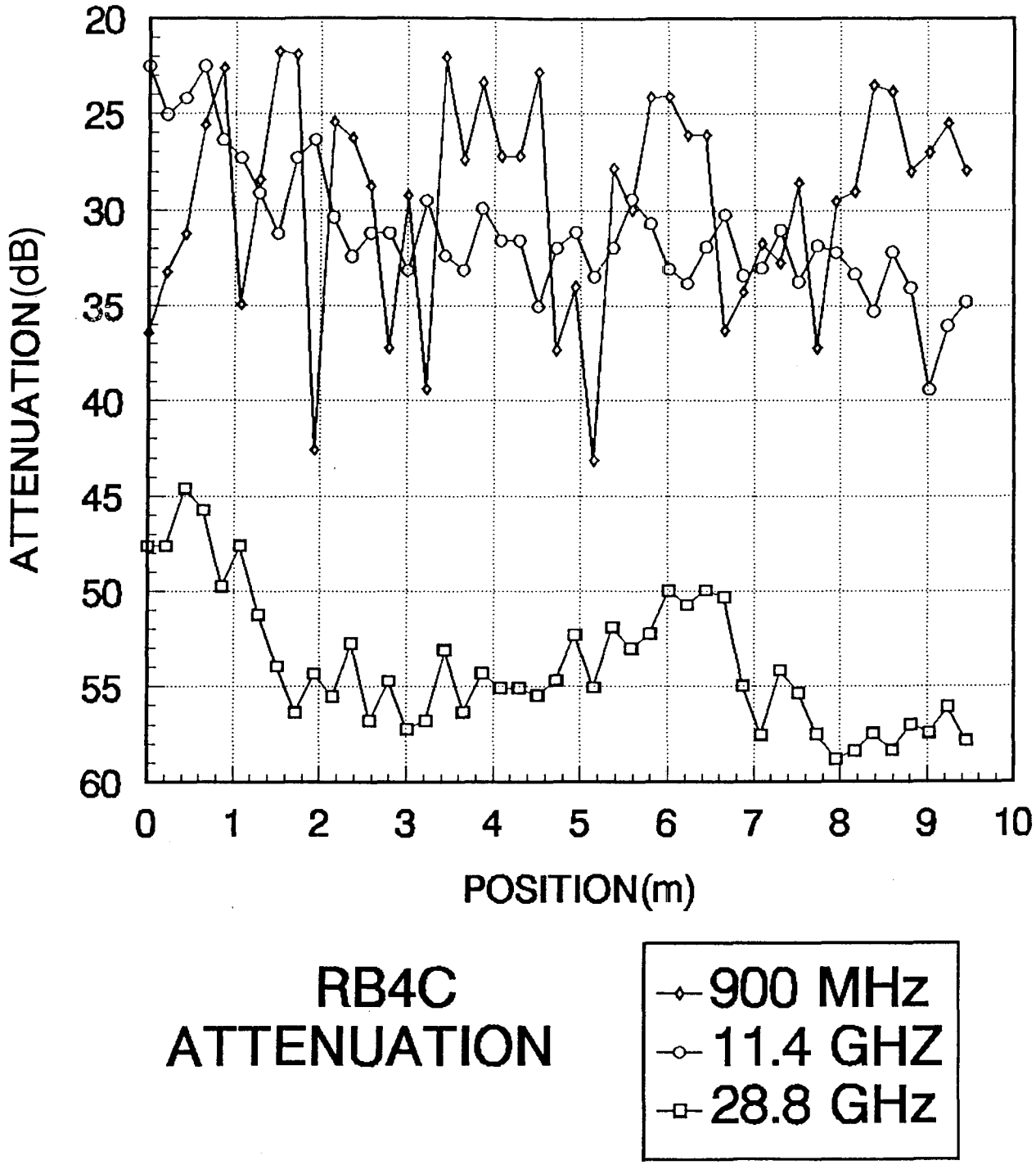

Figure A-7. Penetration loss for Radio Building path RB4C.

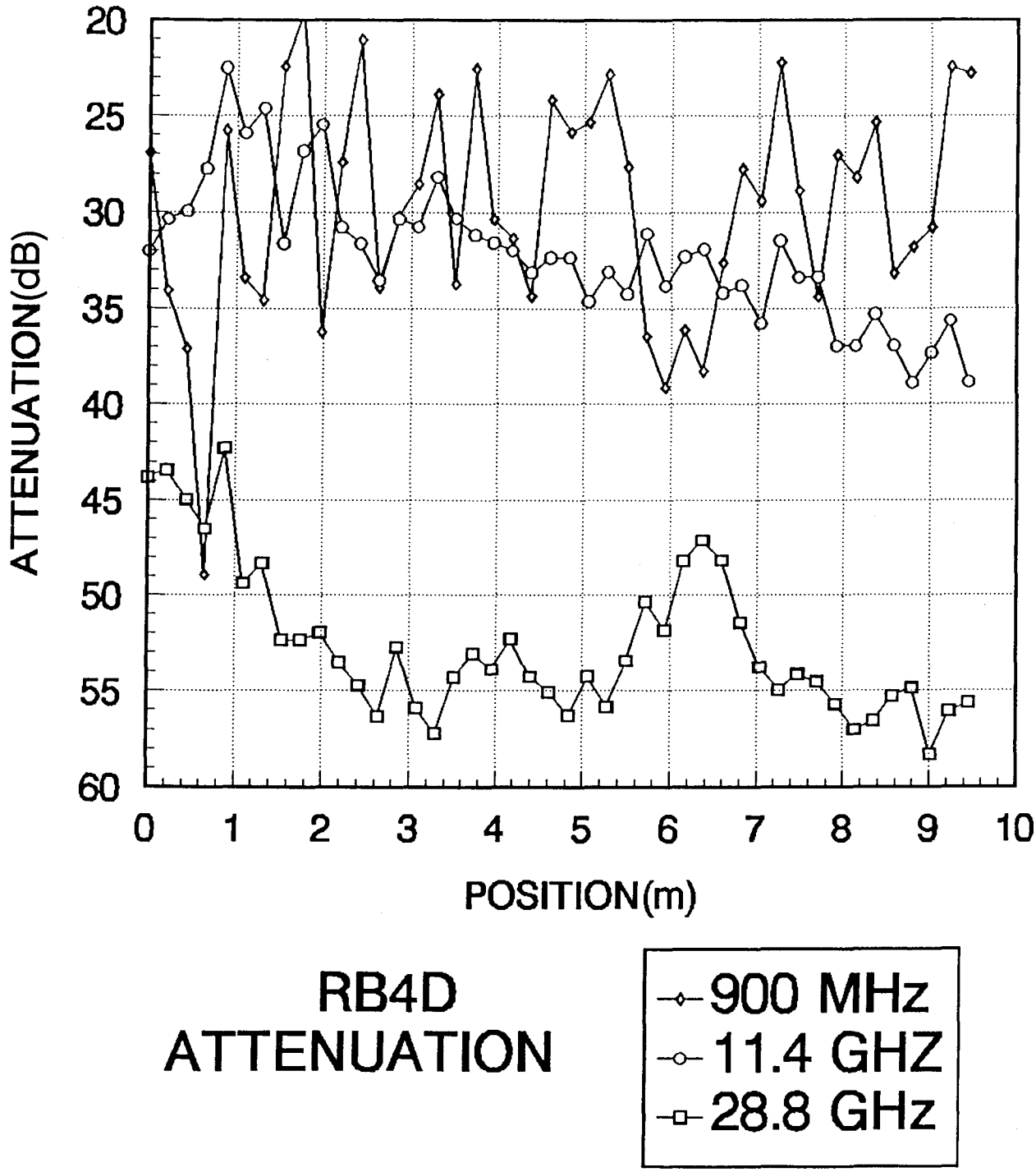

Figure A-8. Penetration loss for Radio Building path RB4D.

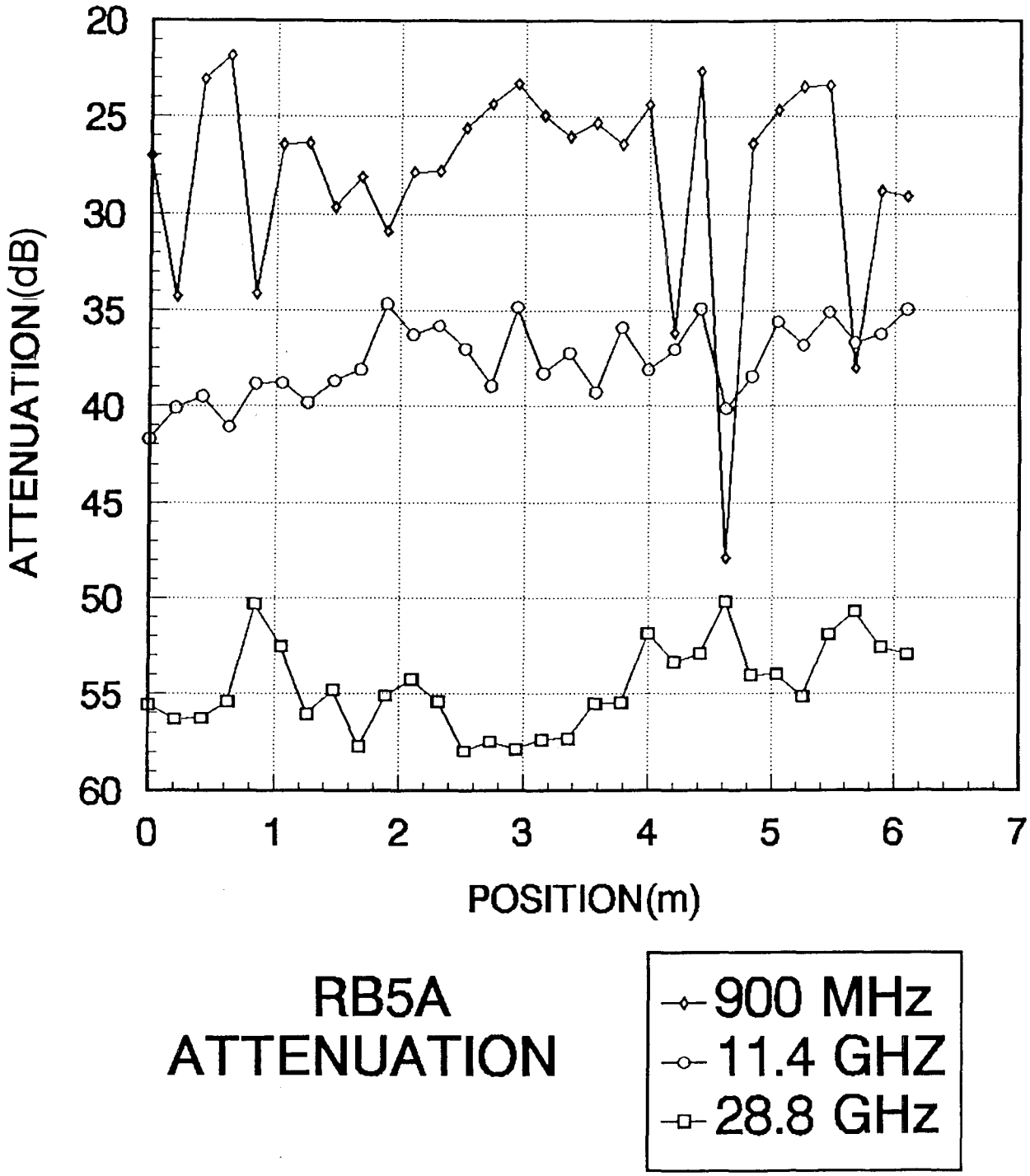

Figure A-9. Penetration loss for Radio Building path RB5A.

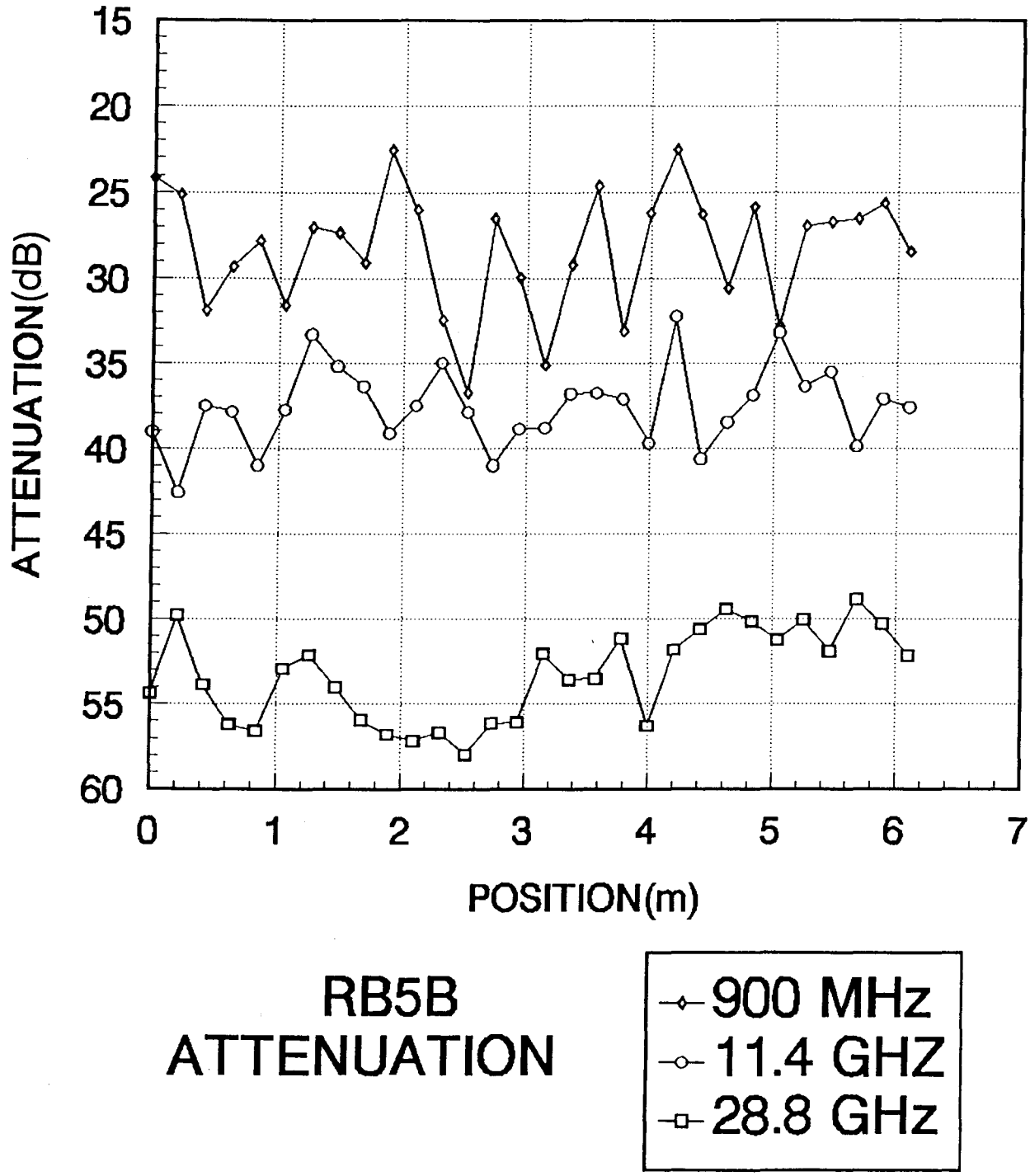

Figure A-10. Penetration loss for Radio Building path RB5B.

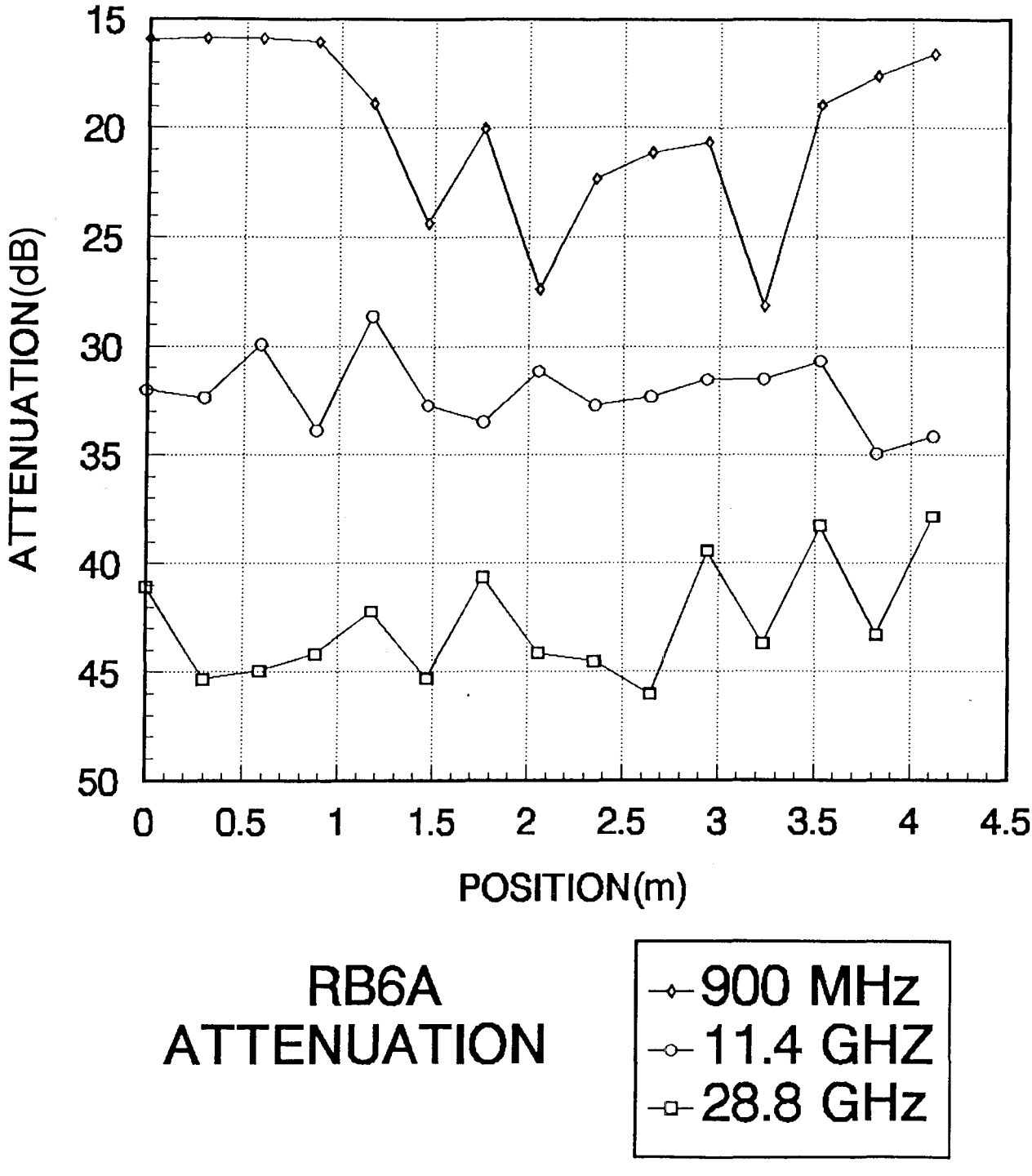

Figure A-11. Penetration loss for Radio Building path RB6A.

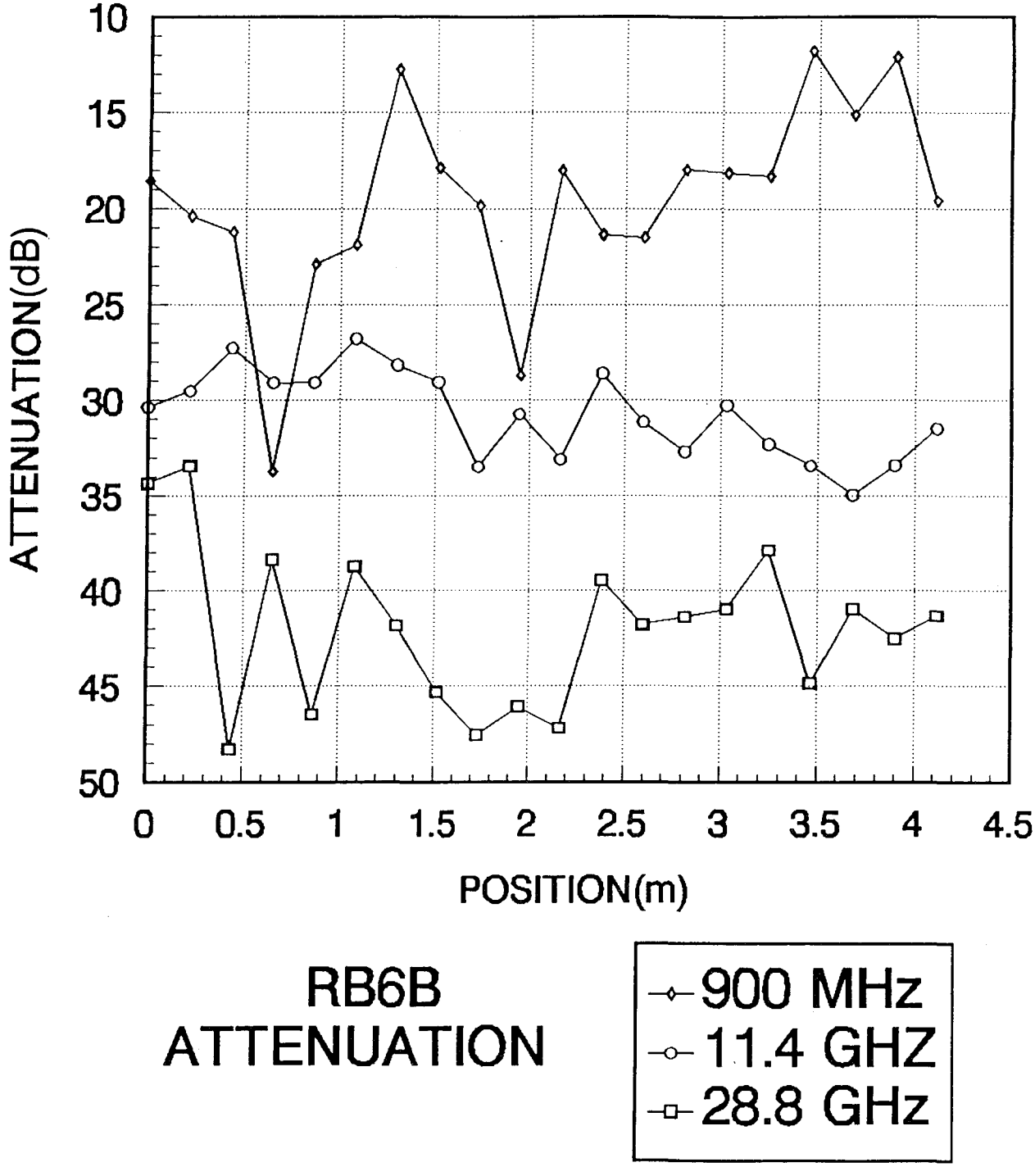

Figure A-12. Penetration loss for Radio Building path RB6B.

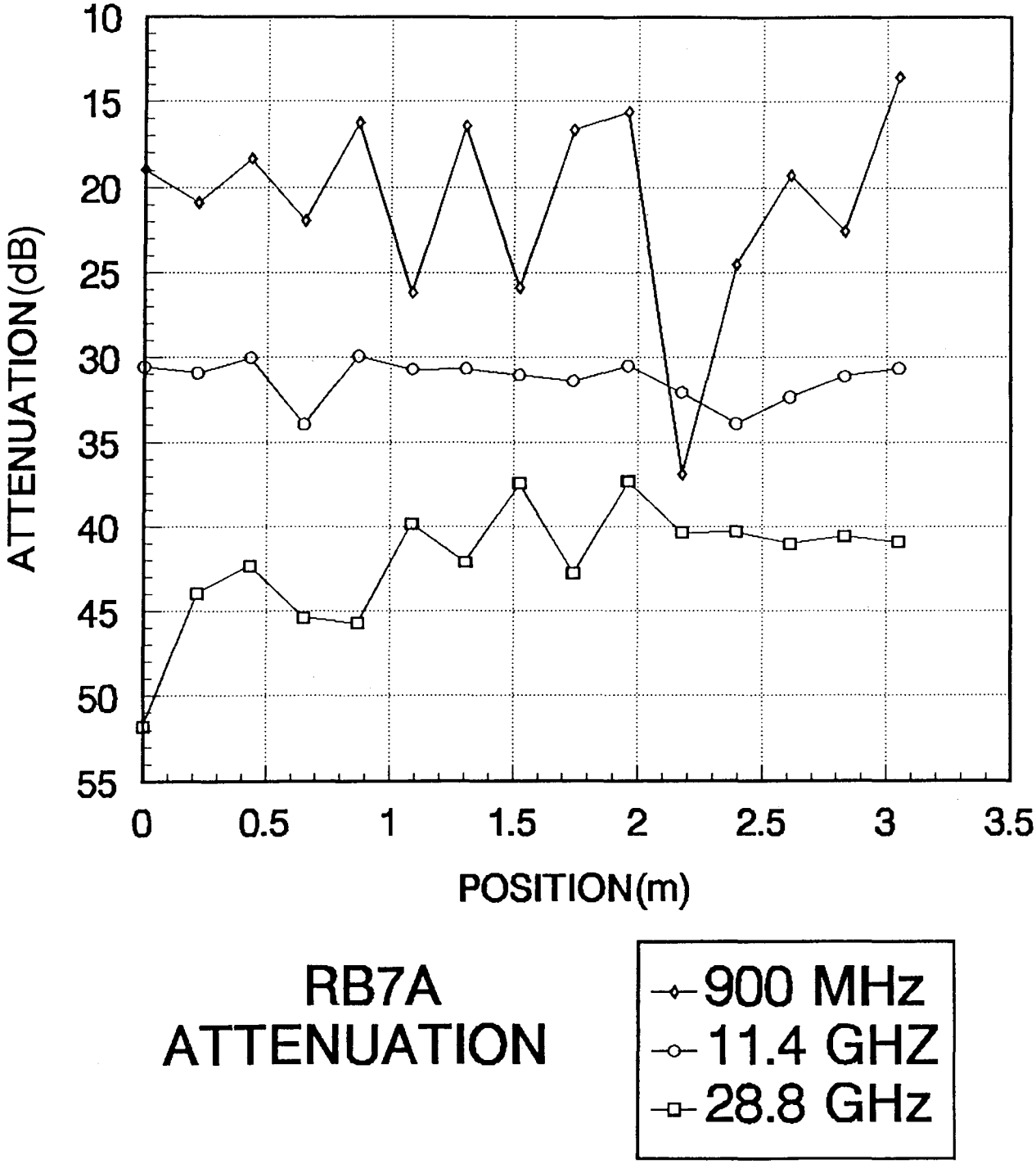

Figure A-13. Penetration loss for Radio Building path RB7A.

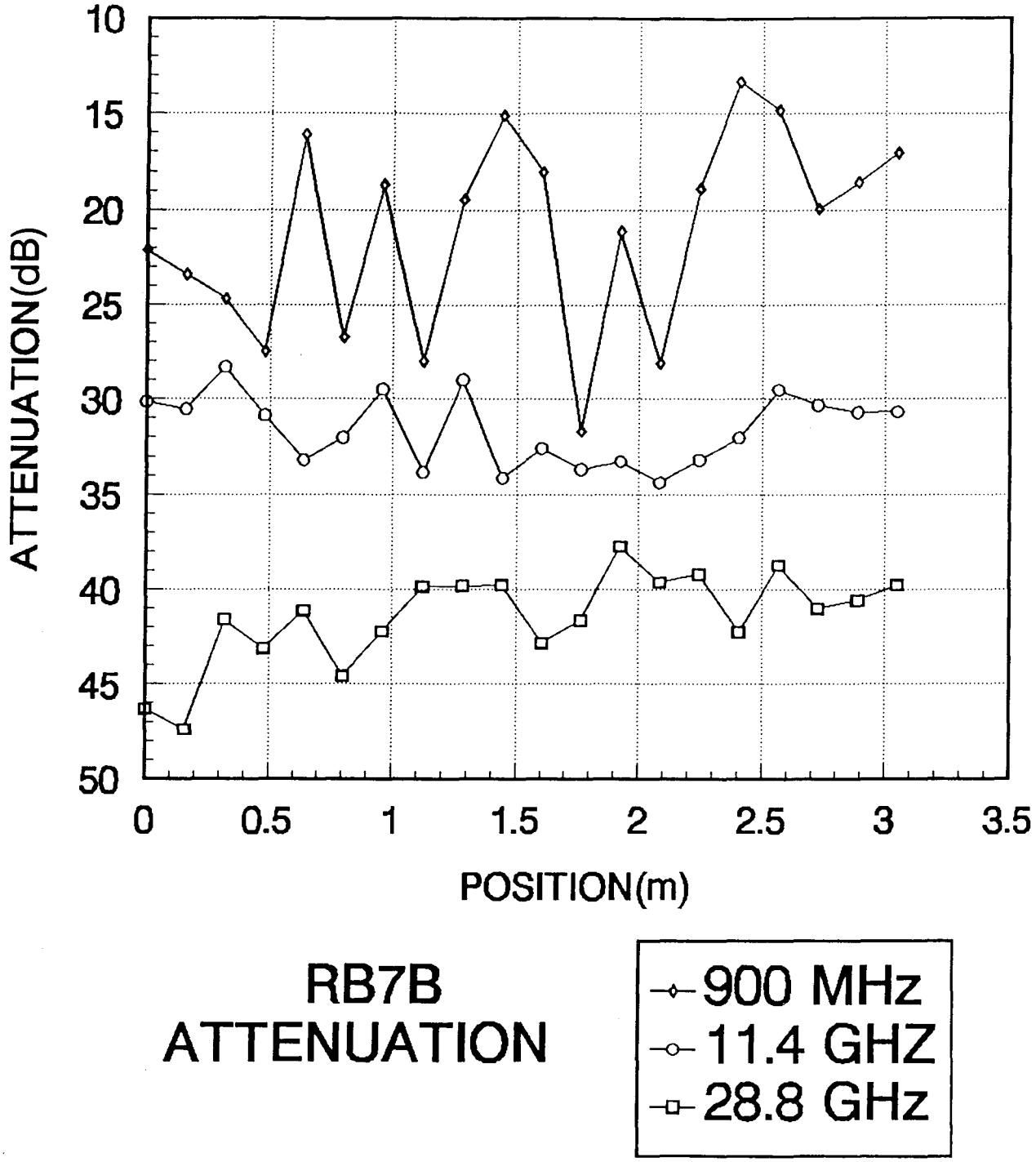

Figure A-14. Penetration loss for Radio Building path RB7B.

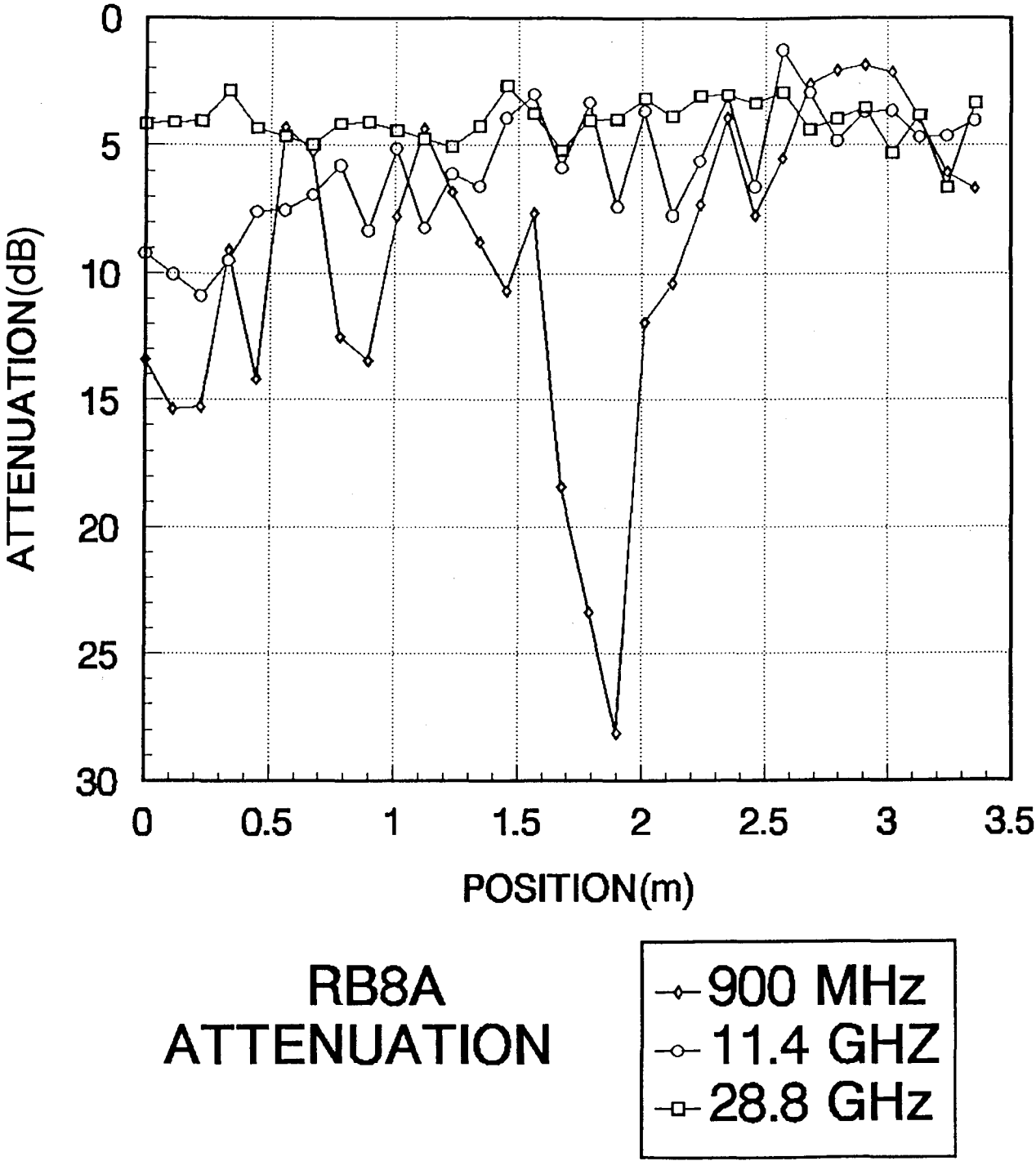

Figure A-15. Penetration loss for Radio Building path RB8A.

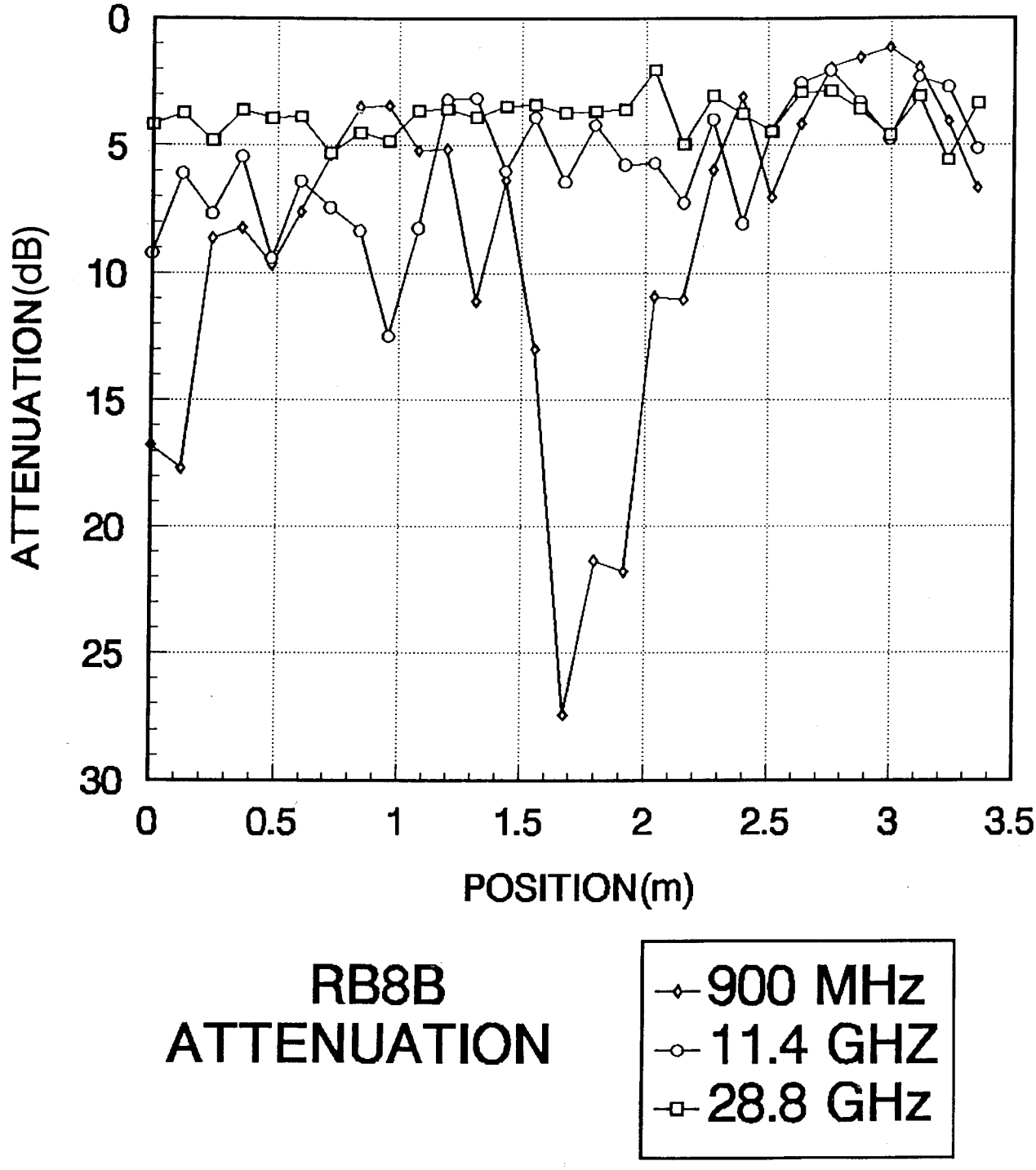

Figure A-16 Penetration loss for Radio Building path RB8B.

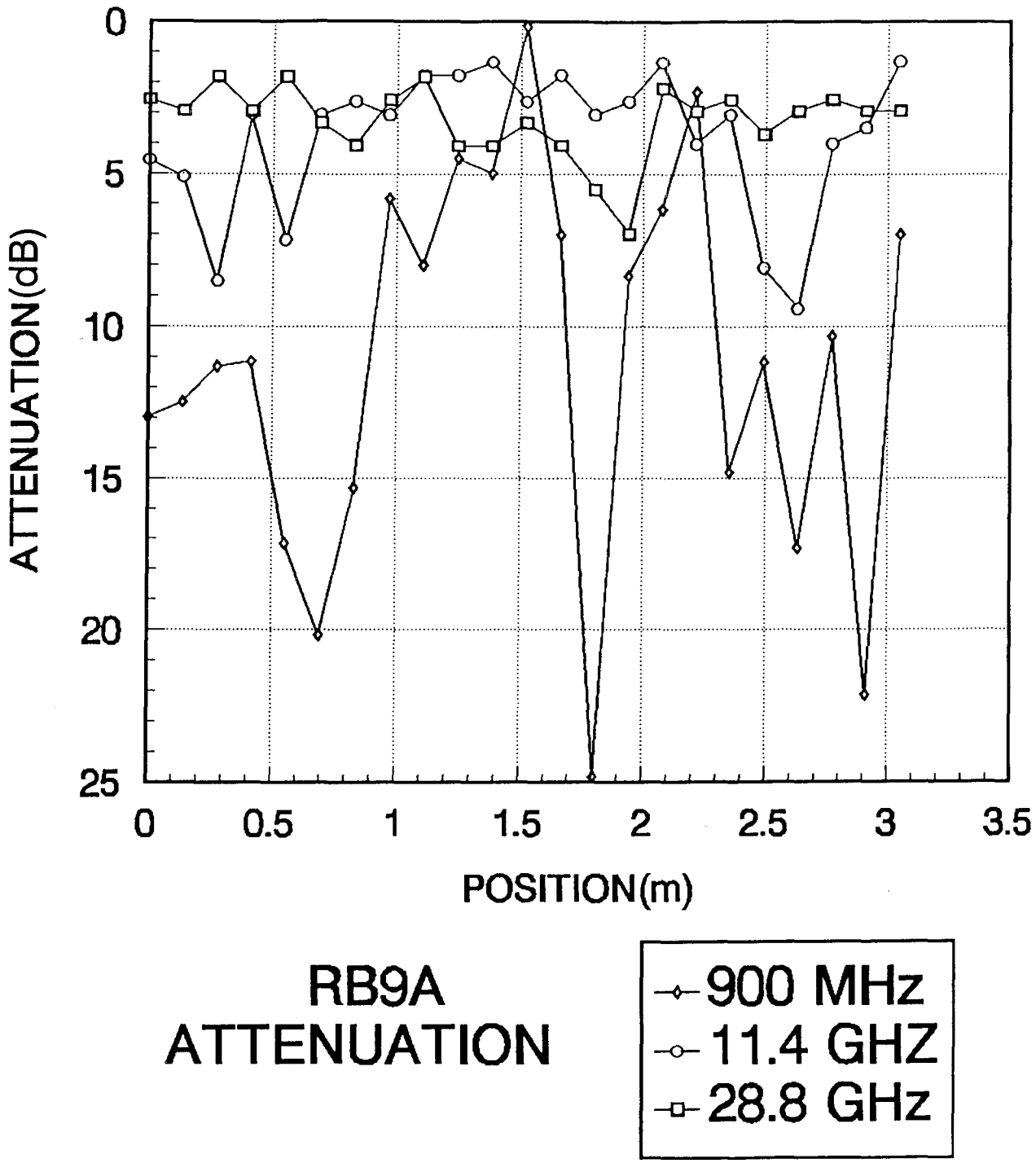

Figure A-17. Penetration loss for Radio Building path RB9A.

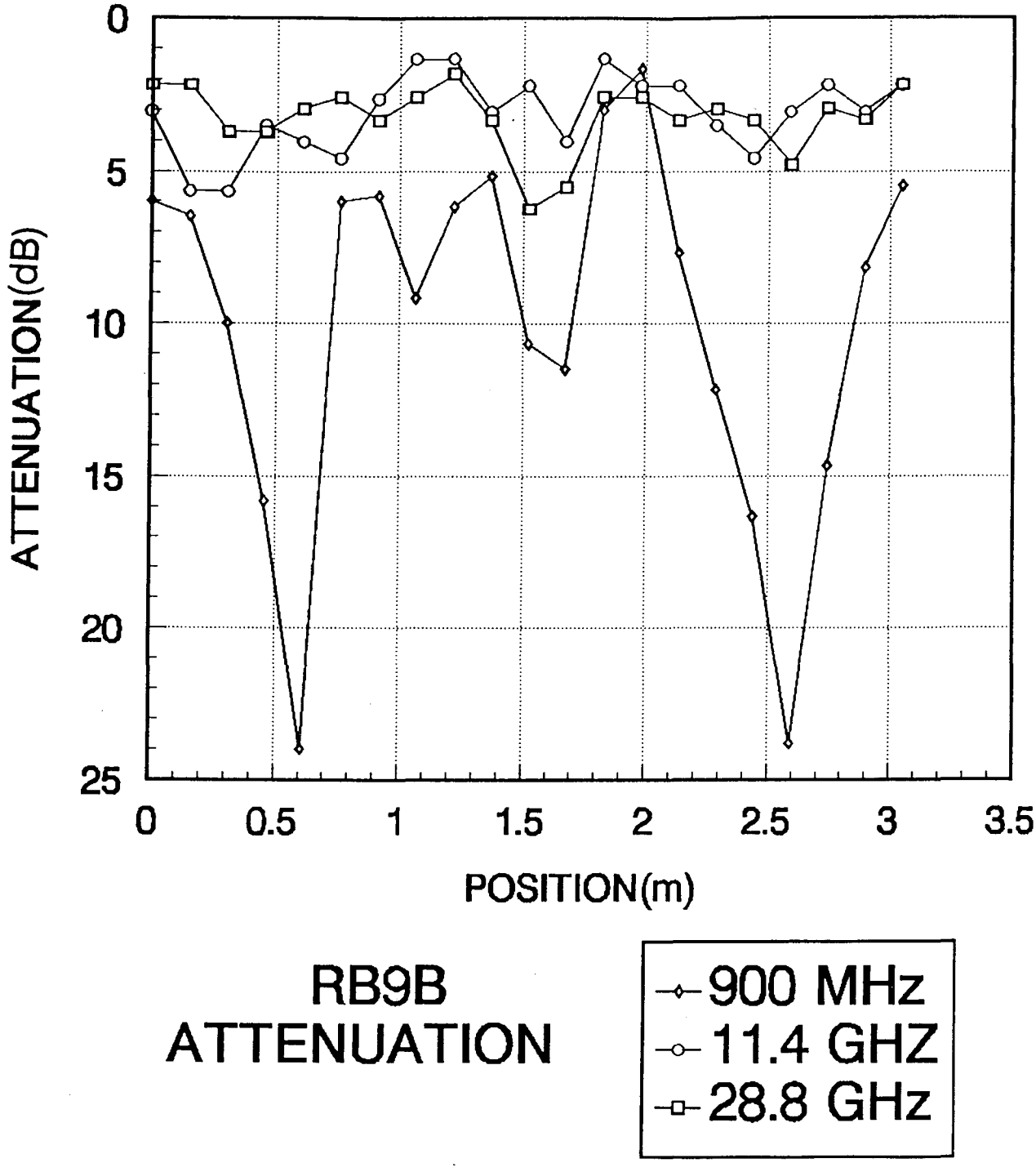

Figure A-18. Penetration loss for Radio Building path RB9B.

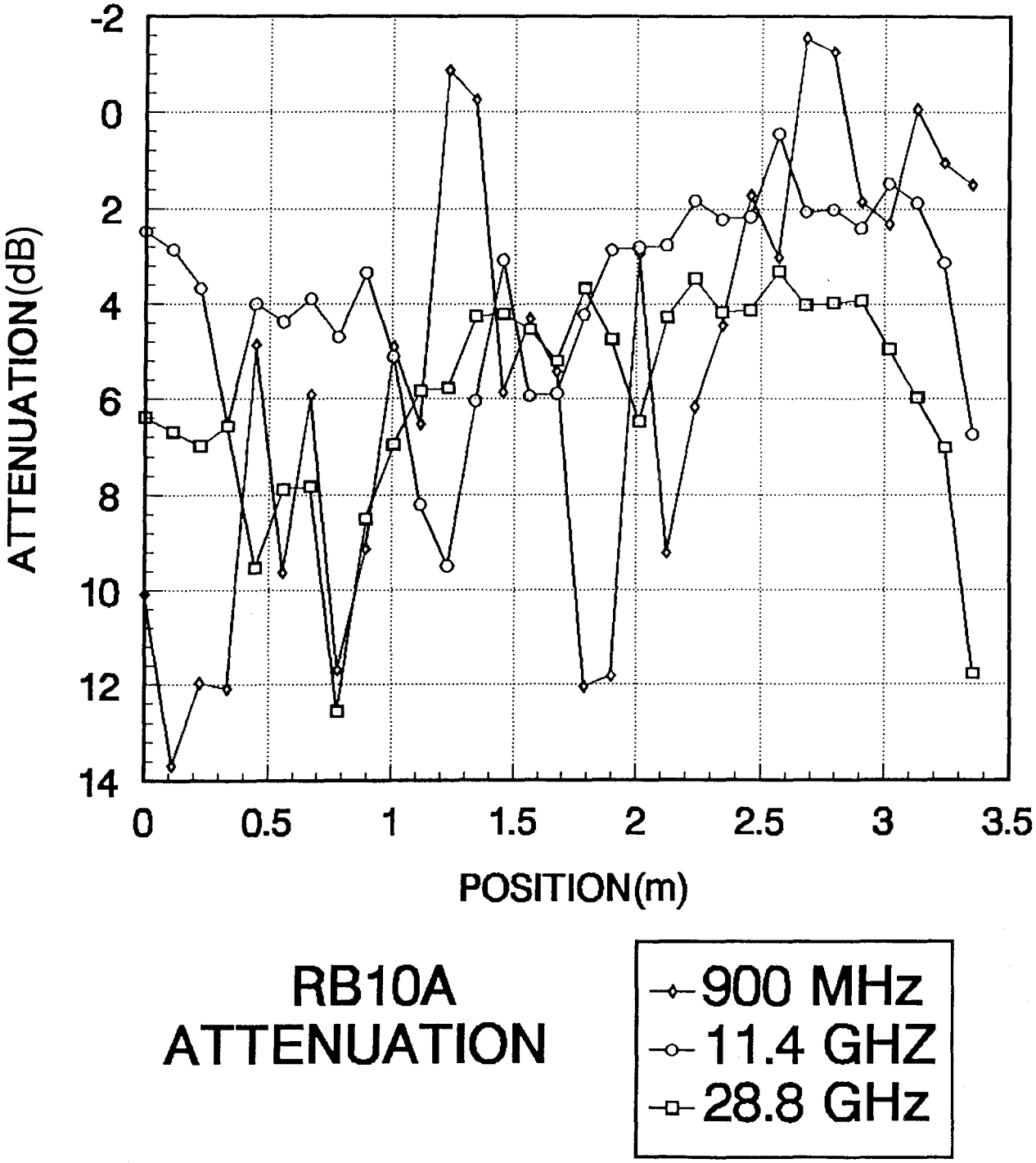

Figure A-19. Penetration loss for Radio Building path RB10A.

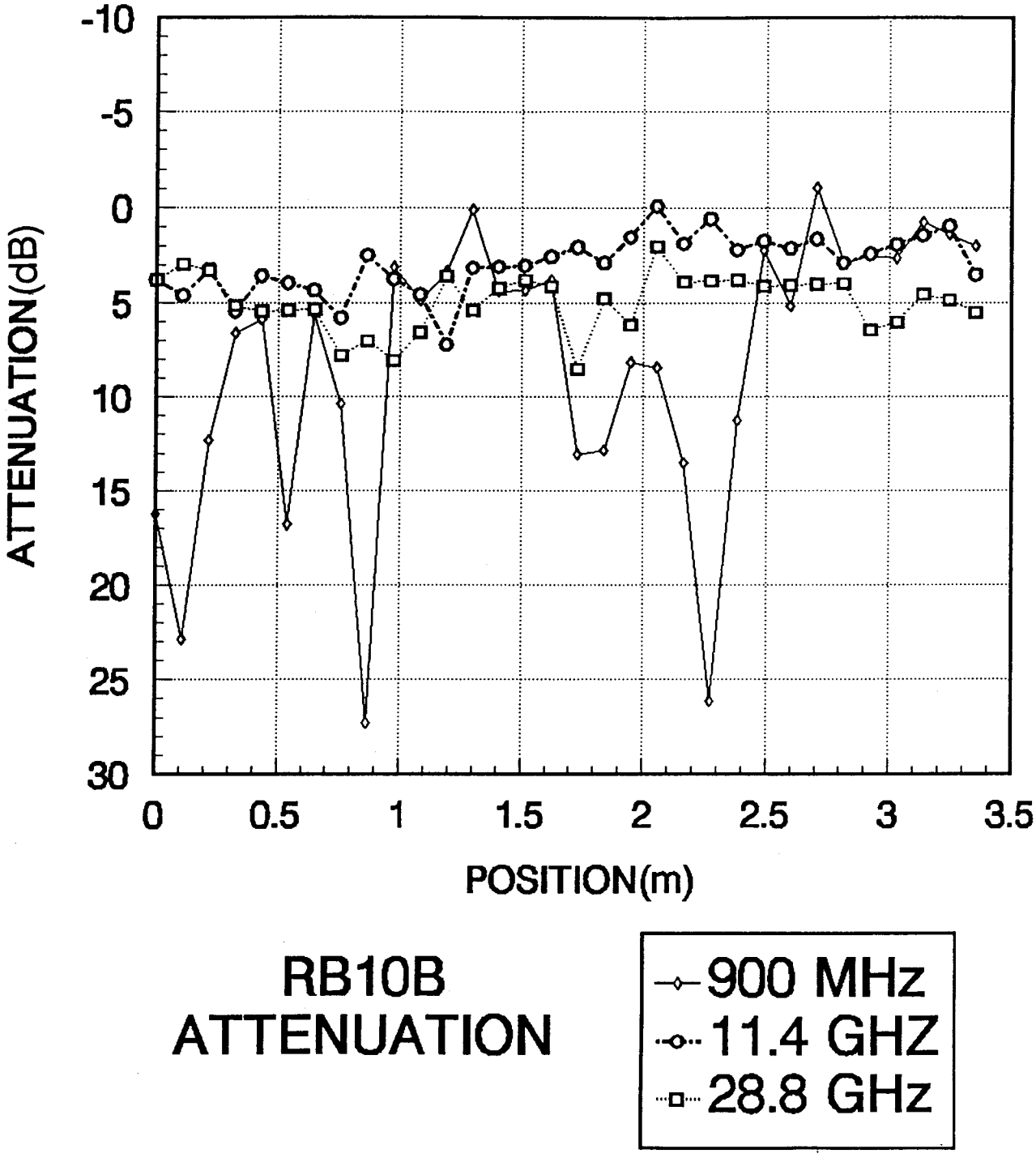

Figure A-20. Penetration loss for Radio Building path RB10B.

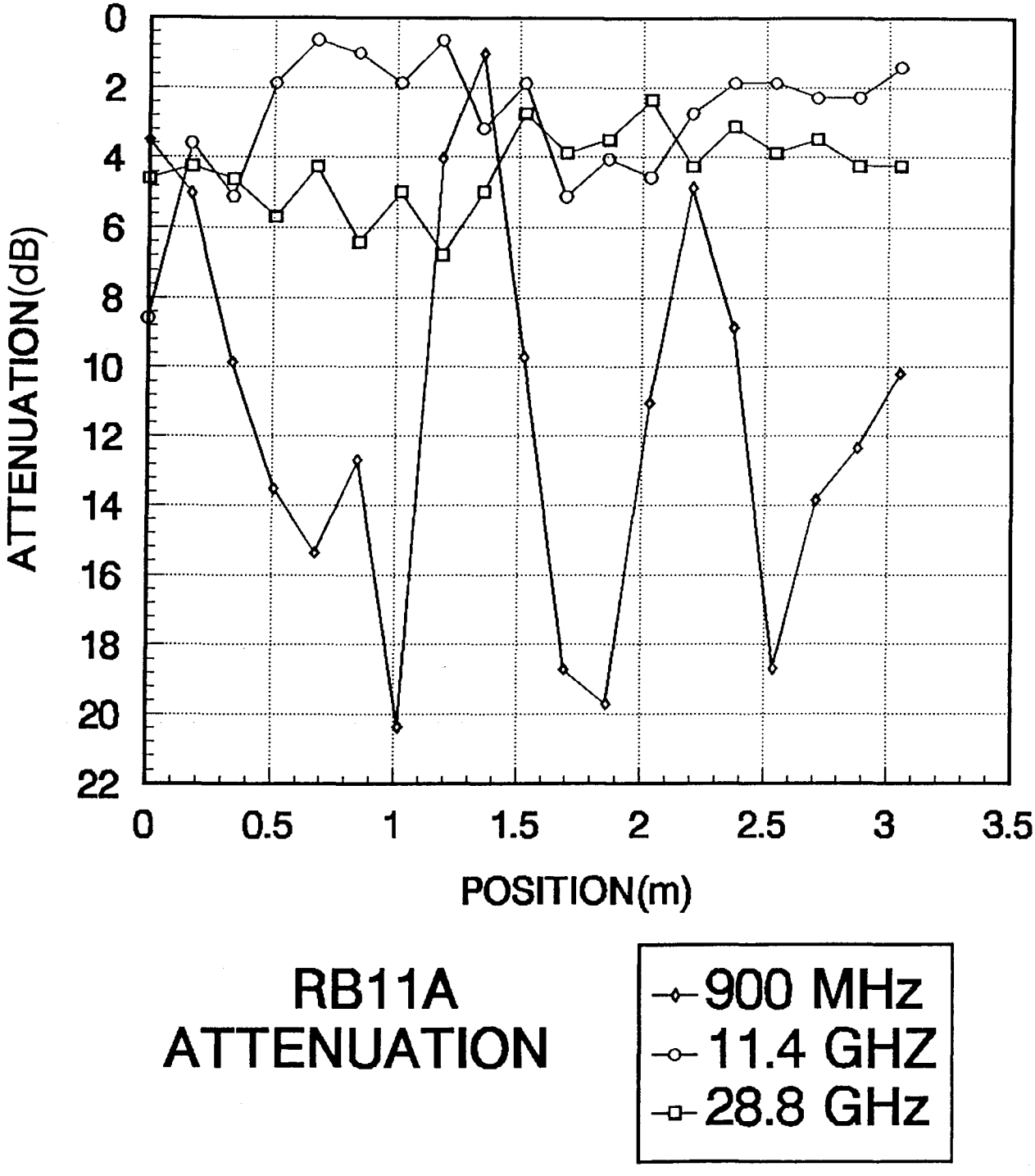

Figure A-21. Penetration loss for Radio Building path RB11A.

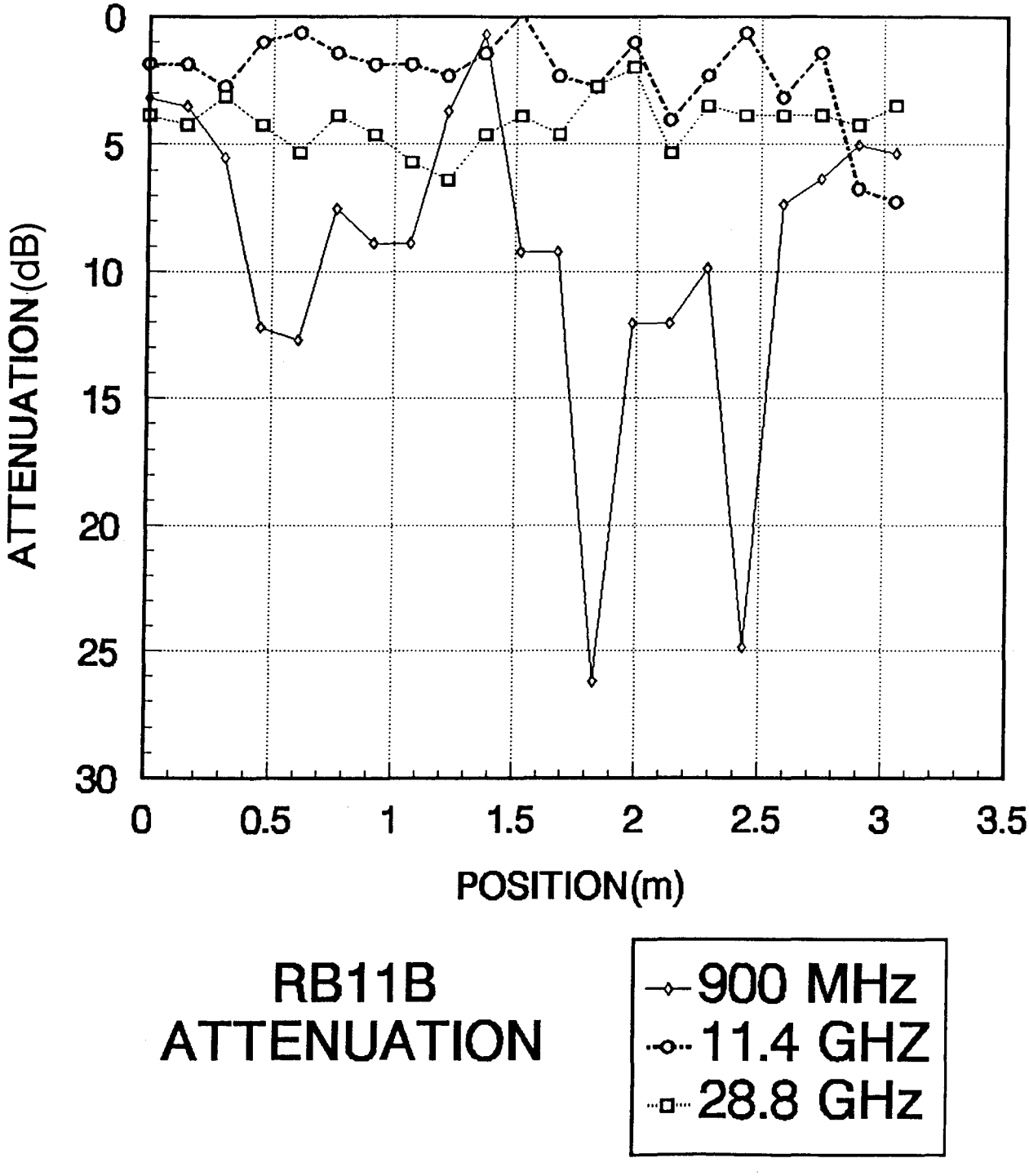

Figure A-22. Penetration loss for Radio Building path RB11B.

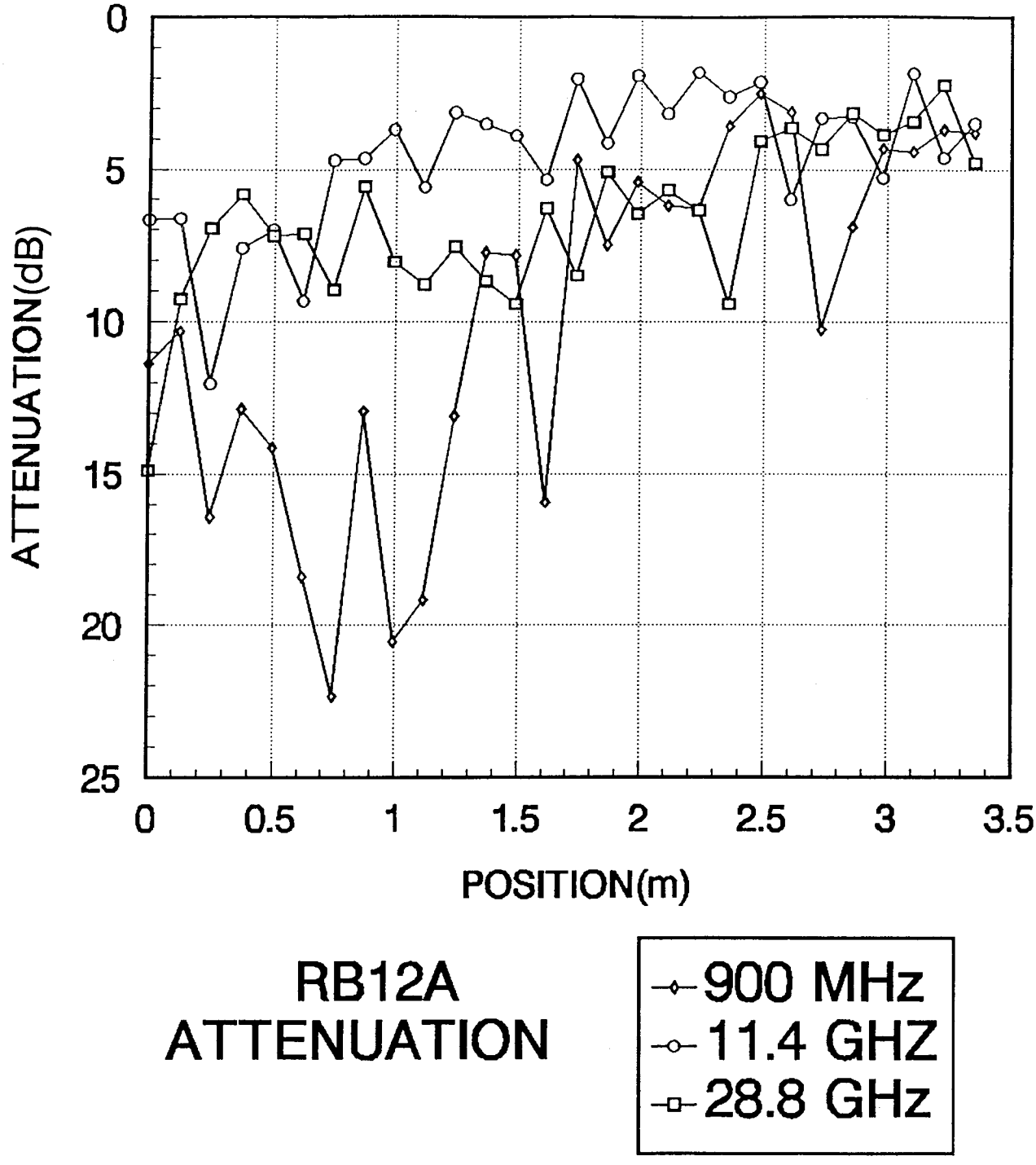

Figure A-23. Penetration loss for Radio Building path RB12A.

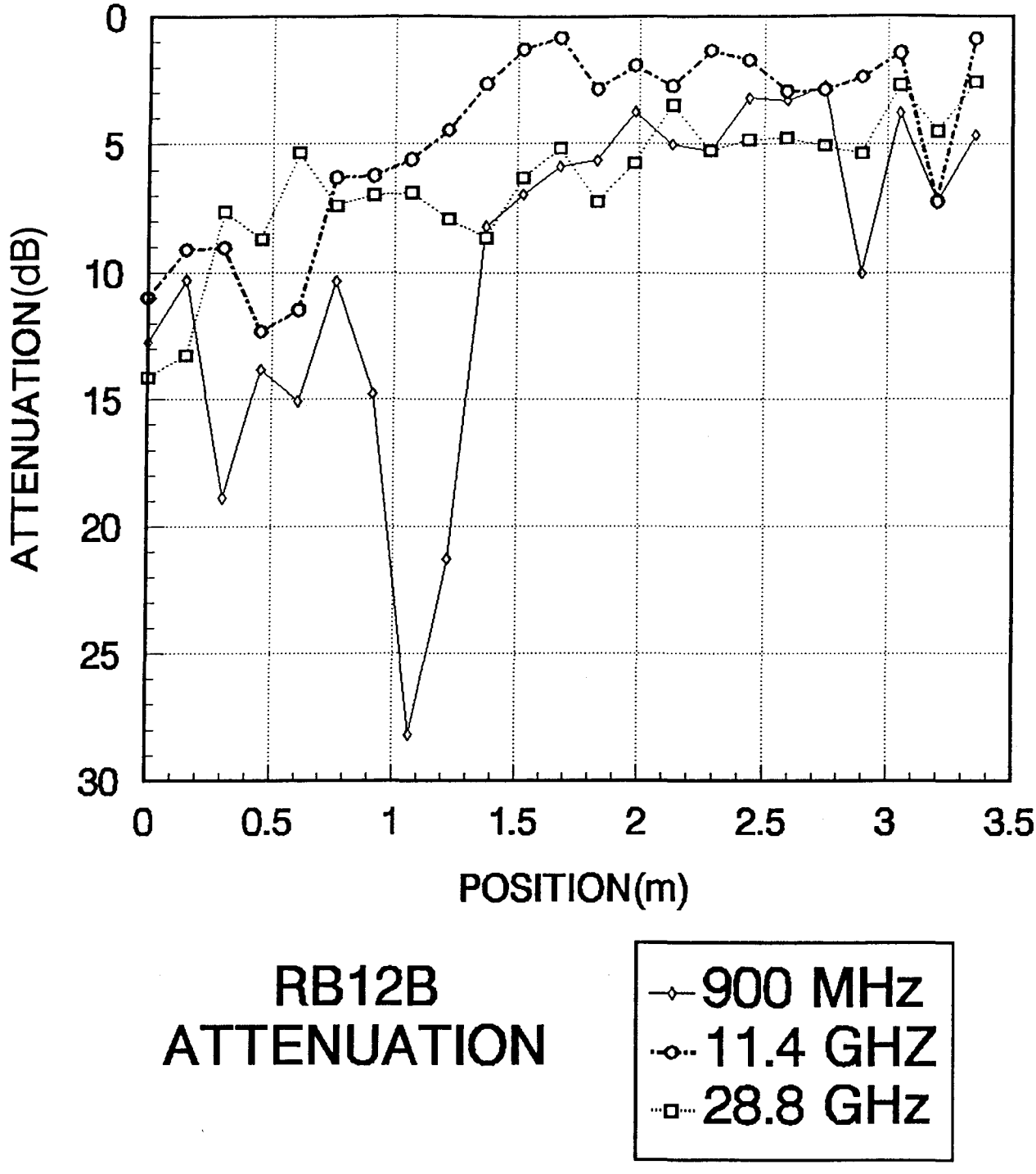

Figure A-24. Penetration loss for Radio Building path RB12B.

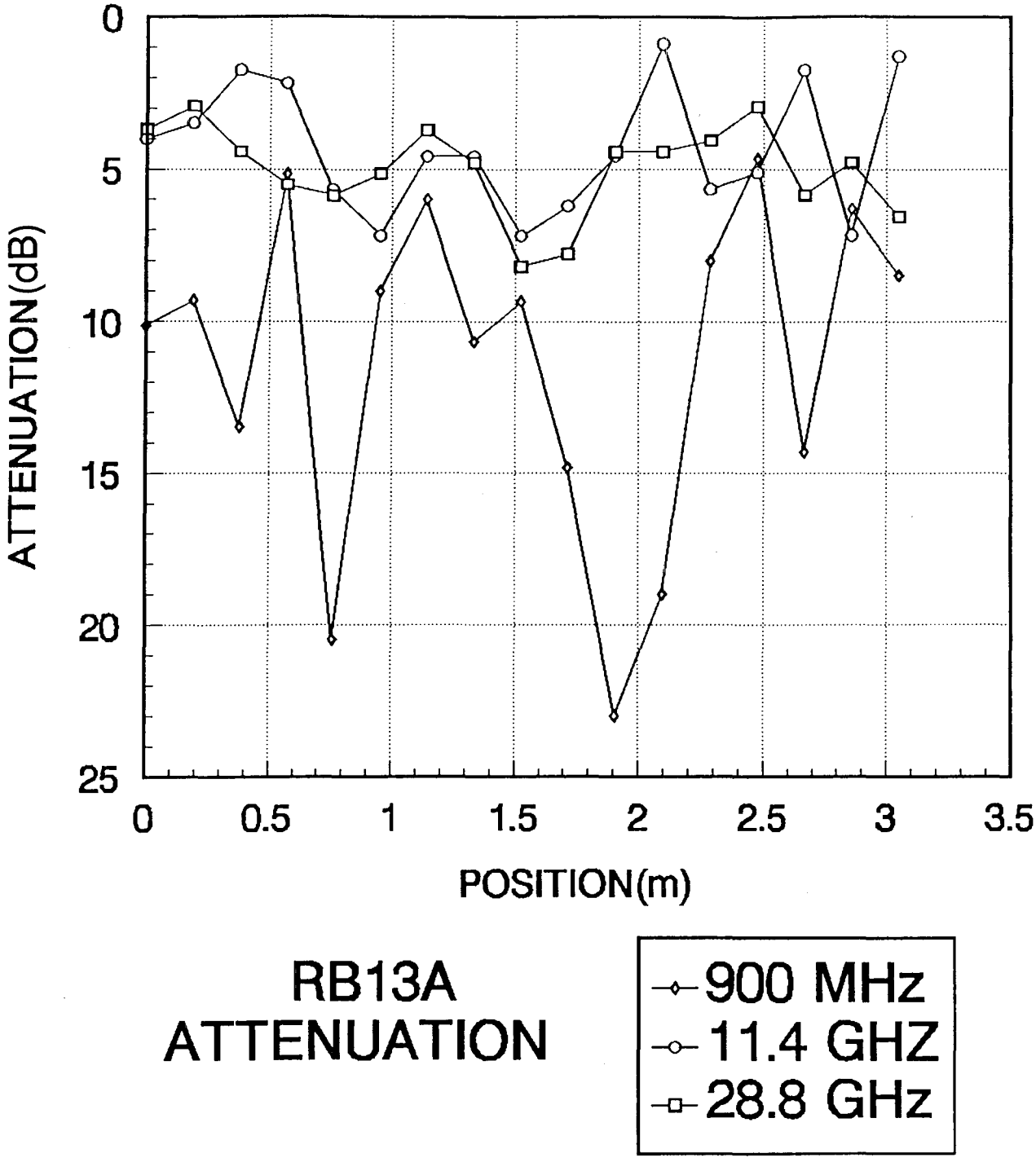

Figure A-25. Penetration loss for Radio Building path RB13A.

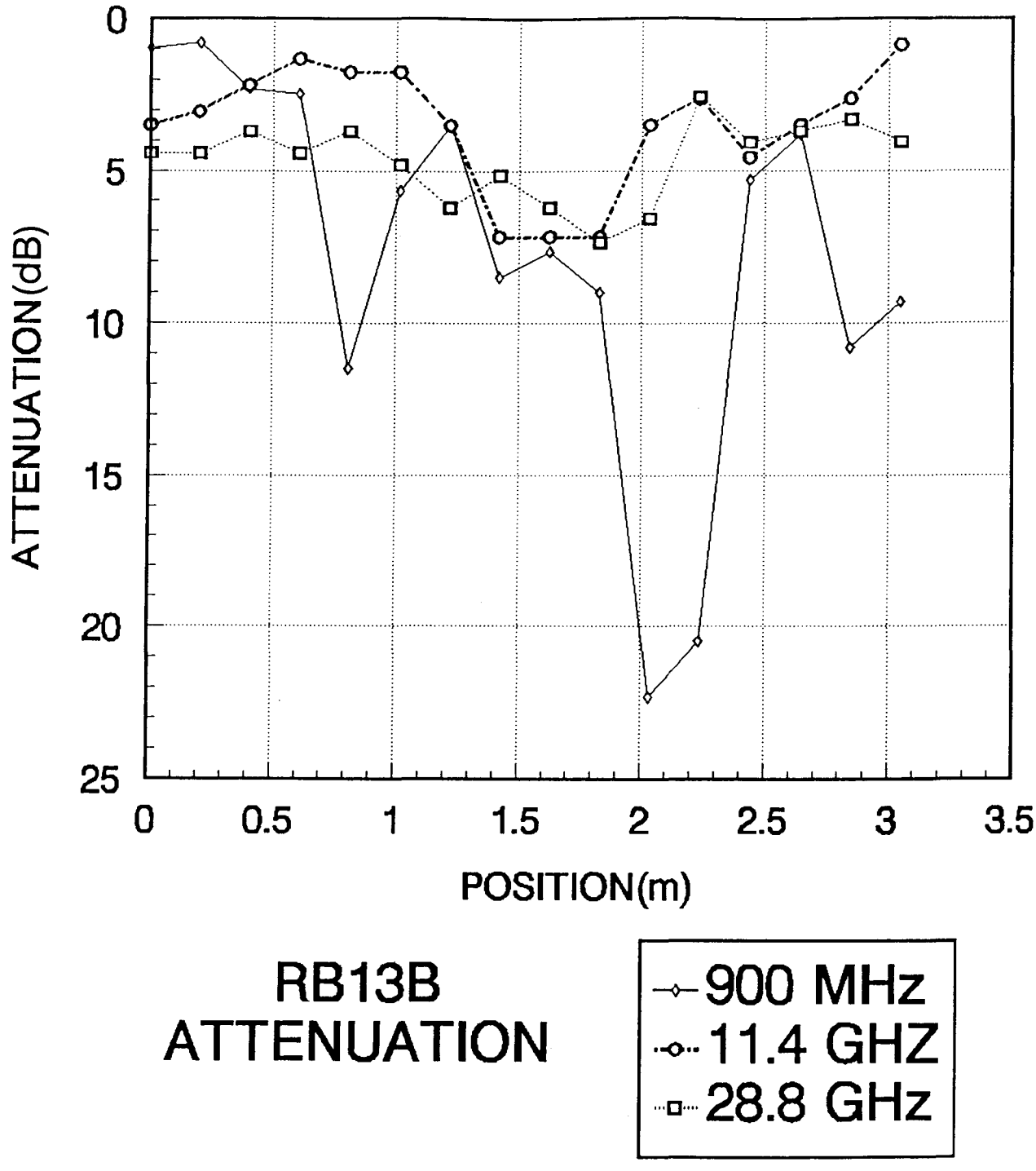

Figure A-26. Penetration loss for Radio Building RB13B.

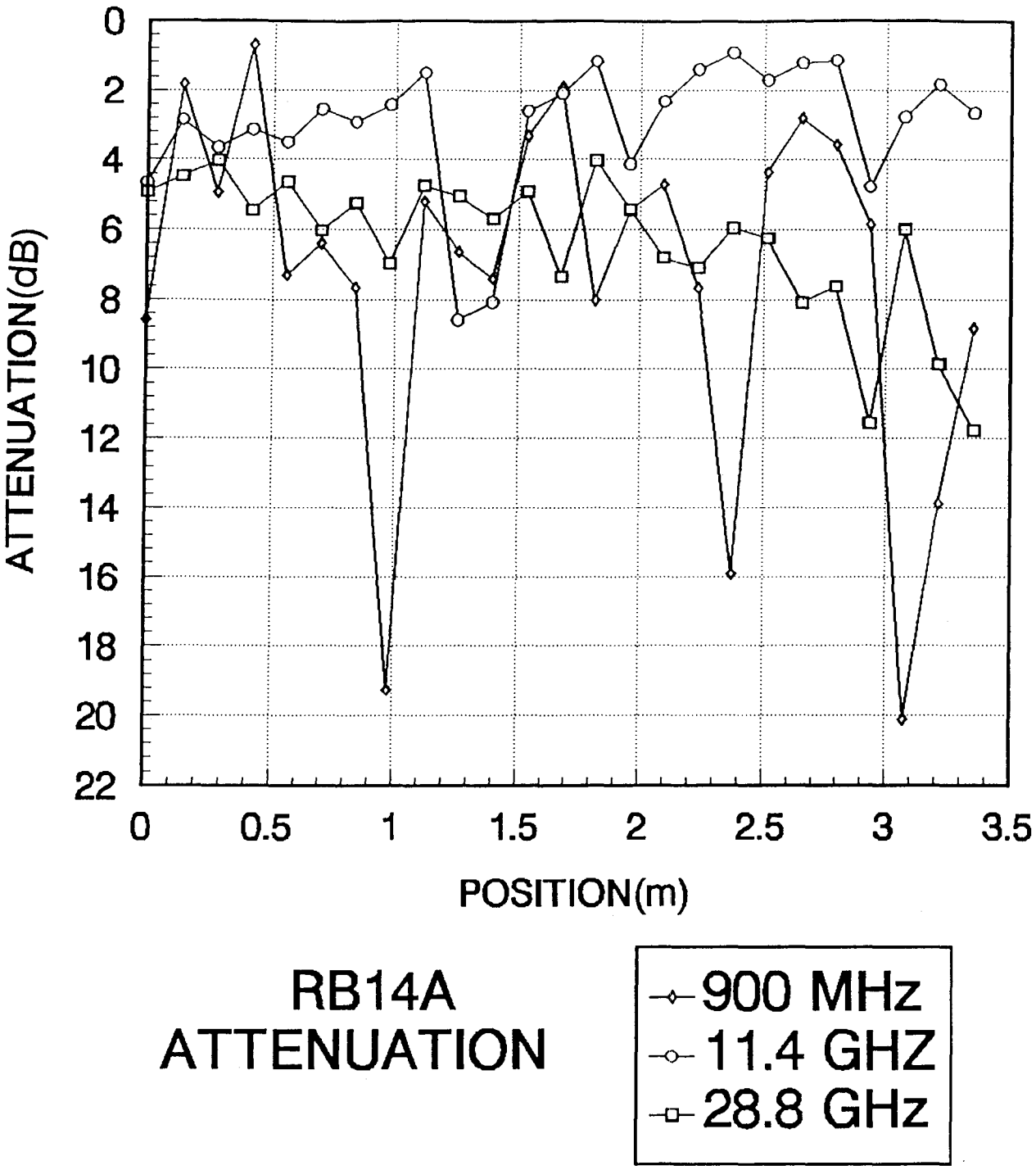

Figure A-27. Penetration loss for Radio Building path RB14A.

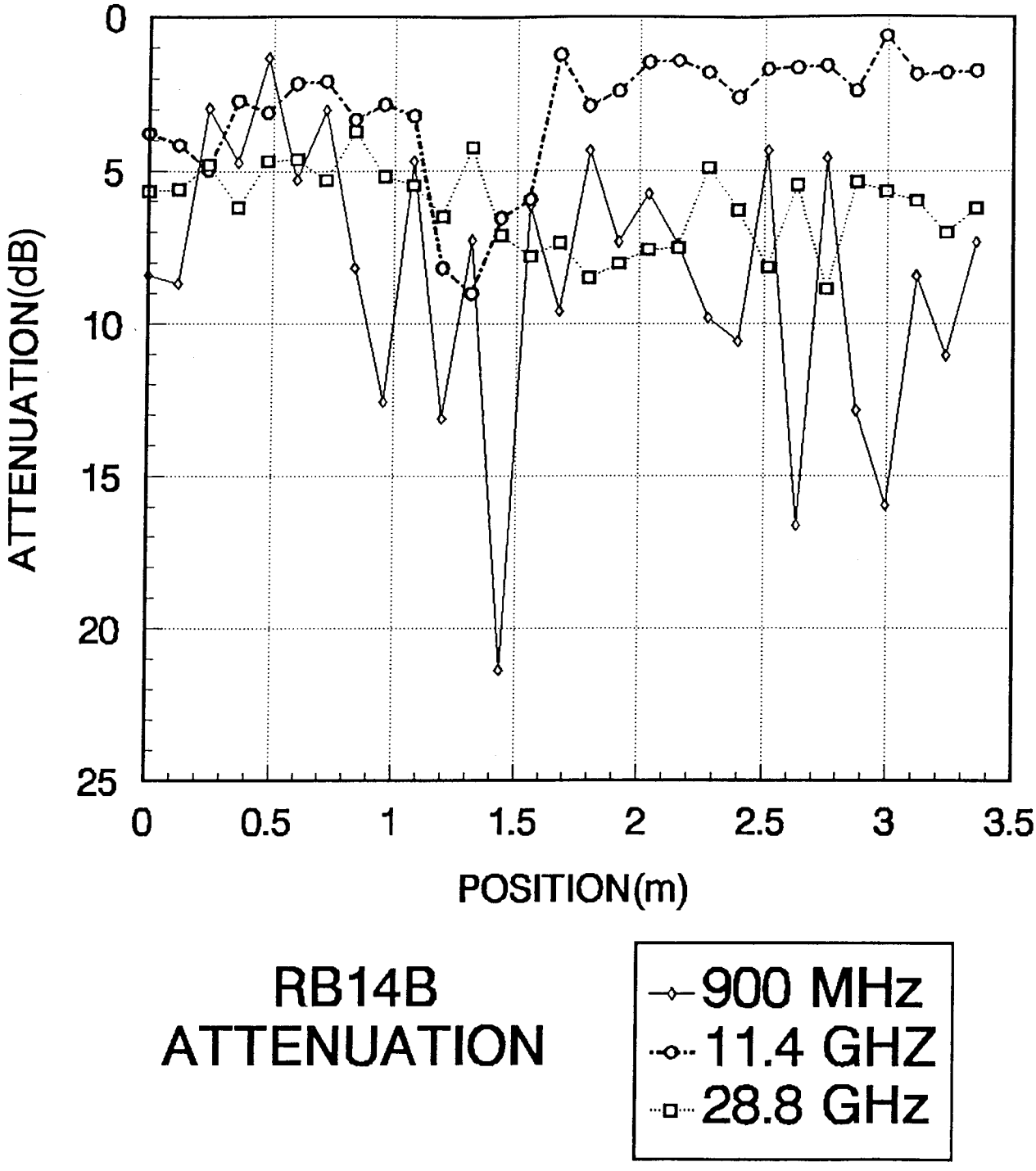

Figure A-28. Penetration loss for Radio Building path RB14B.

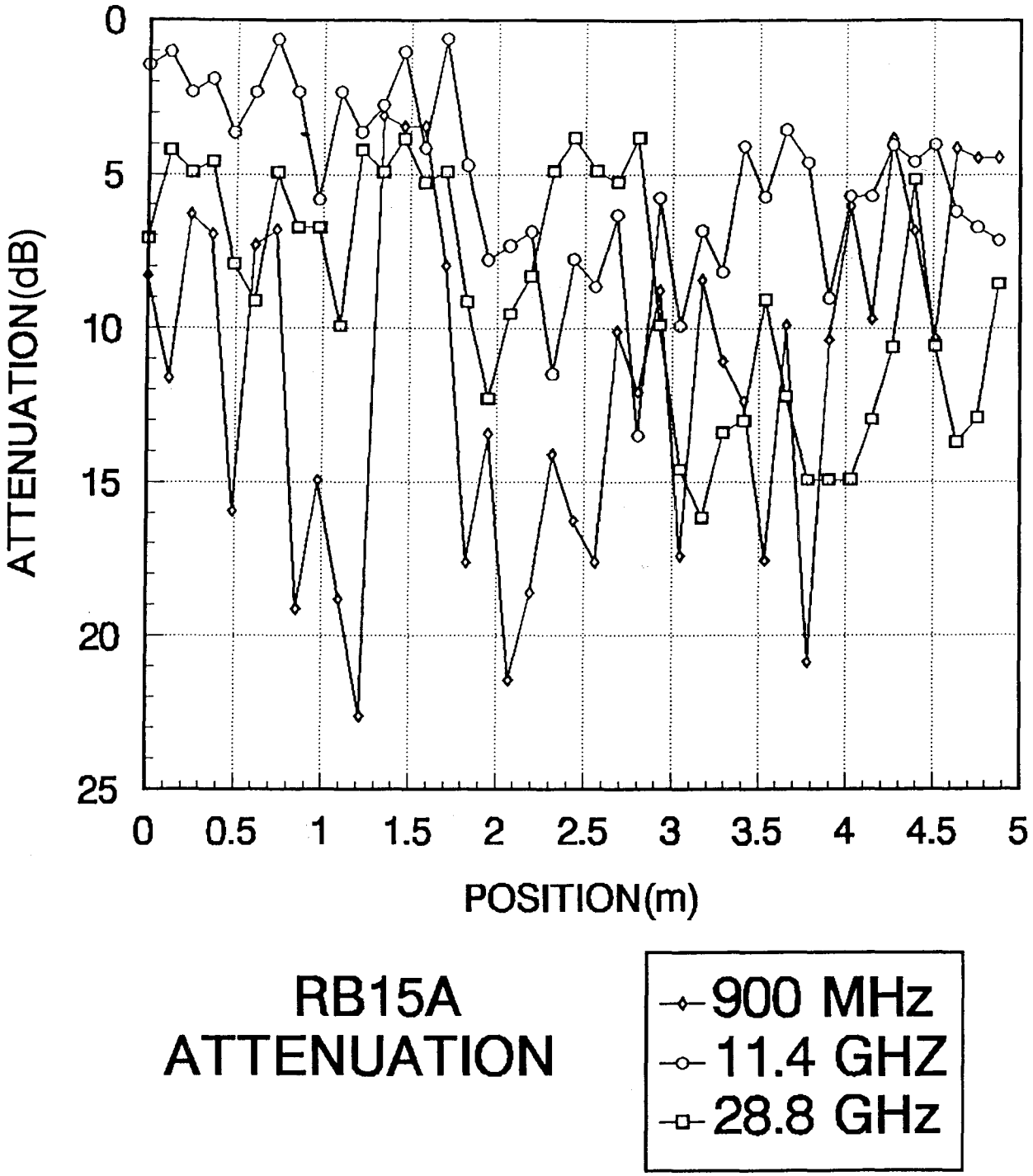

Figure A-29. Penetration loss for Radio Building path RB15A.

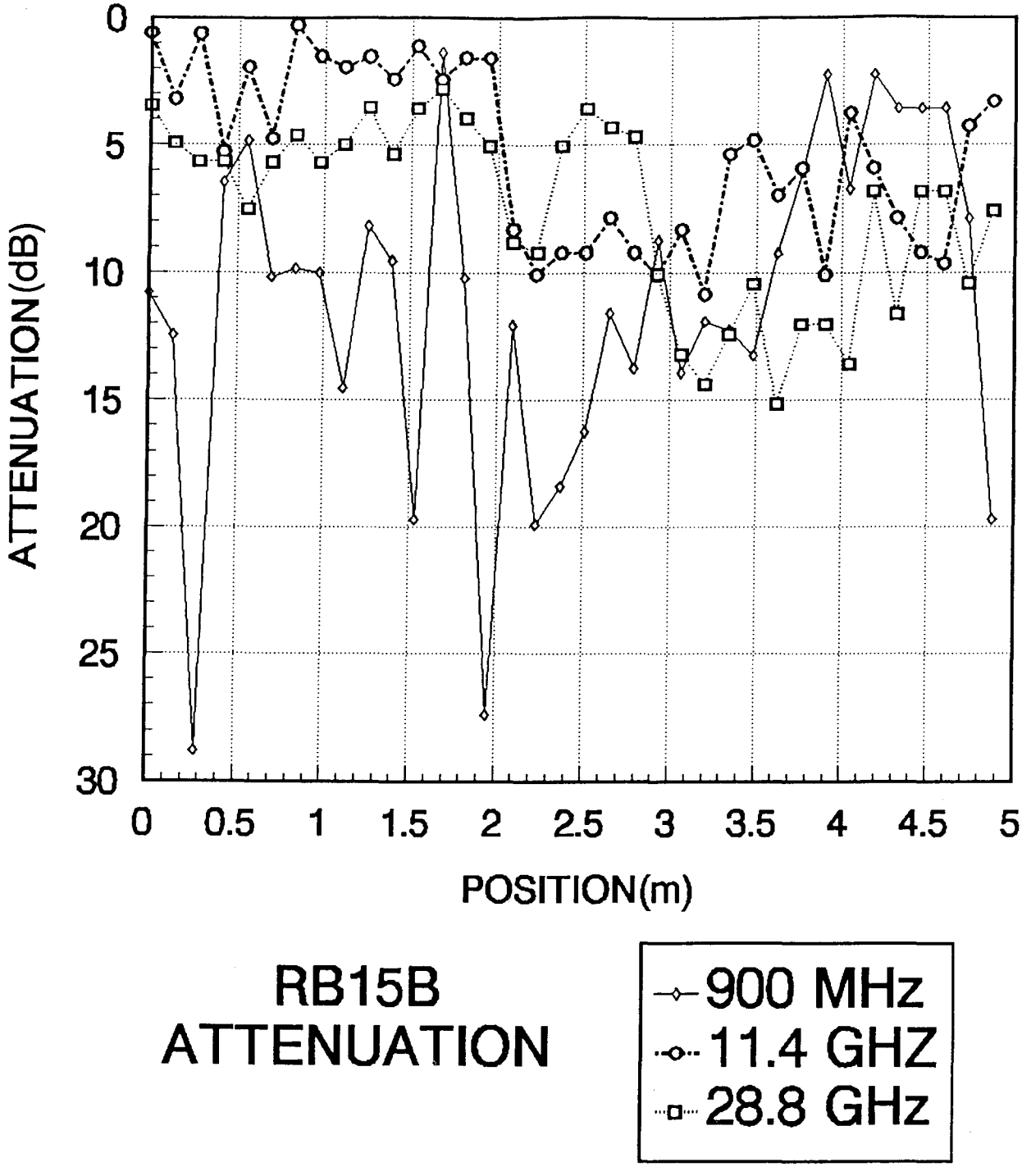

Figure A-30. Penetration loss for Radio Building path RB15B.

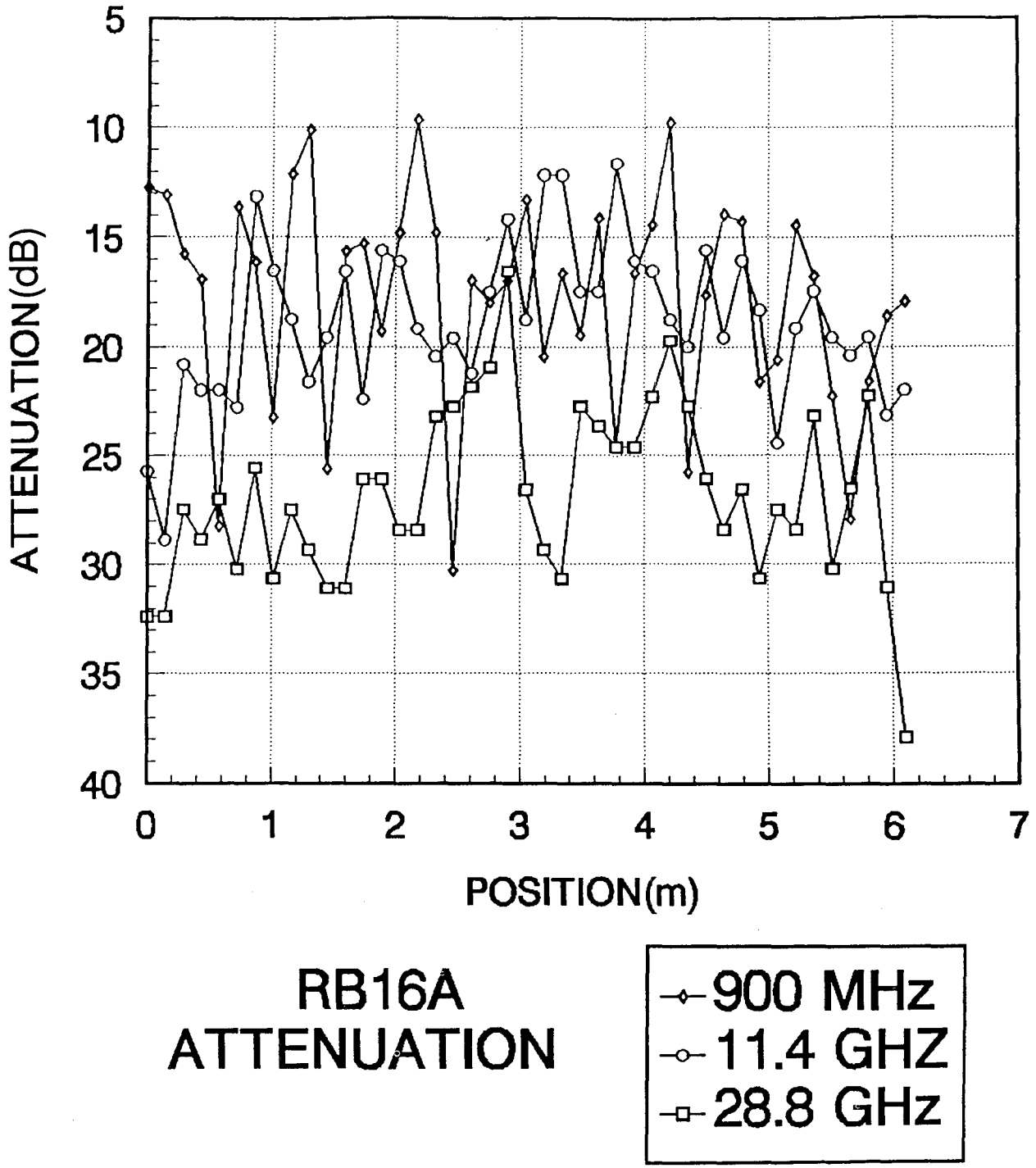

Figure A-31. Penetration loss for Radio Building path RB16A.

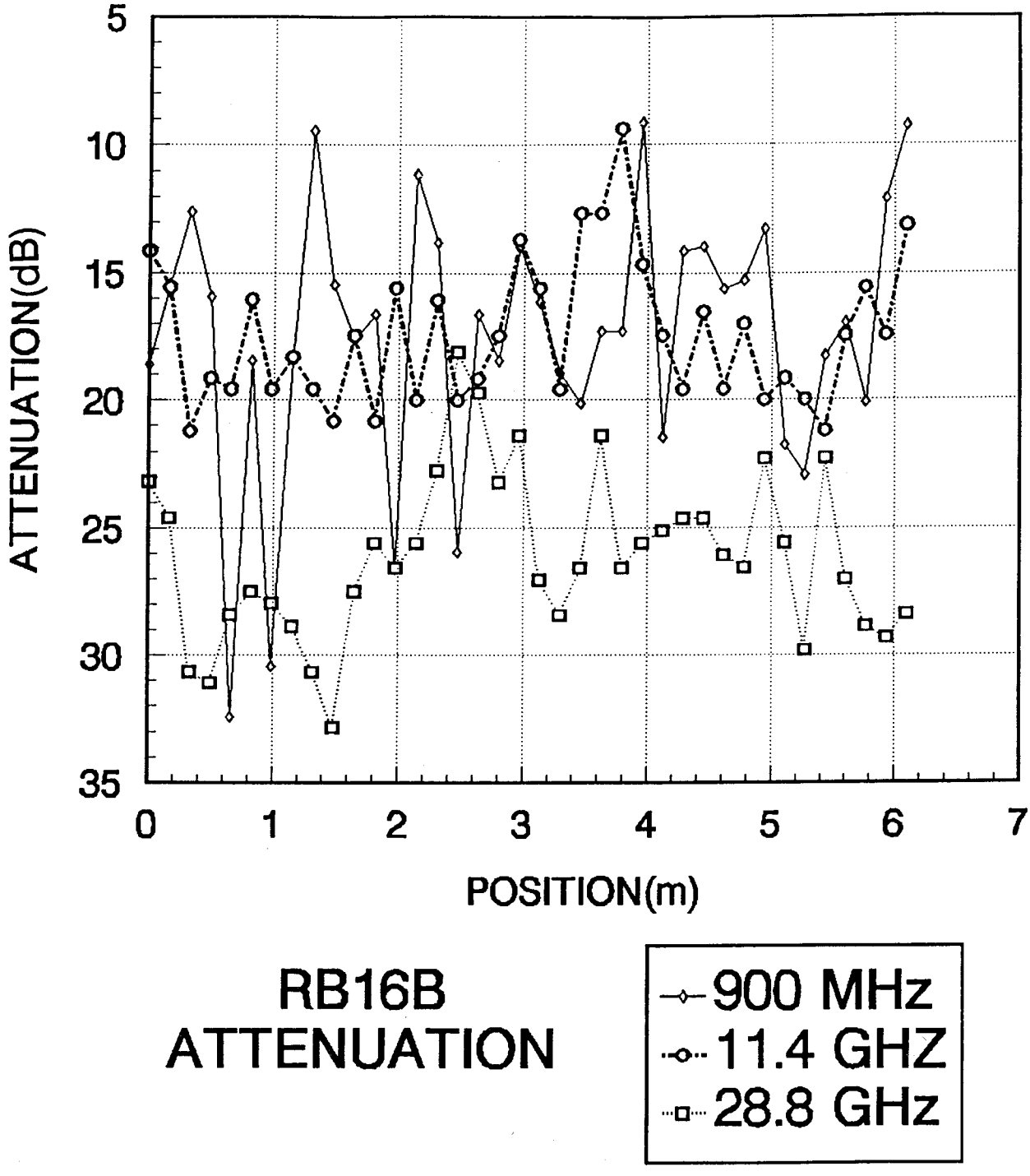

Figure A-32. Penetration loss for Radio Building path RB16B.

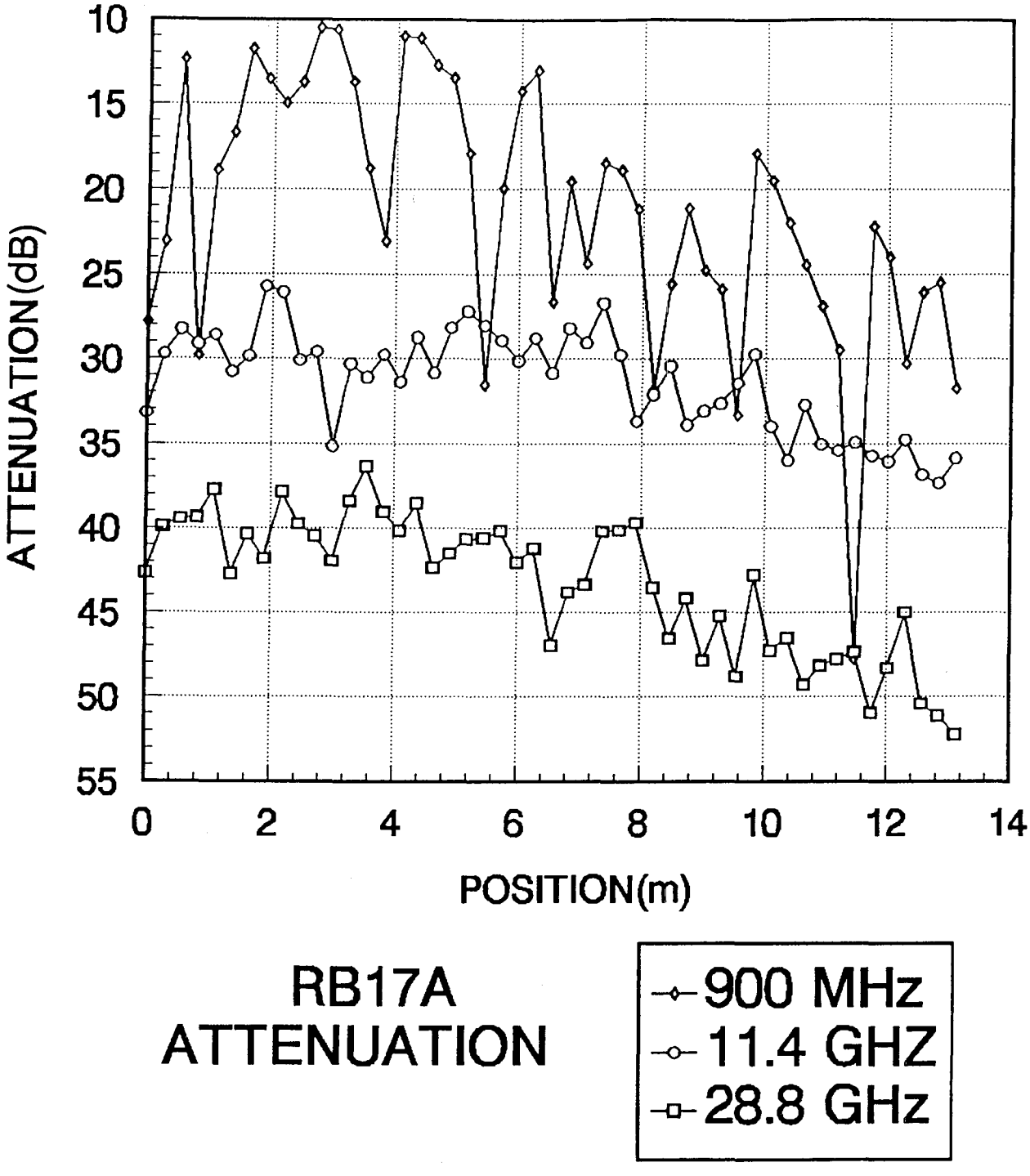

Figure A-33. Penetration loss for Radio Building path RB17A.

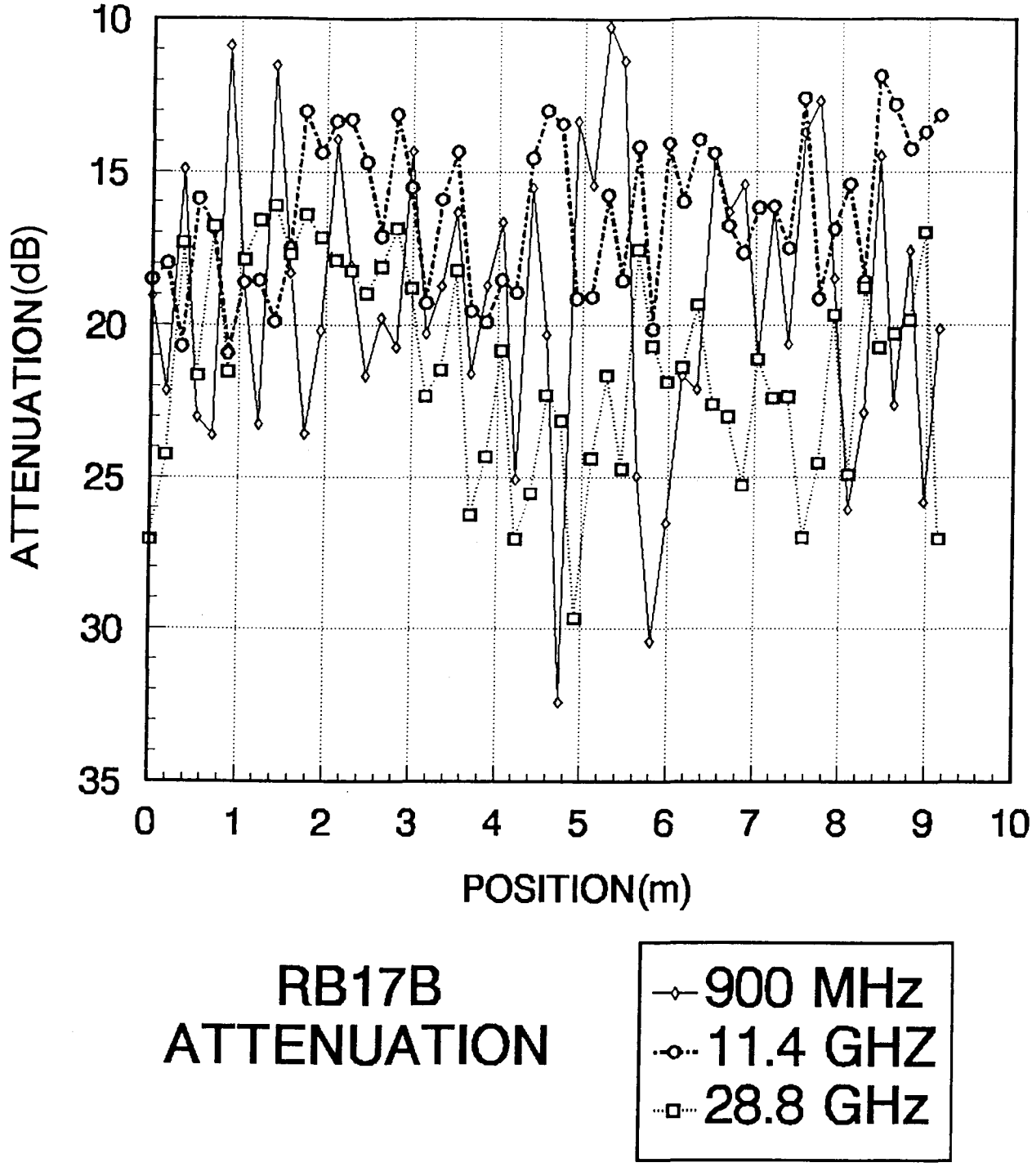

Figure A-34. Penetration loss for Radio Building path RB17B.

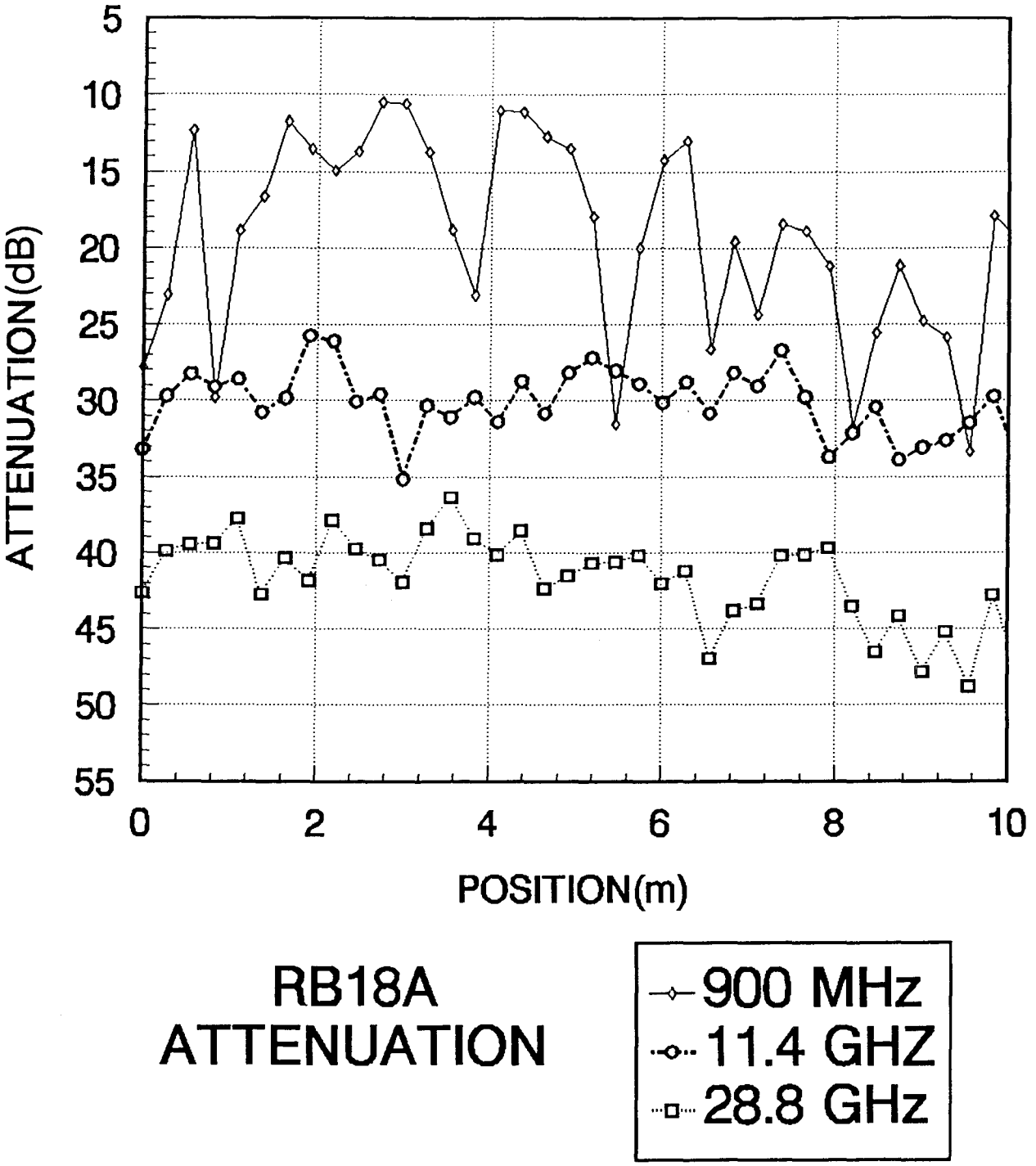

Figure A-35. Penetration loss for Radio Building path RB18A.

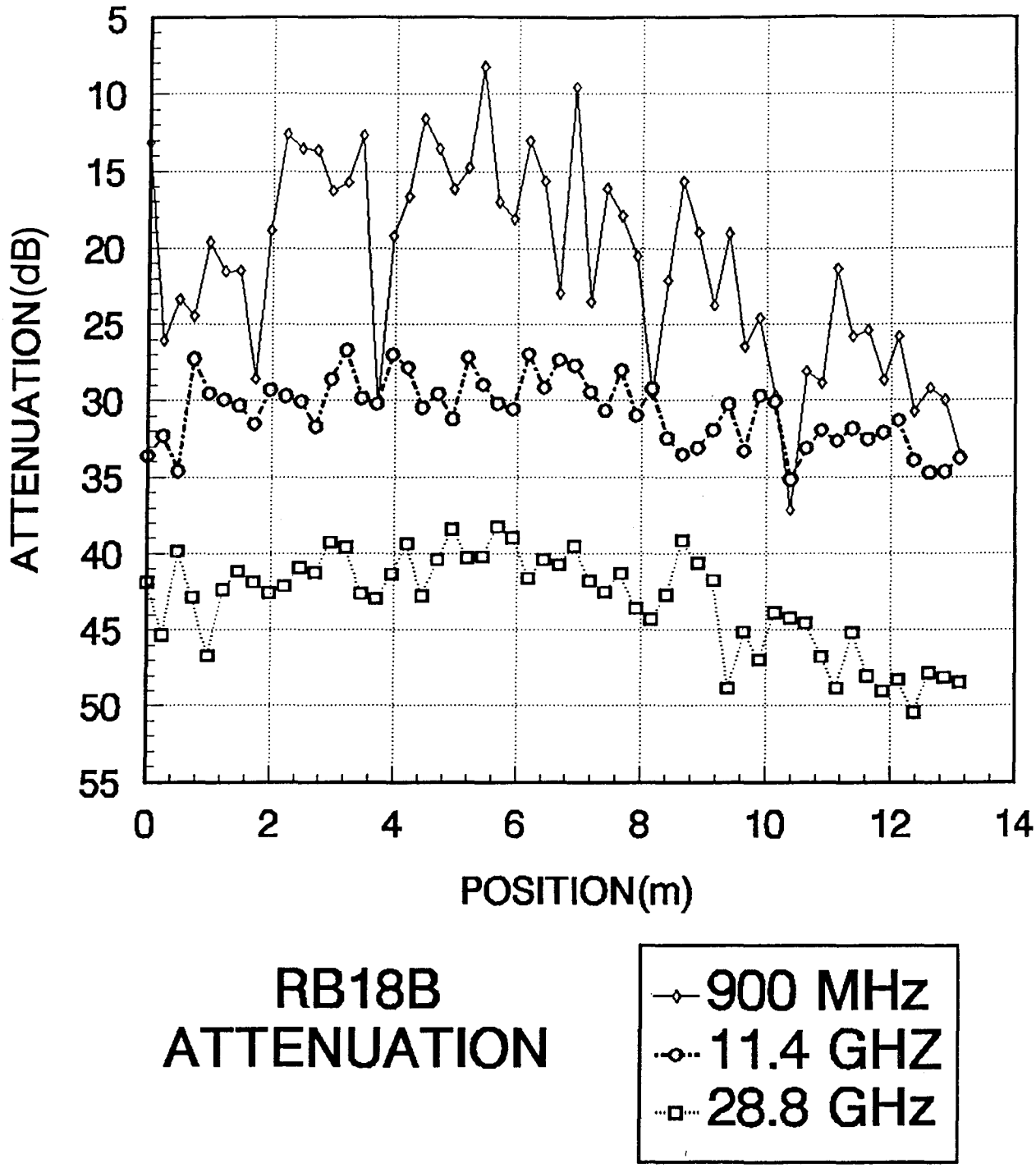

Figure A-36. Penetration loss for Radio Building path RB18B.

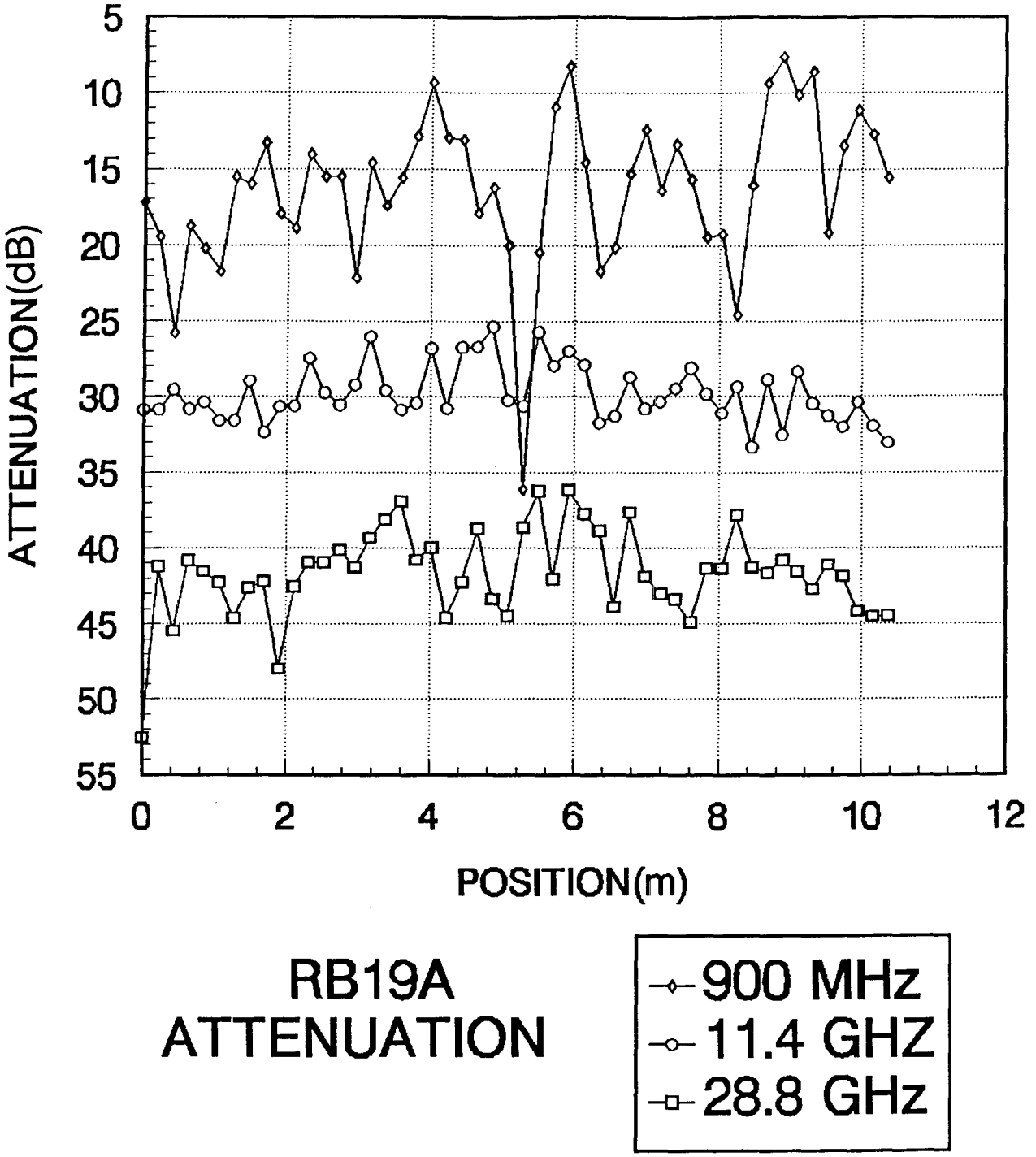

Figure A-37. Penetration loss for Radio Building path RB19A.

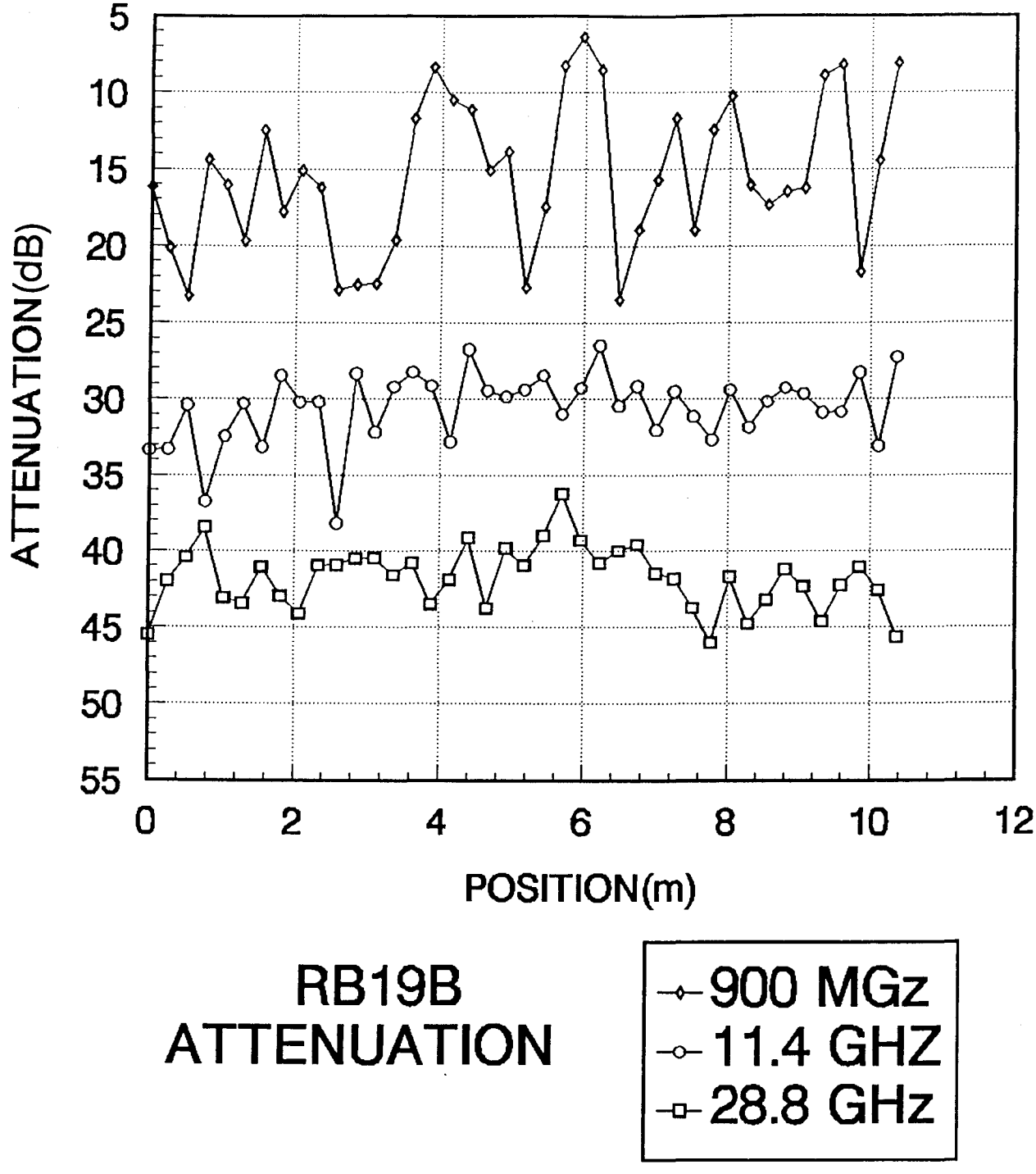

Figure A-38. Penetration loss for Radio Building path RB19B.

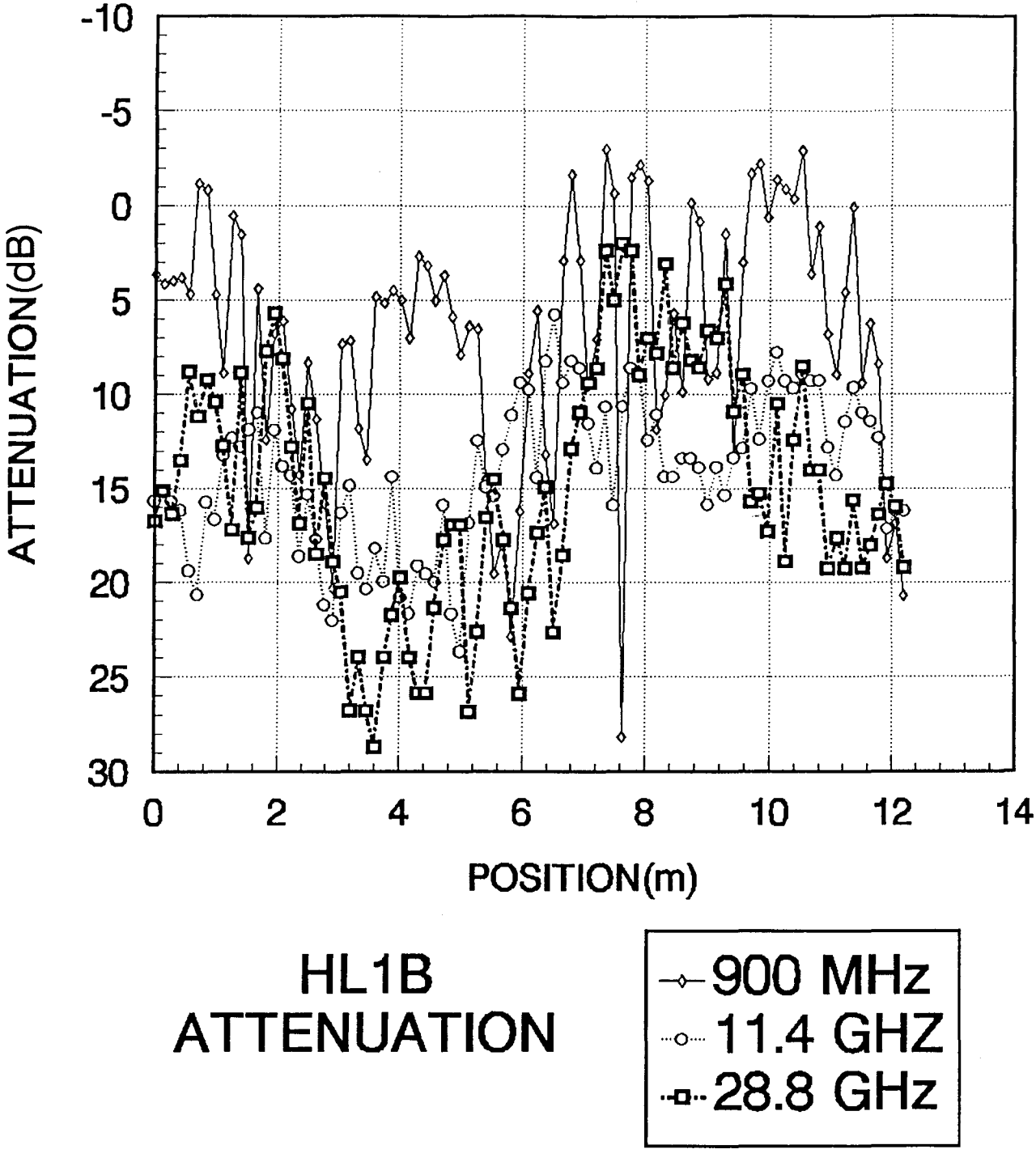

Figure A-39. Penetration loss for private residence path HL1B.

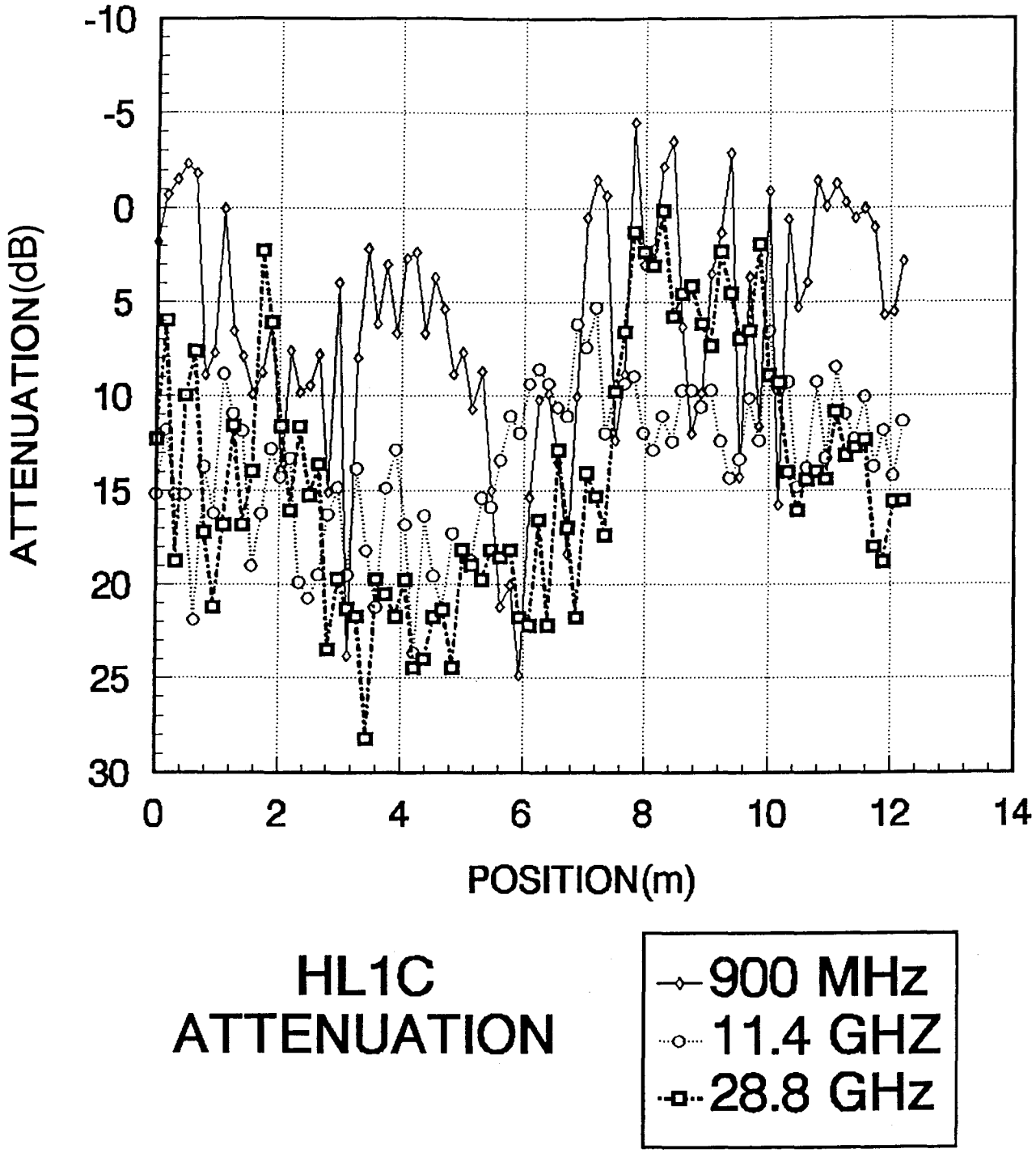

Figure A-40. Penetration loss for private residence path HL1C.

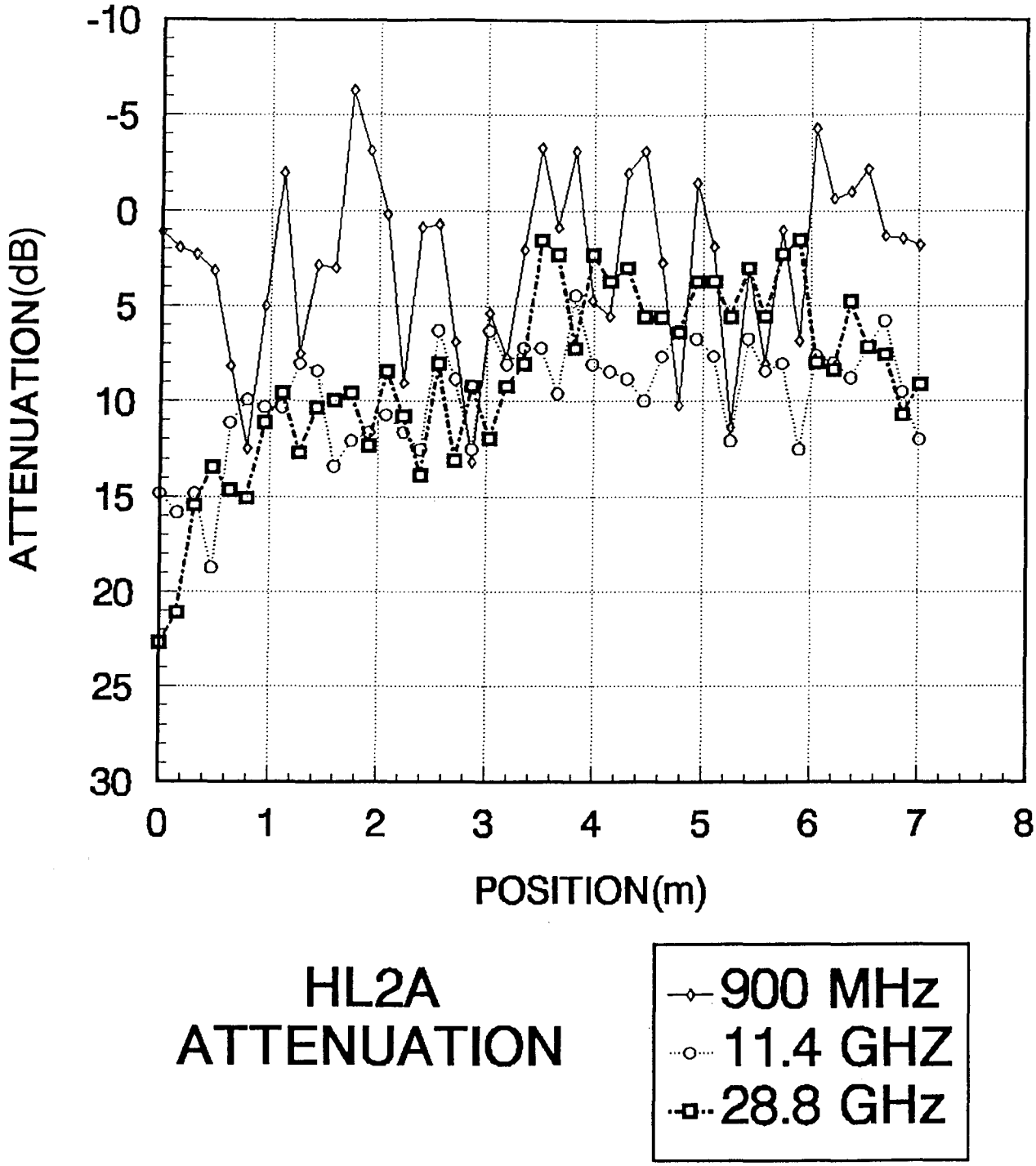

Figure A-41. Penetration loss for private residence path HL2A.

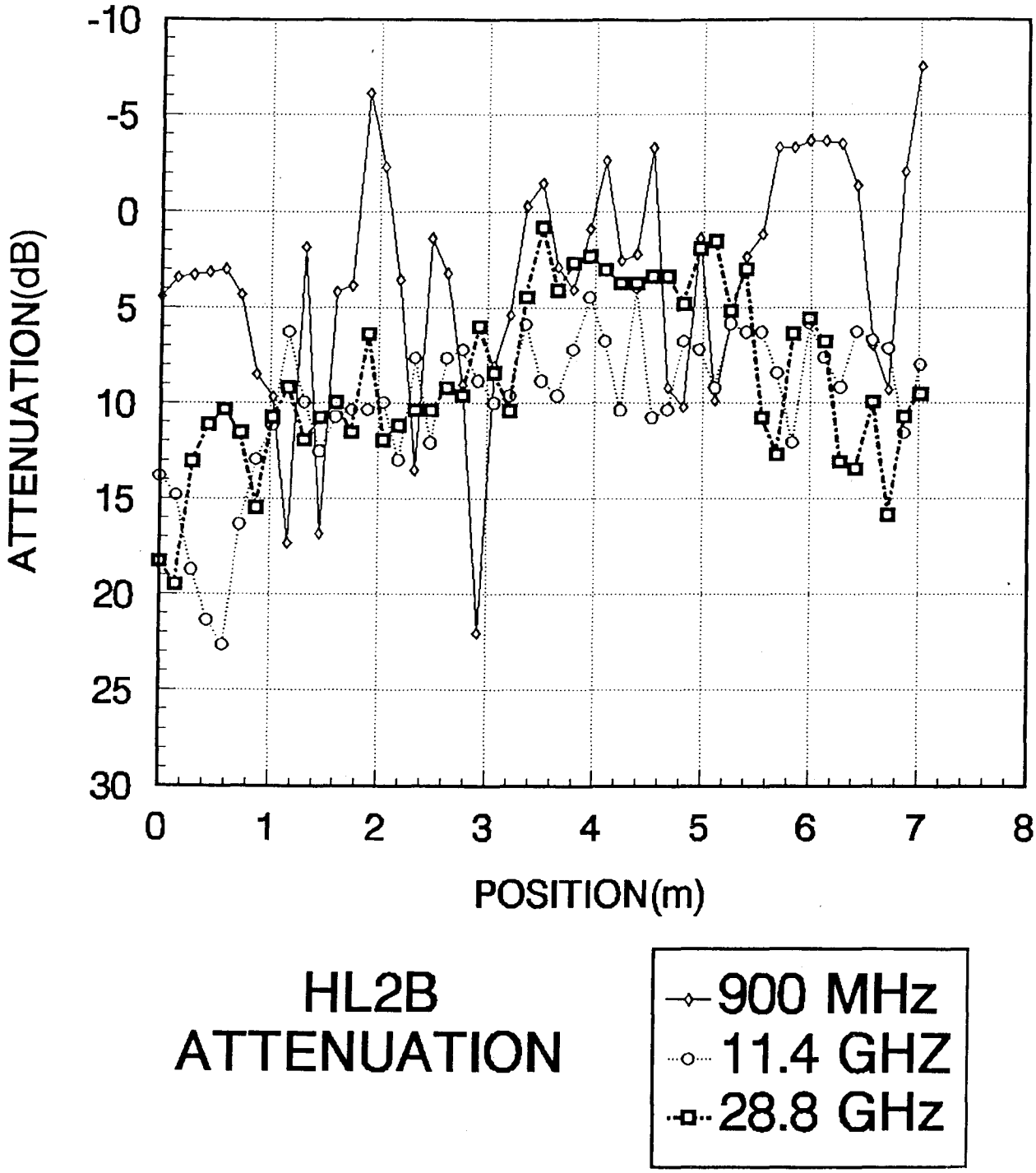

Figure A-42. Penetration loss for private residence path HL2B.

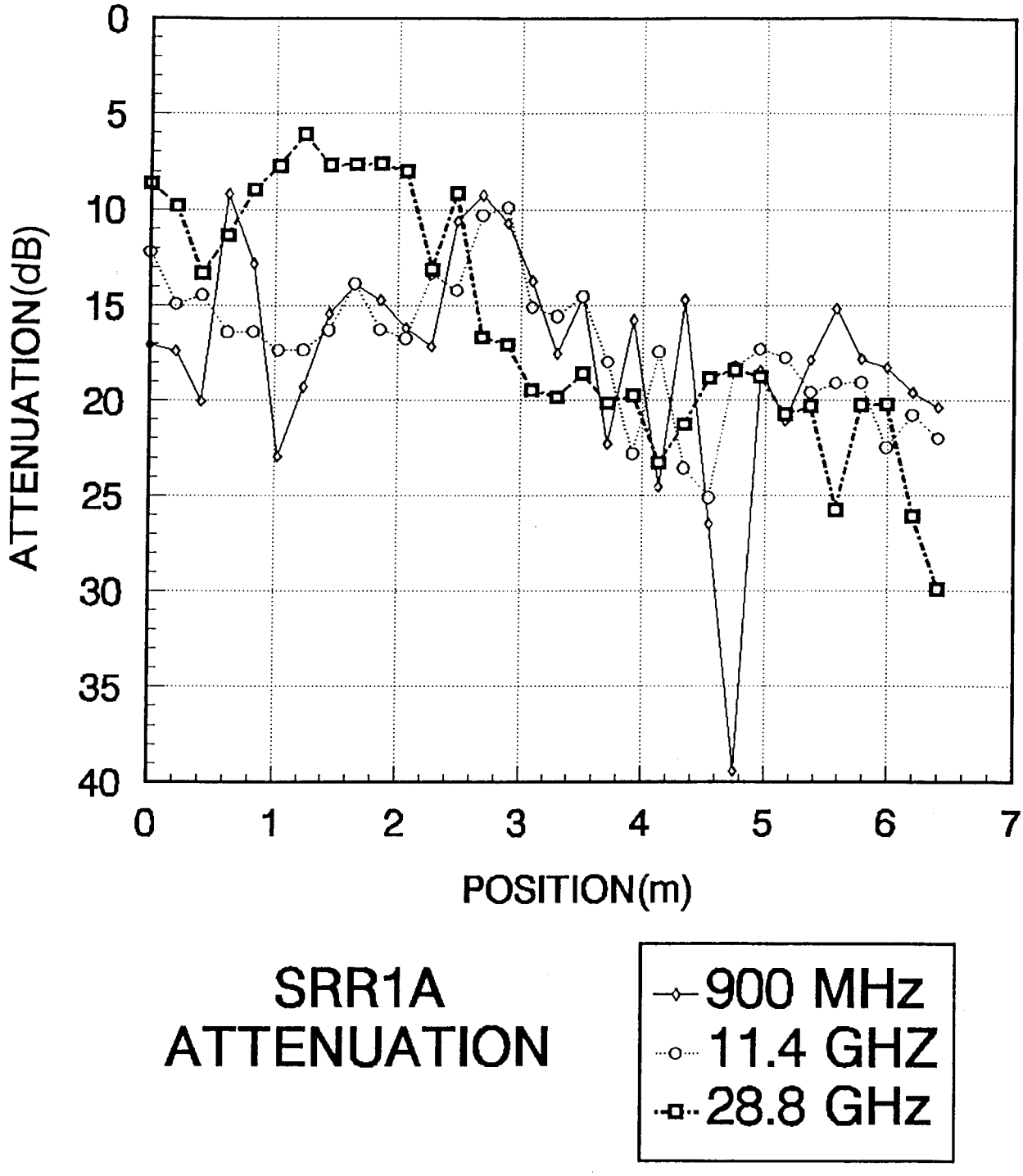

Figure A-43. Penetration loss for storeroom path SRR1A.

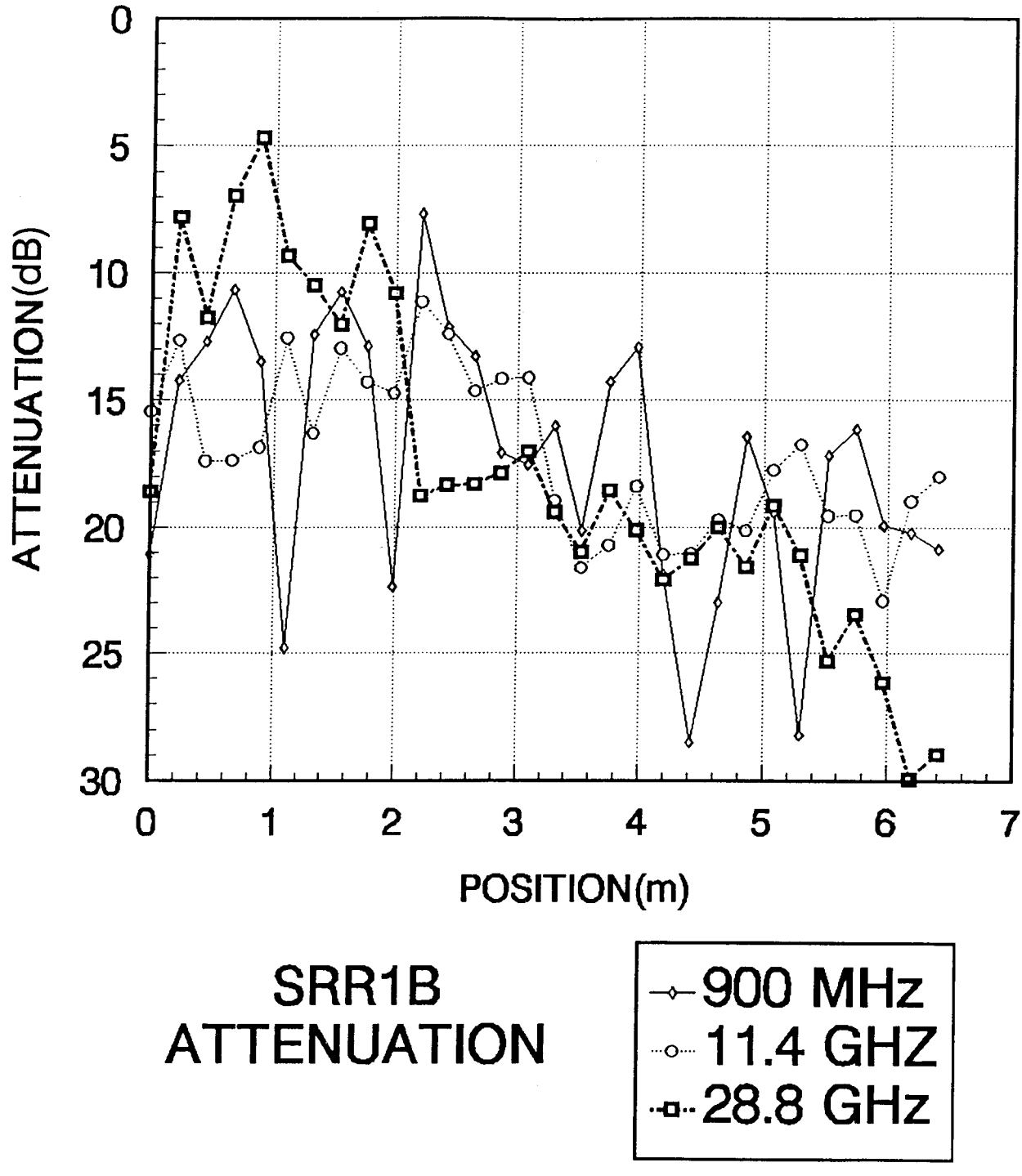

Figure A-44. Penetration loss for storeroom path SRR1B.

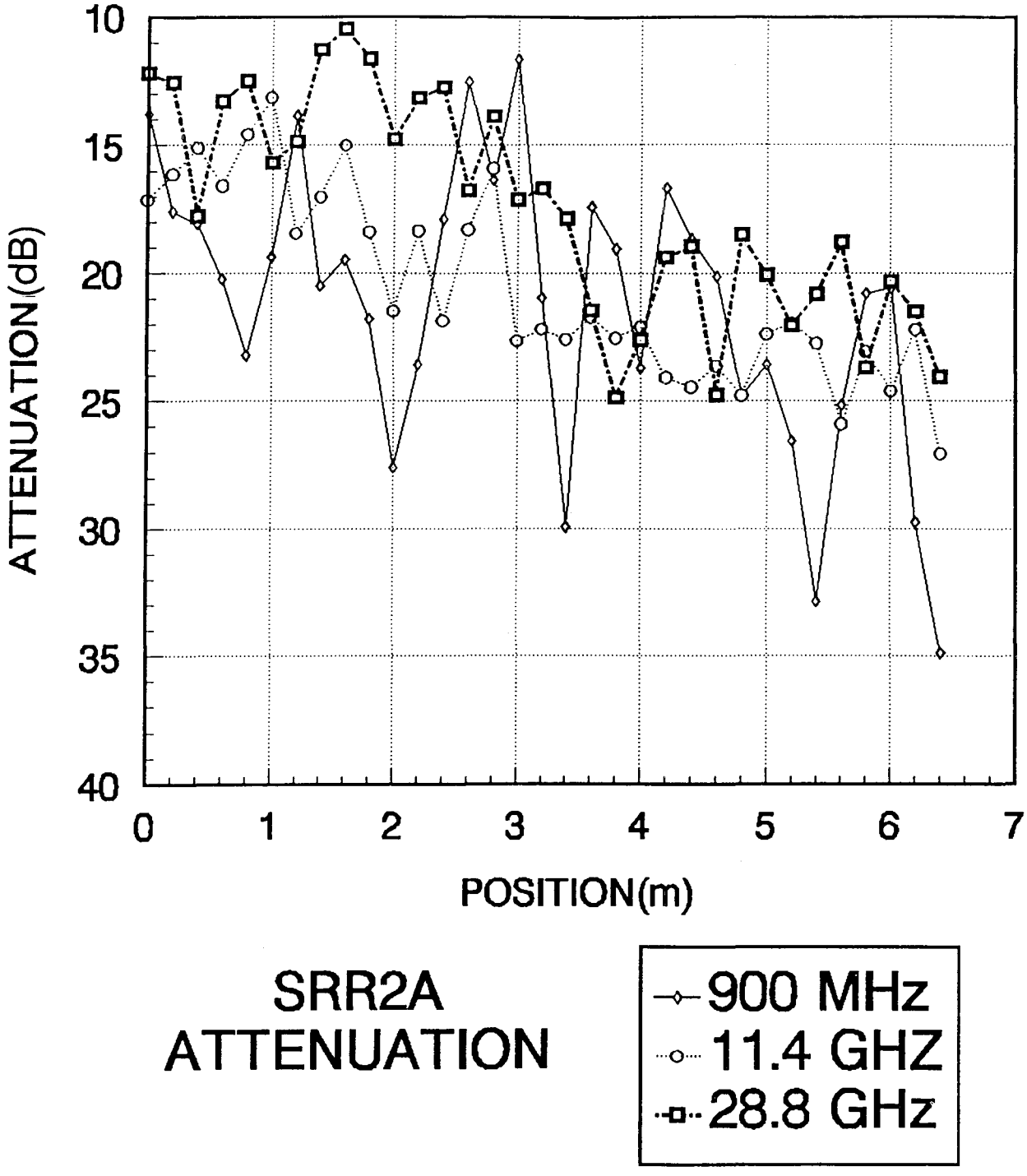

Figure A-45. Penetration loss for storeroom path SRR2A.

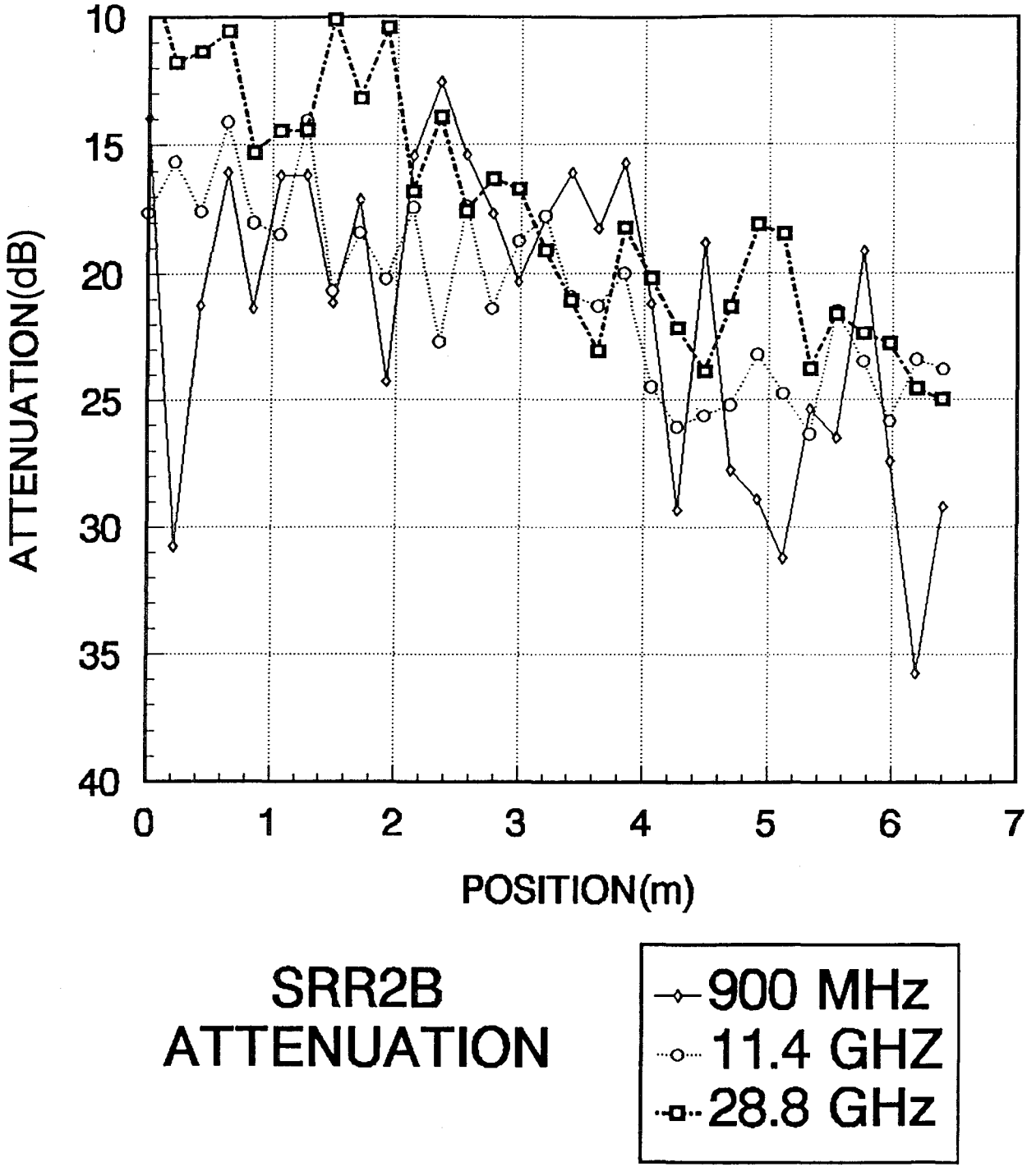

Figure A-46. Penetration loss for storeroom path SRR2B.

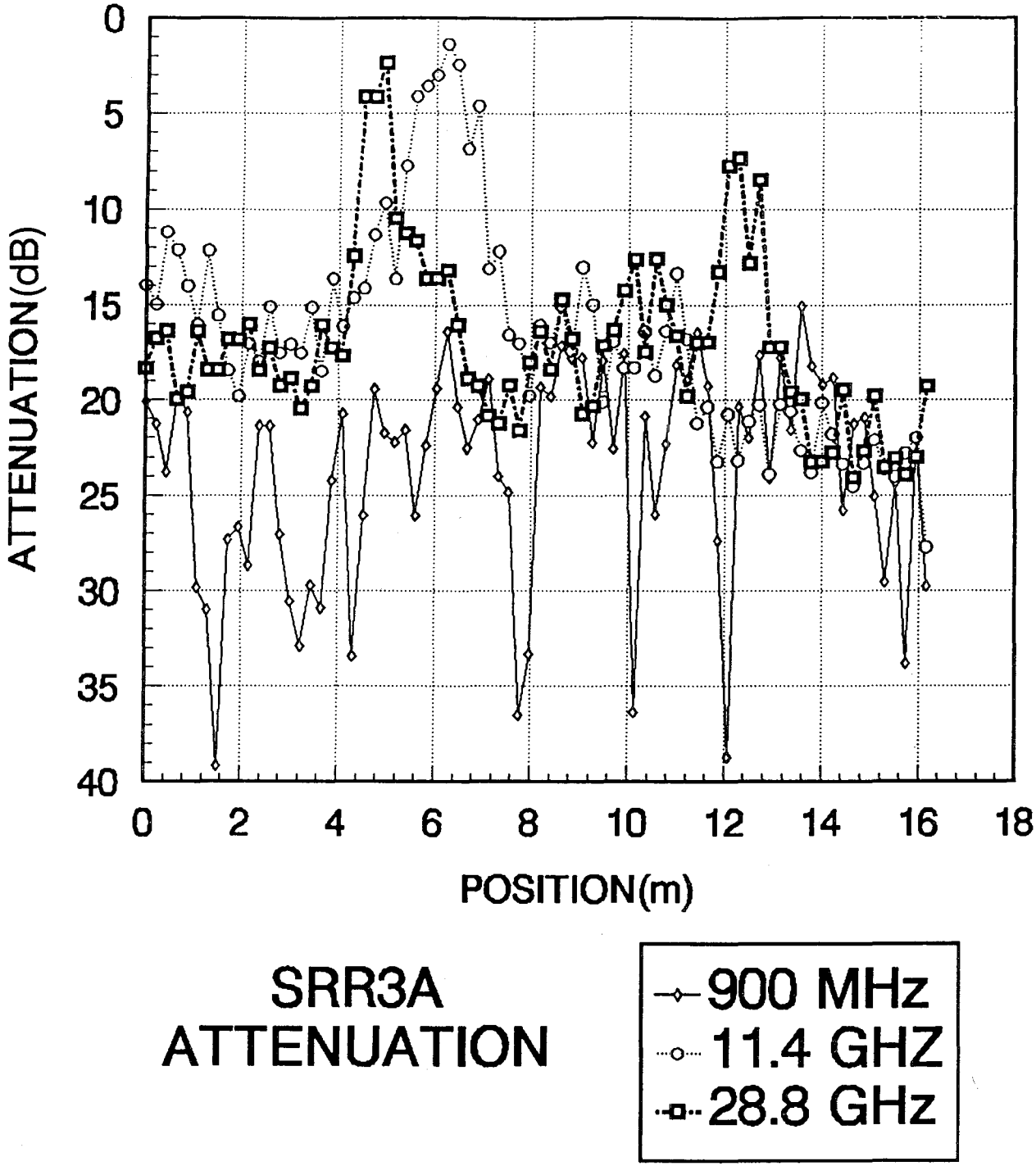

Figure A-47. Penetration loss for storeroom path SRR3A.

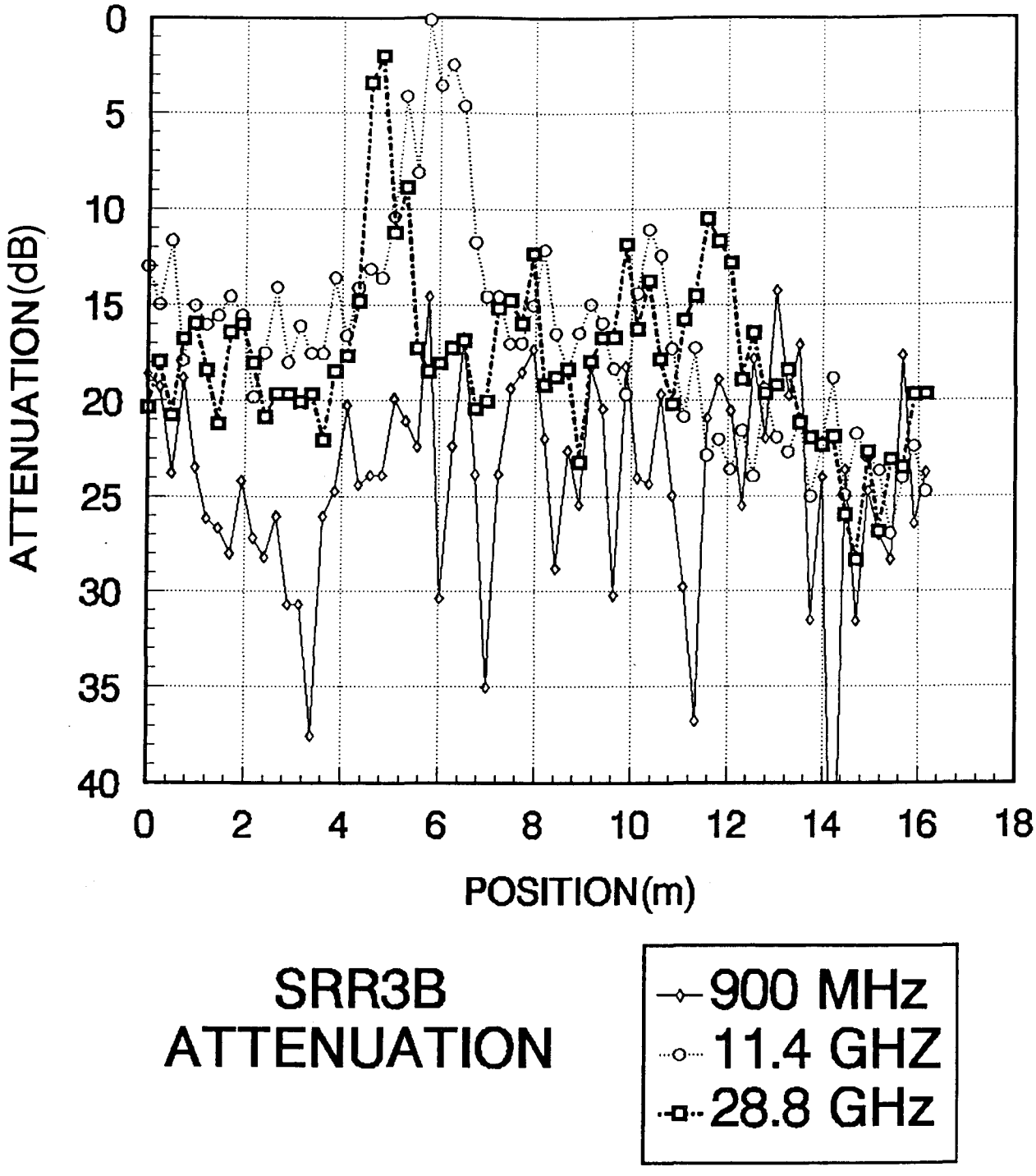

Figure A-48. Penetration loss for storeroom path SRR3B.

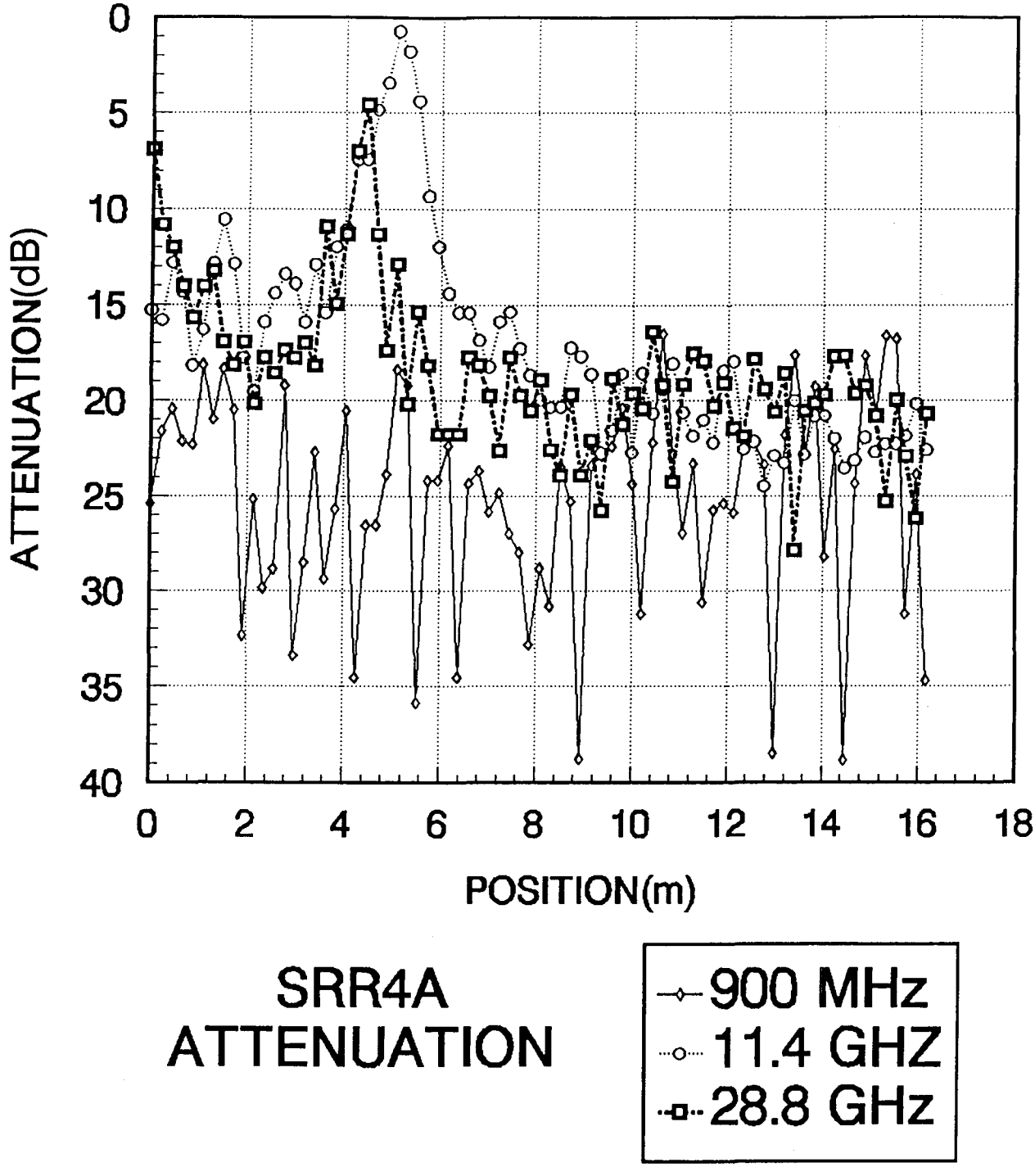

Figure A-49. Penetration loss for storeroom path SRR4A.

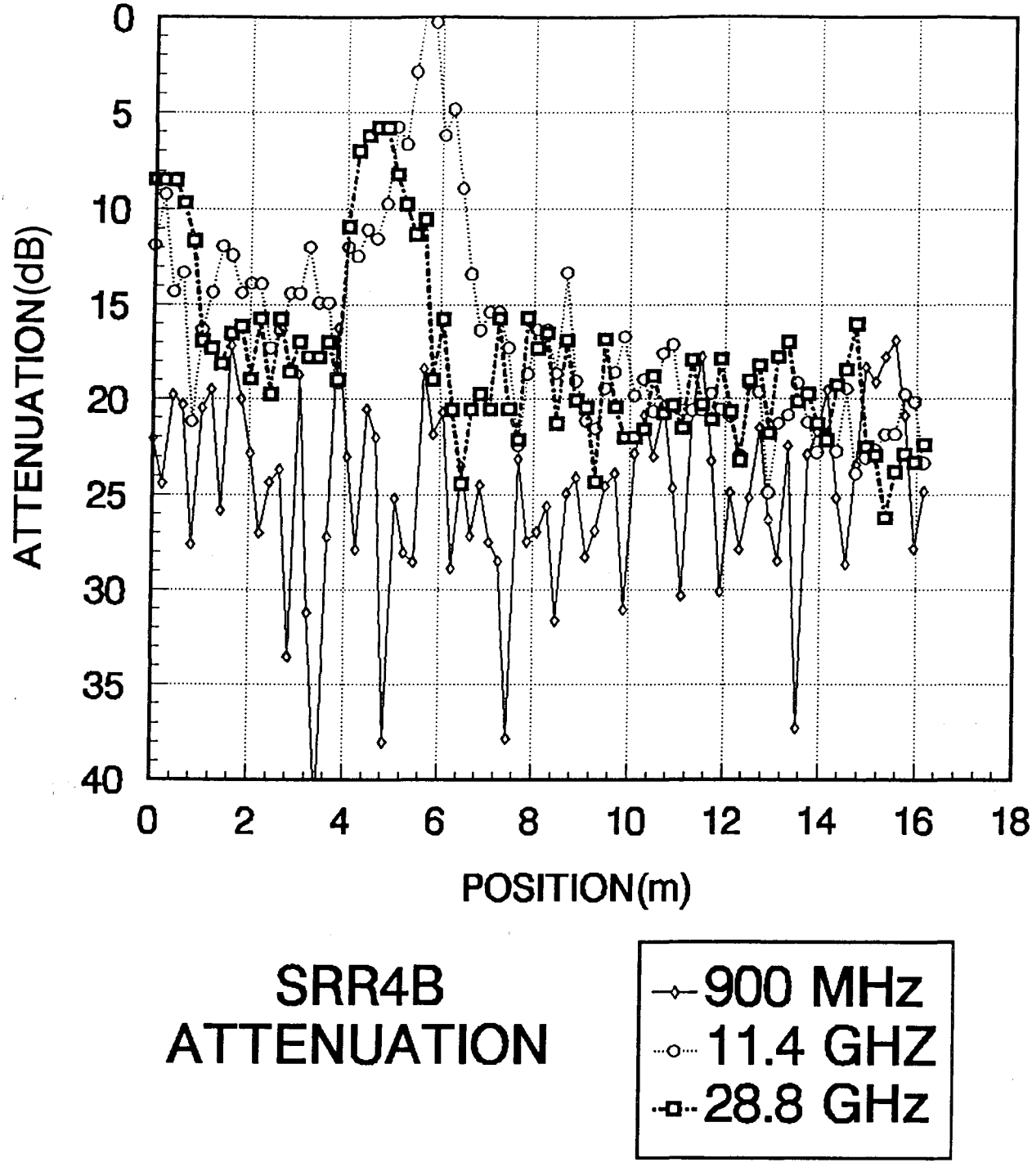

Figure A-50. Penetration loss for storeroom path SRR4B.

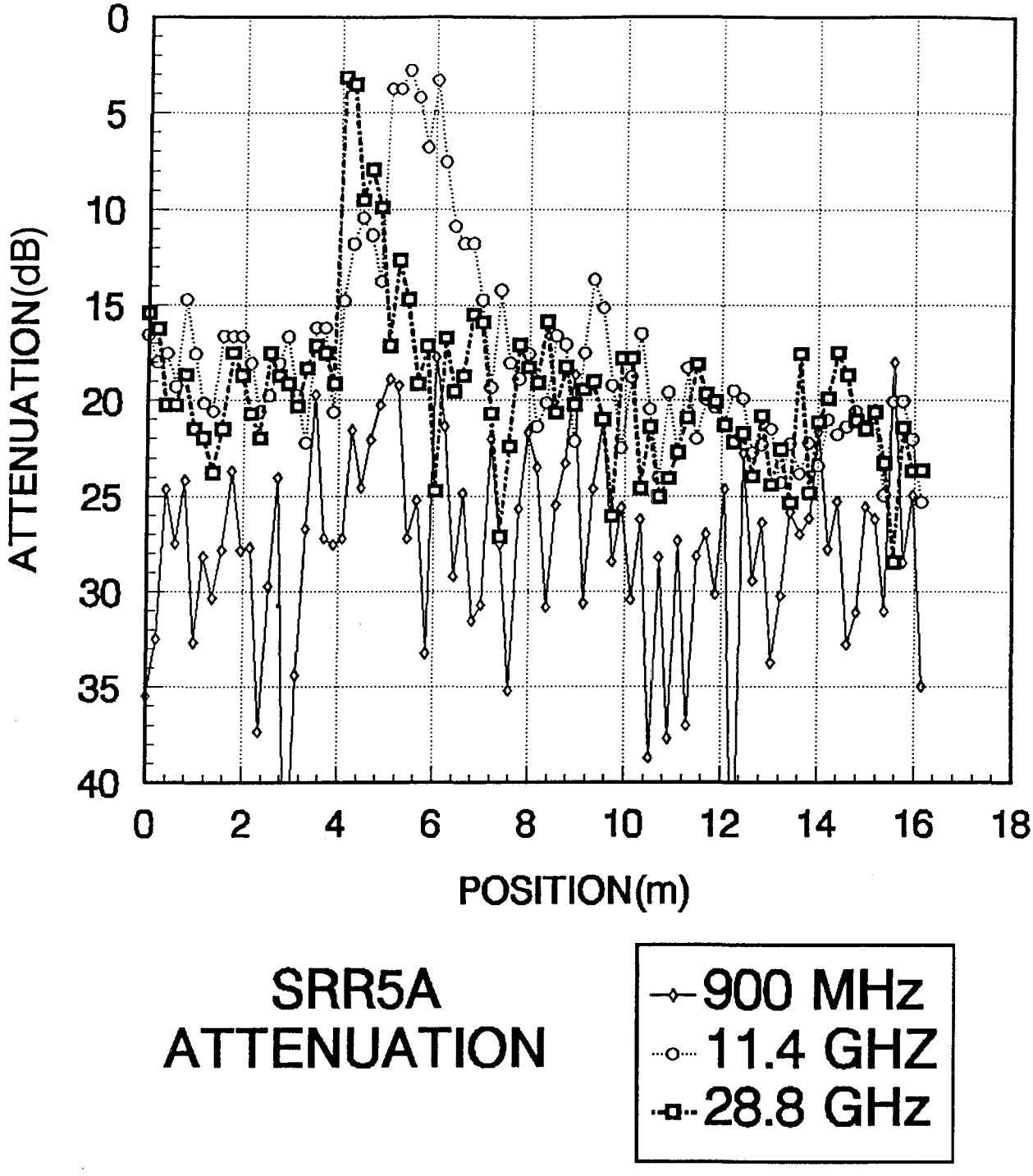

Figure A-51. Penetration loss for storeroom path SRR5A.

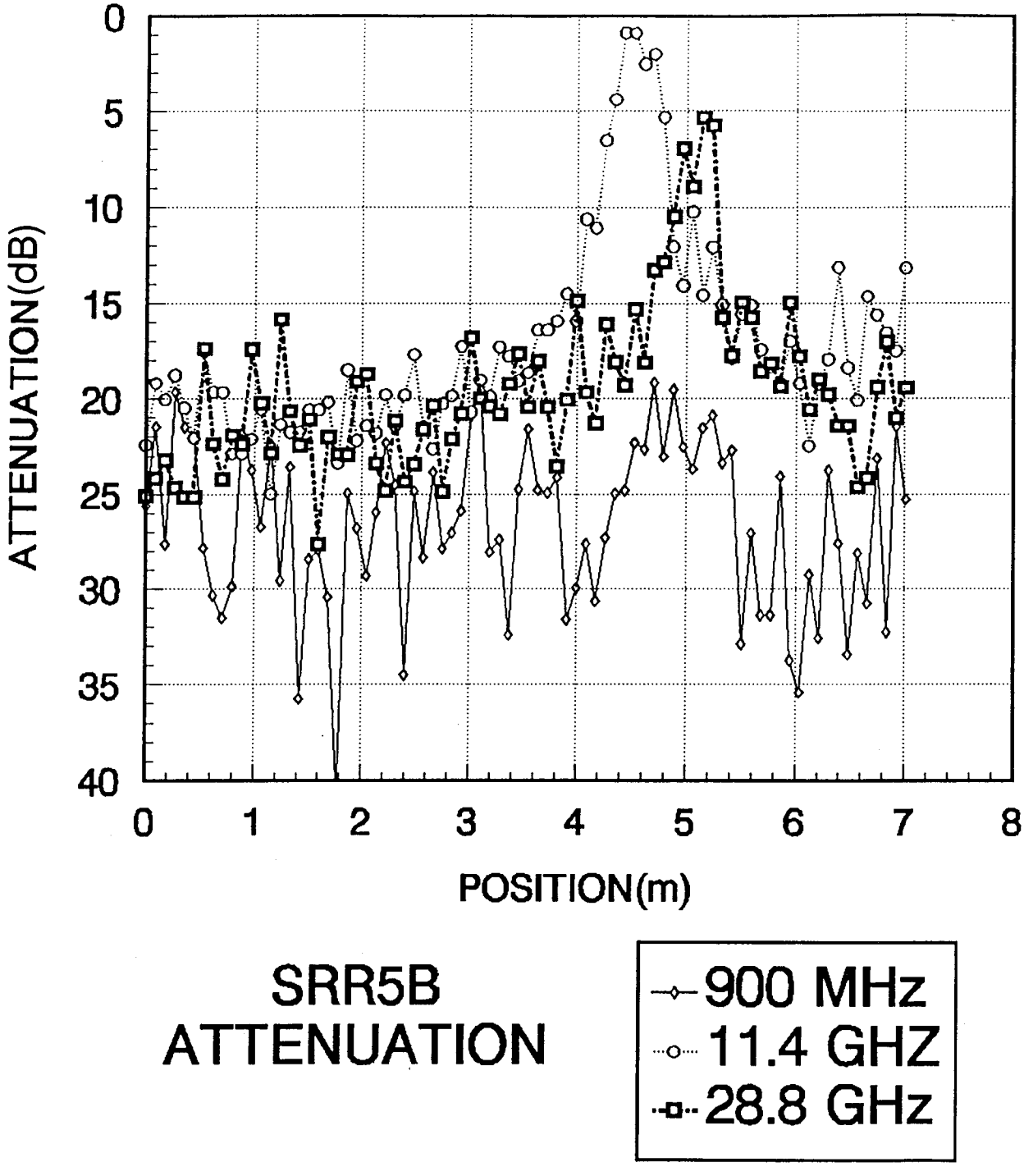

Figure A-52. Penetration loss for storeroom path SRR5B.

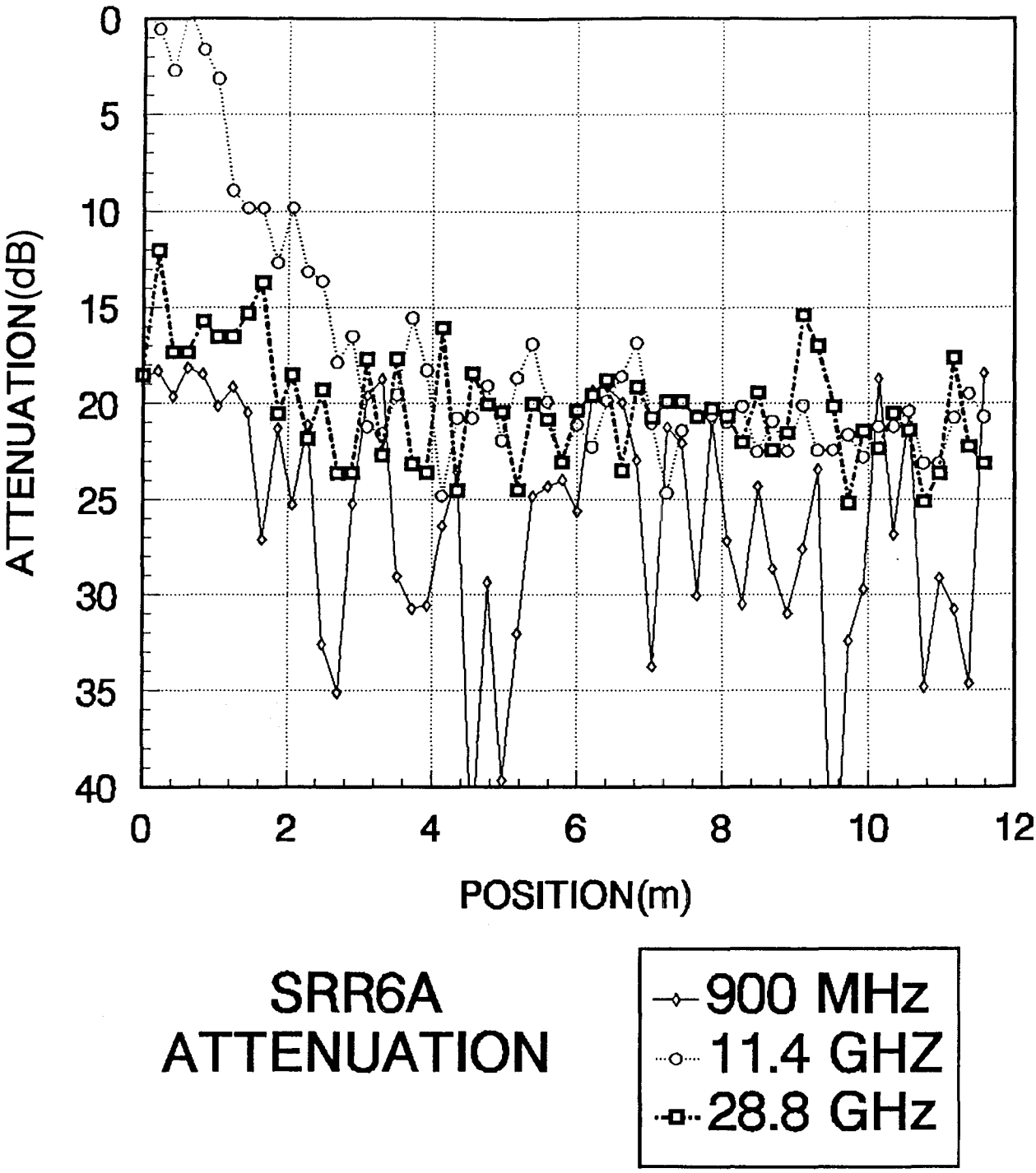

Figure A-53. Penetration loss for storeroom path SRR6A.

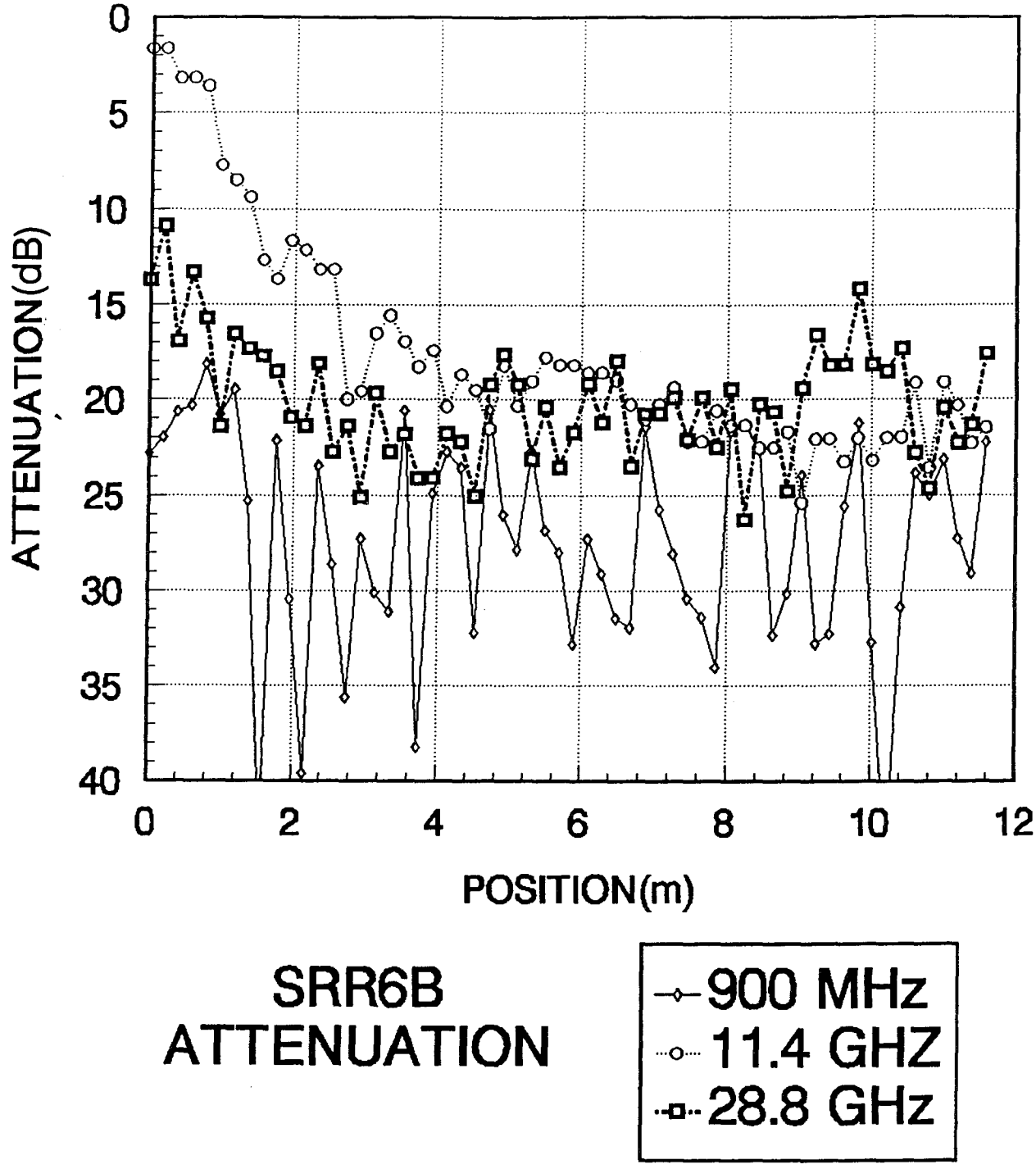

Figure A-54. Penetration loss for storeroom path SRR6B.

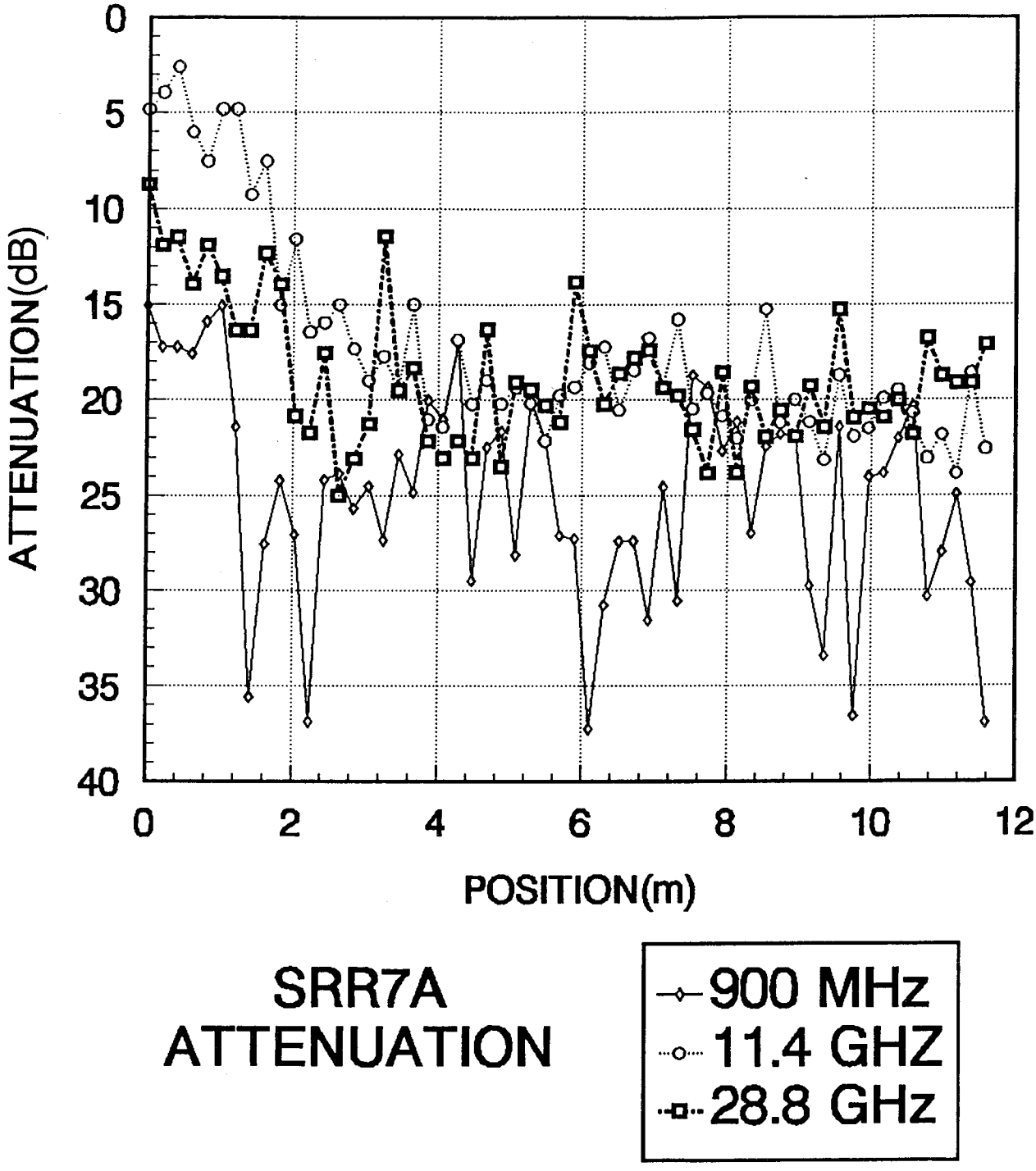

Figure A-55. Penetration loss for storeroom path SRR7A.

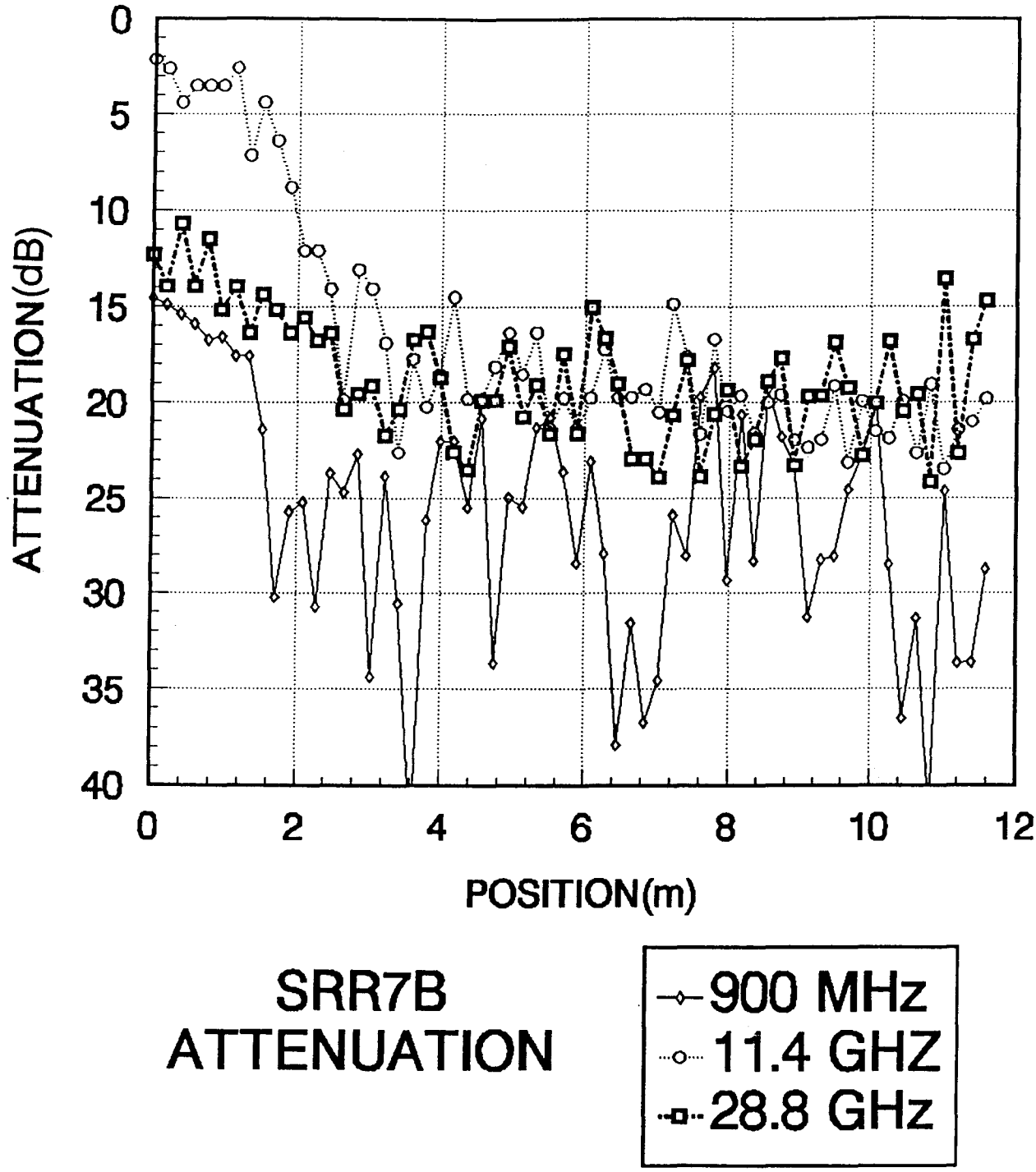

Figure A-56. Penetration loss for storeroom path SRR7B.

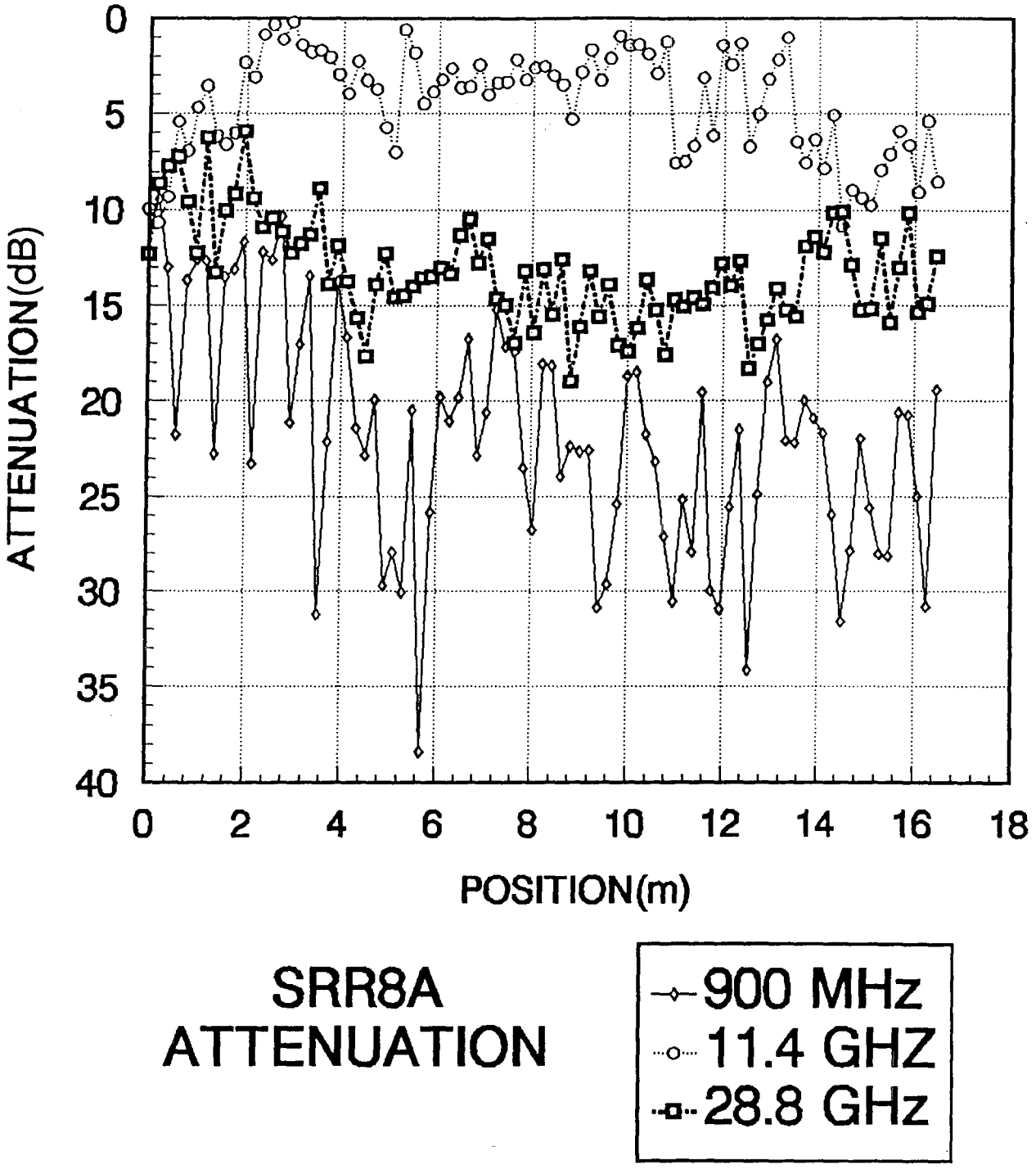

Figure A-57. Penetration loss for storeroom path SRR8A.

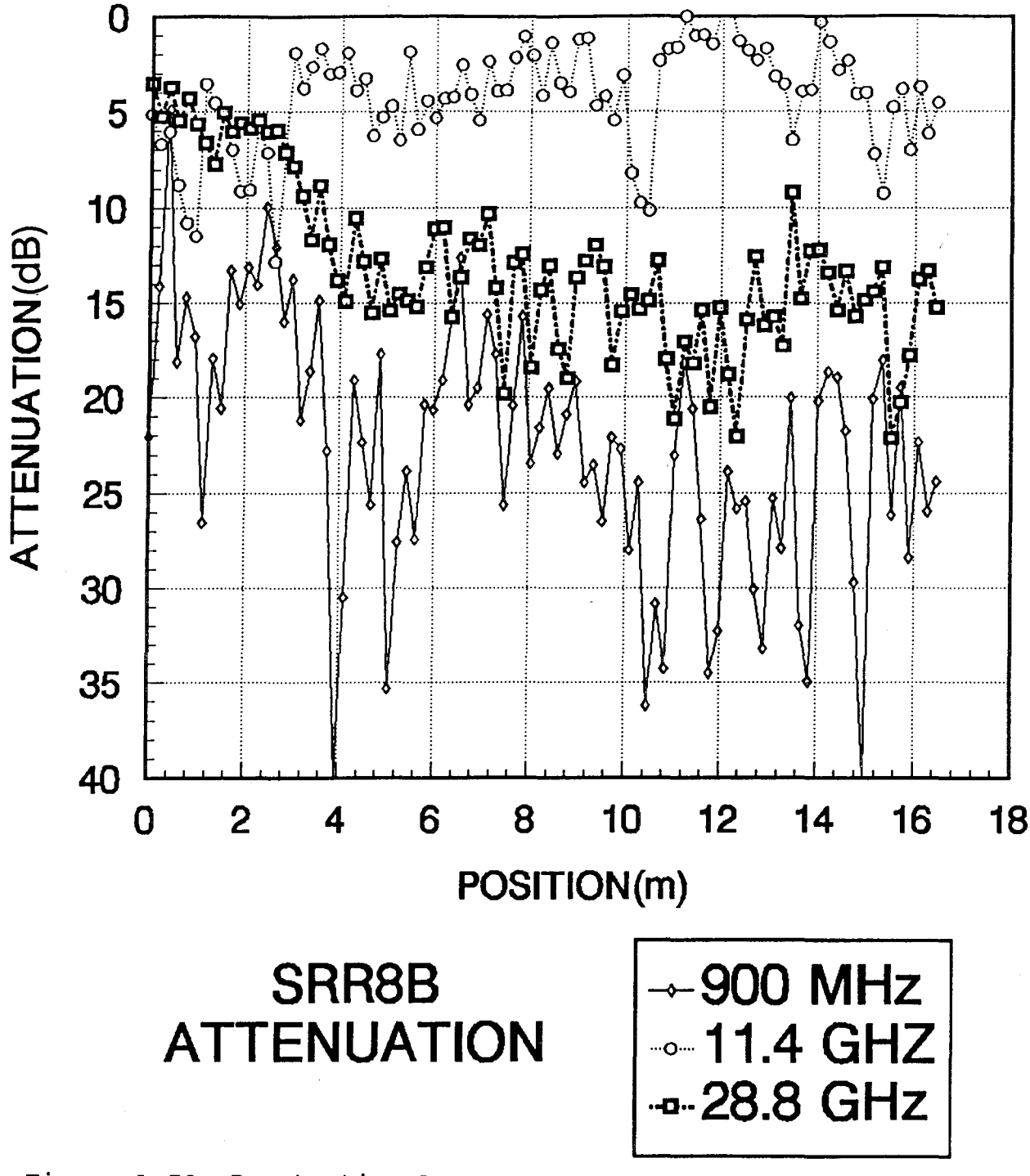

Figure A-58. Penetration loss for storeroom path SRR8B.

FORM **NTIA-29**
(4-80)

U.S. DEPARTMENT OF COMMERCE
NAT'L. TELECOMMUNICATIONS AND INFORMATION ADMINISTRATION

BIBLIOGRAPHIC DATA SHEET

	1. PUBLICATION NO.	2. Gov't Accession No.	3. Recipient's Accession No.
	94-306		

4. TITLE AND SUBTITLE
Building Penetration and Loss Measurements at 900 MHz, 11.4 GHz, and 28.8 GHz.

5. Publication Date
May 1994

6. Performing Organization Code
NTIA/ITS

7. AUTHOR(S)

9. Project/Task/Work Unit No.

8. PERFORMING ORGANIZATION NAME AND ADDRESS
National Telecommunications and Information Administration
Institute for Telecommunication Sciences
325 Broadway
Boulder, CO. 80303

10. Contract/Grant No.

11. Sponsoring Organization Name and Address
National Telecommunications & Information Administration
Institute for Telecommunication Sciences
325 Broadway
Boulder, CO. 80303-3328

12. Type of Report and Period Covered

13.

14. SUPPLEMENTARY NOTES

15. ABSTRACT *(A 200-word or less factual summary of most significant information. If document includes a significant bibliography or literature survey, mention it here.)*

The feasibility of using radio frequencies in the super high frequency (SHF) band (3-30 GHz) for Personal Communications Services (PCS) in buildings depends on the multipath within the structure and the amount of attenuation experienced by the electromagnetic waves passing through the structures. This study measured these effects to obtain a quantitative estimate of the attenuation magnitude. This magnitude can then be used for link margin analysis to determine if personal communications at SHF is practical.

16. Key Words *(Alphabetical order, separated by semicolons)*

Building attenuation; Measurements; Penetration attenuation; Personal communications; PCS.

17. AVAILABILITY STATEMENT	18. Security Class. *(This report)*	20. Number of pages
☒ UNLIMITED.		101
☐ FOR OFFICIAL DISTRIBUTION.	19. Security Class. *(This page)*	21. Price:

*U.S. GOVERNMENT PRINTING OFFICE:1994-573-013/00013